

Existence of Patchiness in Constricted Lungs: from
Experiments to Complex System Modeling **ARCHIVES**

by

Chanikarn Mint Wongviriyawong

Submitted to the Department of Mechanical Engineering
in partial fulfillment of the requirements for the degree of

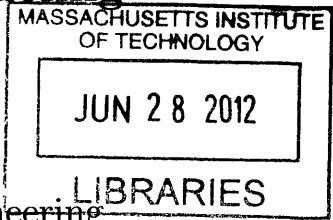
Doctor of Science


at the

MASSACHUSETTS INSTITUTE OF TECHNOLOGY

June 2012

© Massachusetts Institute of Technology 2012. All rights reserved.



Author 

Department of Mechanical Engineering


May 15, 2012

Certified by 

Jose G. Venegas

Associate Professor in Bioengineering

Thesis Supervisor

Certified by 

Roger D. Kamm

Professor of Mechanical Engineering and Biological Engineering

Thesis Reader

Accepted by 

David E. Hardt

Chairman, Department Committee on Graduate Students

Existence of Patchiness in Constricted Lungs: from Experiments to Complex System Modeling

by

Chanikarn Mint Wongviriyawong

Submitted to the Department of Mechanical Engineering
on May 15, 2012, in partial fulfillment of the
requirements for the degree of
Doctor of Science

Abstract

Understanding asthma pathophysiology can directly help researchers and physicians pinpoint mechanisms that govern airway hyperresponsiveness and effectively treat complex respiratory diseases such as asthma. The advancement in this research field has been prompted by the usage of medical imaging technology and computational modeling providing a subject-specific, noninvasive assessment of respiratory structure and function *in vivo*. This thesis features several attempts to study mechanisms of bronchoconstriction and interdependence between respiratory structure and function.

First, with complex system modeling of a network of airways, I investigated the effect of breathing patterns on the catastrophic closure of airways and the emergence of patchiness hypothesized to occur during an asthma attack. Second, from High-Resolution Computed Tomography (HRCT) images of the lung, the effect of longitudinal heterogeneity on resistance to airflow within central airways was studied. Lastly, the relationship between respiratory structure and function estimated from Positron Emission Tomography (PET) and HRCT images was examined. Responses of central airways to a simulated asthma attack was not able to explain the observed ventilation, thus prompting for an estimation of peripheral airway resistance to be added such that the predicted ventilation matched the ventilation observed in PET scans.

Three mechanisms hypothesized to be responsible for airway hyperresponsiveness in asthma and their influences on peripheral airway response were tested in our data set. In conclusion, we successfully identified the mechanism that was directly correlated with hyperresponsiveness of peripheral airways in asthma.

Thesis Supervisor: Jose G. Venegas
Title: Associate Professor in Bioengineering

Thesis Reader: Roger D. Kamm

Title: Professor of Mechanical Engineering and Biological Engineering

0.1 Acknowledgments

Knowing that this section may be the most read section of my thesis, I would like to leave behind words that express my most sincere appreciation for the dedicated efforts of countless number of people who have shaped my life, guiding me to where I am right now. My journey since I came to MIT in 2005 has not always been paved with rose petals. There are always bumps, and often times big ones. But what has kept me going is the reassurance that through all my ups and downs, I have the support of these amazing people who never stop believing in my potential.

Daisaku Ikeda, my life mentor, has taught me how much a single individual who is committed to realizing peace and happiness for all can do. His actions and constant encouragements continue to guide me through all difficulties in my life since 2008. I remember reading over and over again his guidance, embracing it with all my being. He wrote, "The proud mission of those who have been able to receive education must be to serve, in seen and unseen ways, the lives of those who have not had this opportunity." No matter how difficult it is, I would find the exact guidance that lifts up my spirit so that I can dash forward with great pride and self esteem. His compassion and encouragement are great treasures of my life and the reason why I cannot thank enough those who created circumstances that challenged me so that I can manifest my true potential.

My mother, Orawan Wongviriyawong, always loves me unconditionally. She is always by my side supporting me in both seen and unseen ways. Even if no one believes in me, she does. Even if no one is there when I am down, I can always count on her. Her love has been the sole source of light in darkness. I owe my life to her and my mentor. I vow to work tirelessly for the sake of happiness of others as the only way to repay my debts of gratitude to my mother and my mentor throughout my life. My sister, Titima Wongviriyawong, is the reason why I am alive. My life gains purposes since she has been born into this world. Kawin Setsompop has always been my pillar when I am weak, warmth when I feel cold, and much more.

Many others are my mentors in my professional development including Jose Venegas,

Christine Ortiz, Roger Kamm, Peter So, and Thaweesak Koanantakool. They have guided me through many difficult challenges I have had during my PhD, giving me strict yet compassionate training to become better a scientist and researcher. I am sincerely grateful for their guidance in my life.

Moreover, I want to thank my SGI family who without them I would not be alive today. I want to thank my comrades in faith who are always fighting by my side—Eric Reker, Anna Ikeda, Yi-Chun Lu, Masami Tabata, Mai Koyo, Mia Harvey, Emanda Thomas, Yumi Masui, Woei Ling Leow, Victor Ng, Jessie Calkins, and many more whose name I cannot finish listing here. Without my SGI family, life would be so lackluster. Like the wise man say, happiness when shared is doubled, sadness when shared is more than halved. I am determined to live my life with the spirit to repay my debts of gratitude to everyone by living the most fulfilling life contributing to world peace until the last moment.

Contents

0.1	Acknowledgments	5
1	Introduction	25
1.1	Existence of Patchiness in Constricted Lungs	25
1.2	Thesis Organization	26
2	Mechanical Ventilation and the Network Model of the Lung	29
2.1	Network Model of the Lung	31
2.2	Simulations	32
2.3	Effects of Mechanical Ventilation	36
2.3.1	Transition from VCV to PCV	39
2.3.2	Sensitivity of VT and regional ventilation to selection of P_I	42
2.3.3	Ventilation heterogeneity and ASM dynamic behavior	44
2.4	Methodological considerations	46
2.5	Emergence of Patchiness, Catastrophic Airway Closure and Dynamics of Tidal Volume	47
2.6	Summary	52
3	Central Airways	55
3.1	Function Effect of Longitudinal Heterogeneity in Constricted Airways Before and After Lung Expansion	55
3.1.1	Introduction	55
3.1.2	Methods	56

3.1.3	Results	64
3.1.4	Discussion	73
3.2	Paradoxical Dependency of Airway Distensibility on Airway Wall Area in Asthma	77
3.2.1	Introduction	77
3.2.2	Methods	78
3.2.3	Results	81
3.2.4	Discussion	90
4	Peripheral Airways	93
4.1	Image-Based Modeling Approach for Estimating Peripheral Airway Constriction in Human Lungs	93
4.1.1	Introduction	93
4.1.2	Methods	95
4.1.3	Results	106
4.1.4	Discussion	111
4.2	Topographic Modulation of Peripheral Airway Response in Asthma	116
4.2.1	Introduction	116
4.2.2	Results	120
4.2.3	Discussion	126
A	Derivations of Specific Pathway Admittance	145
A.1	Model 1	145
A.2	Model 2	146
A.3	Model 3	146
B	Estimating Apparent Compliance	149

List of Figures

2-1	Simulation Protocols. A: relative smooth muscle activation (Tr) plotted breath by breath. B: response of peak airway opening pressure ($P_{ao,p}$) relative to positive end-expiratory pressure (PEEP). The dashed line divides the 2 simulation protocols (volume-controlled ventilation (VCV) and pressure-controlled ventilation (PCV) with the inspiratory pressure (P_I) set at a fraction of $P_{I,0}$). $P_{I,0}$ is the P_I that yields the tidal volume (VT) immediately after the transition equal to VT_0 during VCV.	34
2-2	Airway response and changes in airway opening pressure with progressive bronchoconstriction during VCV. A: Tr plotted breath by breath. B: Response to the changes in Tr of lumen radii of terminal airways normalized by their corresponding fully dilated radii (r/r_0). Data from 256 representative airways are presented. In the pseudo-ventilation images at 2 steady conditions, the values of acinar ventilation normalized by total ventilation were represented in a color scale. C: Response of $P_{ao,p}$ relative to PEEP.	37

2-3	Airway response and changes in airway opening pressure during progressive bronchoconstriction with PCV with $Tr_0 = 0.5$. A: Tr plotted breath by breath. B: Response to the changes in Tr of lumen radii of terminal airways normalized by their corresponding fully dilated radii (r/r_0). Data from 256 representative airways are presented. In the pseudo-ventilation images at 2 steady conditions, the values of acinar ventilation normalized by total ventilation were represented in a color scale. C: Response of VT normalized by VT_0 . D: Response of $P_{ao,p}$ relative to PEEP	38
2-4	Airway response and changes in airway opening pressure during progressive bronchoconstriction with PCV with $Tr_0 = 0.9$. A: Tr plotted breath by breath. B: Response to the changes in Tr of lumen radii of terminal airways normalized by their corresponding fully dilated radii (r/r_0). Data from 256 representative airways are presented. In the pseudo-ventilation images at 2 steady conditions, the values of acinar ventilation normalized by total ventilation were represented in a color scale. C: Response of VT normalized by VT_0 . D: Response of $P_{ao,p}$ relative to PEEP.	40
2-5	Effect of the setting of P_I during PCV on the VT normalized by VT_0 , the VT during VCV, and ventilation distribution during maximal ASM activation ($Tr_0 = 1$). Tr was initially increased to 1.0 and kept constant to ensure a steady state (until the 900 th breath). At that point, the ventilatory mode was transitioned to PCV with P_I set at different values as a fraction of $P_{I,0}$. The pseudo-ventilation images illustrate the effect of different P_I on ventilation distribution.	41

2-6 Steady state VT (VT_{ss}) during PCV as a function of P_I for simulations with maximal ASM activation ($Tr_0=1$). VT_{ss} was normalized by the VT during VCV (VT_0) and P_I by the P_I yielding a first-breath VT following the transition equal to VT_0 ($P_{I,0}$). The solid line connects data points obtained from different simulations that were run with different values of $P_I/P_{I,0}$. The dashed line connects data points obtained from a single simulation that was run with successive step increases in $P_I/P_{I,0}$ from 0.9 to 1.1 and successive step decreases from 1.1 back to 0.9 (the direction of change is indicated by arrows). 43

2-7 The sensitivity of VT_{ss} to the selection of P_I was estimated from multiple simulation runs with independent changes in P_I (solid line in Fig. 2-6). Note that the sensitivity of VT_{ss} to the values of P_I is exceptionally high around $P_I = 1.03 P_{I,0}$ 43

2-8 Histograms and spatial distributions of ventilation normalized by the average ventilation during VCV at maximal ASM activation ($Tr_0=1$). Histograms and pseudo-ventilation images from 3 simulations of the identical VT_{ss} were compared. Both data sets were during steady state after the transition from VCV to PCV with $P_I=1.04 P_{I,0}$. However, in **A**, the dynamic properties of active ASM were present, while **B** absent. 44

2-9	<p>Histograms and spatial distributions of ventilation normalized by the average ventilation during VCV at maximal ASM activation ($Tr_0=1$). Histograms and pseudo-ventilation images from 3 simulations with identical VT_{ss} were compared. Each simulation was run under the following 3 conditions. A: During steady state, VCV before the transition to PCV. B: During steady state, after the transition from VCV to PCV with P_I selected so that VT_{ss} equaled VT_0 ($P_I=1.031 P_{I,0}$) and the dynamic properties of active ASM were present. C: During steady state after the transition from VCV to PCV with P_I selected so that VT_{ss} equaled VT_0 ($P_I=1.031 P_{I,0}$) and the dynamic properties of active ASM were absent.</p>	45
3-1	<p>3D rendered airway tree of an asthmatic subject after MCh challenge imaged at mean lung volume (MLV). A: Labels of all 35 defined central airways (0 – 6th generation) that were included in our analysis. B: A close-up of an airway (colored in blue) illustrating the presence of large longitudinal heterogeneity in the cross sectional area. To calculate the resistance of three airway models (See text and Fig. 3-2), dimensions of the five luminal cross sections (marked in white) equally spaced over the middle half of each airway were used. See text for an explanation.</p>	60
3-2	<p>Three models of the airway used for calculating three airway resistances (R_{avg}, R_T and R_A). A: Model of a cylindrical airway with a constant radius of r_{avg} and total length of L used for computing R_{avg}. B: Model of an airway with both longitudinal variability in the cross sectional area and non-circularity of the cross sectional shape used for computing R_T. The cross section was assumed elliptical with a major and minor radius of a_i and b_i, and the segmental length of l_i. C: Model of an airway with circular cross sections with the radius r_i and the longitudinal variability in the cross sectional area used for computing R_A.</p>	61

3-3 Cumulative distribution functions (CDF) of underestimations of airway resistance grouped for all airways of all asthmatic subjects (AS, left) and of non-asthmatic subjects (NA, right) after MCh challenge at mean lung volume (grey) and TLC (black). A: CDF of the total underestimation of airway resistance due to ignoring all longitudinal heterogeneity ($\%U_{total}$). B: CDF of the contribution to $\%U_{total}$ caused by longitudinal heterogeneity in the airway cross sectional area ($\%U_{area}$). C: CDF of the contribution to $\%U_{total}$ caused by a non-circular shape ($\%U_{shape}$). See text for explanation. 65

3-4 Changes in average underestimations of airway resistance caused by MCh challenge and an increase of lung volume to TLC. Each point represents the average of all airways for each asthmatic (AS, left) and non-asthmatic (NA, right) subject. A: Average underestimation of resistance caused by ignoring longitudinal heterogeneity in the airway cross sectional area and the non-circularity of the cross sectional shape ($\%U_{total}$). B: Average contribution to $\%U_{total}$ caused by longitudinal heterogeneity in the cross sectional area ($\%U_{area}$). C: Average contribution to $\%U_{total}$ caused by a non-circular shape ($\%U_{shape}$). BM denotes the image taken at baseline during breath-hold at mean lung volume (MLV). MM denotes the image taken post MCh challenge at MLV. MT denotes the image taken post MCh challenge at total lung capacity (TLC). Pairwise comparison based on the two-way ANOVA model with repeated measurements: *P<0.05, **P<0.005, and ***P<0.0001. 68

3-5 The distribution of the longitudinal heterogeneity in the cross sectional area quantified by $CV^2(A)$ and the non-circularity of the shape of the airway cross section (ϵ). A: The distribution of $CV^2(A)$ in all airways of all subjects under 3 conditions. Skewness of this distribution was measured using statistical software, SAS, to be 3.24 with the median of 0.009. B: The distribution of eccentricity of the assumed-elliptical cross section (ϵ). The average ϵ was 0.611. 69

- 3-6 Correlation between the contribution to $\%U_{total}$ caused by longitudinal heterogeneity in the airway cross sectional area ($\%U_{area}$) and $CV^2(A)$ (the square of the coefficient of variation in the cross sectional area along that airway). Data are taken from all airways in all subjects in all three imaging conditions. A least-square linear regression of the log-transformed data shows high correlation between $\log(\%U_{area})$ and $\log(CV^2(A))$ had a goodness of fit $R^2 = 0.997$ 71
- 3-7 Correlation between the contribution to $\%U_{total}$ caused by the non-circular shape ($\%U_{shape}$) and ϵ (the eccentricity of the assumed-elliptical cross section). Data are taken from all airways in all subjects in all three imaging conditions. A least-square linear regression of $\log(\%U_{shape})$ and ϵ had a goodness of fit $R^2 = 0.966$ 71
- 3-8 Changes in longitudinal heterogeneity in the cross sectional area caused by the lung volume increase to TLC in airways of various sizes. The average luminal area of an airway at baseline (A_{BM}) was plotted against the ratio in longitudinal heterogeneity in the cross sectional area ($CV^2(A)$) at TLC over that at mean lung volume (MLV) of the same airway. The plot includes all airways of all subjects. A_{BM} was imaged at MLV. The subscript MM denotes the image taken after MCh challenge at MLV; MT after MCh challenge at TLC. Airways with reduction in $CV^2(A)$ after the increase in lung volume to TLC would be below the unity line. Airways were binned into 4 quartiles with an equal number of airways (indicated by vertical lines). Note that in airways with the largest A_{BM} the increase in lung volume to TLC did not significantly change the longitudinal heterogeneity. 72

3-9 The apparent wall area during bronchoconstriction at the mean lung volume (MLV), ω and the apparent wall area during bronchoconstriction at total lung capacity (TLC), ω_T , belonging to one asthmatic subject. The least-square linear regression line was drawn in the solid black line. k is the slope of the regression line. ω^* is the apparent wall area where the predicted $\omega =$ the predicted ω_T based on the linear regression. 80

3-10 The intra-subject change in the measured wall area (WA) and the intra-subject average apparent wall area (ω). The data were taken from 3 images taken at: (1) BM: baseline at mean lung volume (MLV), (2) MM: post MCh challenge at MLV, and (3) MT: post MCh challenge at total lung capacity (TLC). The left column (blue) represents data from asthmatic (AS) subjects. The right column (red) represents data from non-asthmatic (NA) subjects. A: The intra-subject average of the WA_{MM} or WA_{MT} relative to WA_{BM} . In both AS and NA subjects, WA increased after MCh challenge ($P < 0.05$) and following the lung volume increase to TLC during bronchoconstriction ($P < 0.0001$). B: The intra-subject average ω . Following the lung volume increase to TLC during bronchoconstriction, the apparent wall area decreased in both AS and NA subjects ($P < 0.0001$). 82

3-11 The change in the airway wall area (WA) before and after lung expansion to TLC during bronchoconstriction. Data from all airways in all asthmatic (AS) and non-asthmatic (NA) subjects were plotted in A and B, respectively. WA of each airway are colored according to their airway type: small (blue), medium (yellow), and large (red). The significant difference of the change in WA between AS and NA subjects was observed only in large airways. The extent to which WA increased in large airways of AS subjects is higher than that in large airways of NA subjects following lung expansion to TLC. 83

- 3-12 The apparent wall area before and after lung expansion to TLC in 8 asthmatic subjects. The apparent wall area during bronchoconstriction at MTLV (ω_{MM}) and at TLC (ω_{MT}) from small, medium, and large airways were plotted in blue, yellow, and red, respectively. A least-square linear regression was generated for each subject and drawn in the solid black line. See text for explanation. 84
- 3-13 The apparent wall area before and after lung expansion to TLC in 9 non-asthmatic subjects. The WA during bronchoconstriction at MTLV (ω_{MM}) and at TLC (ω_{MT}) from small, medium, and large airways were plotted in blue, yellow, and red, respectively. A least-square linear regression was generated for each subject and drawn in the solid black line. See text for explanation. 85
- 3-14 The slope of the linear regression (k) and relative change in lung volume (VL_{MM}/VL_{MT})^{2/3}. Data from each of the 8 asthmatic (AS) subjects (colored in blue) and 9 non-asthmatic (NA) subjects (colored in red) were plotted with a least-square linear regression line (colored in light blue) that was forced to go through (1,1) ($R = 0.53$). See text for explanation. 86
- 3-15 The estimated lung volume (VL) at three imaging conditions of all asthmatic (AS) and non-asthmatic subjects (NA). The lung volume were taken from 3 images taken at: 1) BM: baseline at mean lung volume (MLV), 2) MM: post MCh challenge at MLV, and 3) MT: post MCh challenge at total lung capacity (TLC). The left column (colored in blue) represents data from AS subjects. The right column (colored in red) represents data from NA subjects. In AS subjects, VL increased both following the MCh challenge ($P < 0.05$) and lung expansion to TLC ($P < 0.05$). In NA subjects, VL increased both following the MCh challenge ($P < 0.0001$) and lung expansion to TLC ($P < 0.0001$). 87

3-16	The apparent wall area at mean lung volume (MLV) before and after MCh challenge in 8 asthmatic subjects. The apparent wall area at MLV before MCh challenge (ω_{BM}) and after MCh challenge (ω_{MM}) from small, medium, and large airways were plotted in blue, yellow, and red, respectively. See text for explanation.	88
3-17	The apparent wall area at mean lung volume (MLV) before and after MCh challenge in 9 non-asthmatic subjects. The apparent wall area at MLV before MCh challenge (ω_{BM}) and after MCh challenge (ω_{MM}) from small, medium, and large airways were plotted in blue, yellow, and red, respectively. See text for explanation.	89
4-1	A: 3D volume rendering of an airway tree, lung, and a sublobar region imaged at TLC. B: Diagram of 35 defined central airways and their labels used in our analysis. Of these, the 19 most distal airways, colored in blue, were used to define respective sublobar regions each airway subtended. C: Diagram of the lumped parameter network model of the airway tree consisting of 35 defined central airways with individual conductance of G_c . For each of the 19 most distal airways, a resistive element (R_p) representing resistance of peripheral airways within each sublobar region and elastic element with apparent compliance of Ca were appended in series. These model parameters were estimated from airway tree morphometry quantified from HRCT images, and the distribution of ventilation among sublobar regions (\dot{V}) estimated from dynamic PET scans. Each pathway was connected to a common pleural pressure (P_{pl}).	98

- 4-2 A: Fraction of gas content (F_{gas}) within each sublobar region located at a normalized distance d from the most ventral part of the lung ($d = 0$ most ventral, 1 most dorsal) taken at baseline (BASE), after MCh challenge (POST), and at TLC (PostTLC). F_{gas} was highest at TLC the top (supine position) and decreased toward dependent regions of the lung with increasing dependency on d as lung volume deviated from TLC. B: Regional gas volume (V_{gasi}) normalized by its TLC value vs. gas volume of the lung (V_{gas_L}) normalized by TLC. Slopes of these lines (belonging to each sublobar region) represented specific compliance of a sublobar region relative to that of the lung (blackBASE, redPOST). 101
- 4-3 Individual conductance (G_c) of 35 defined central airways in a representative non-asthmatic subject at baseline (BASE: open circles) and post MCh challenge (POST: filled circles) and gas volumes of regions that each airway subtended (V_{sub}) estimated from the PostTLC image. $\log(G_c)$ scaled linearly with $\log(V_{sub})$ at PostTLC. 103
- 4-4 Mean-normalized data of specific ventilation measured from PET scans ($s\dot{V}^*$) and specific ventilation predicted from the lumped parameter network model ($s\dot{V}_{pred}^*$) for each pathway in a representative non-asthmatic subjects at baseline (BASE: open circles) and post MCh challenge (POST: filled circles). Data for $s\dot{V}_{pred}^*$ computed from Model 1, 2 and 3 are shown in A, B and C, respectively. In Model 1 and 2, the prediction of were reasonable at baseline, but not after the challenge. In Model 3, we were able to match with by adding the appropriate estimates of R_p with less 1% prediction error. 104

4-5 Cumulative distributions of the central component of specific pathway conductance ($s\tilde{G}_c$) at baseline (BASEsolid line) and post MCh challenge (POST-dashed line) in 19 pathways for A) all non-asthmatic (NA), and B) all asthmatic (AS) subjects. MCh challenge caused a significant reduction in $s\tilde{G}_c$ in both groups ($P<0.01$). Peripheral component of specific pathway conductance (sG_p) at baseline (BASEsolid line) and post MCh challenge (POSTdashed line) in 19 pathways were plotted for C) all NA, and D) all AS subjects. In both groups, we found a significant reduction in sG_p after MCh challenge ($P<0.001$). 108

4-6 Geometric mean (μ_g) and variance (σ_g^2) of the central and peripheral component of specific pathway conductance (and sG_p , respectively). Individuals μ_g of $s\tilde{G}_c$ and sG_p are shown in Fig. A and B. σ_g^2 of $s\tilde{G}_c$ and sG_p within each individual are shown in Fig. C and D. Bronchoconstriction (POST) caused a reduction in μ_g of $s\tilde{G}_c$ in both non-asthmatic (NA) and asthmatic (AS) subjects ($P<0.05$) and a substantial reduction in μ_g of sG_p in both groups ($P<0.005$). The geometric mean of $s\tilde{G}_c$ were at least an order of magnitude higher than that of sG_p . The change in geometric variance was not systematic in either group. See text for further explanation. 109

4-7 Cumulative distributions of peripheral resistance (R_p) relative to the total pathway resistance (R_T). The plot includes data from 19 pathways of all non-asthmatic (NA) and asthmatic (AS) subjects at baseline (BASE) and post MCh challenge (POST). At BASE, R_p/R_T was elevated in AS compared to NA subjects ($P<0.005$). R_p/R_T significantly increased in both groups after MCh challenge ($P<0.0001$). 110

4-8	<p>A 3D volume renders of the lung, airway tree and 3 representative sublobar regions and patient-specific parameters derived from HRCT and PET images.</p> <p>B Structure of the lumped parameters network model of the lung, corresponding lumped elements in each pathway, and regional parenchymal distension ($V_{gas,i}/V_{tis,i}$). Input and output parameters of the lumped parameter network model previously presented in section 4.1 are listed below 4-8.</p>	119
4-9	<p>The sum of square (SS) of the relative difference between the mean normalized $s\dot{V}$ and $s\dot{V}_{pred}$ was plotted against the geometric variance of the normalized corner frequency (f_c/f_b). Each data point represents data from an individual subject at baseline (BASE-white) and after MCh challenge (CHAL-grey). Corresponding cumulative distributions from two representatives are plotted on the right with arrow indicating individual data points on the main plot. SS was highly correlated with geometric variance of f_c/f_b (R=0.88). Most geometric variance of f_c/f_b increased in NA subjects after the challenge, whereas the trend in the AS group is not clear.</p>	122
4-10	<p>Parenchymal distending capacity δ_{IC} and peripheral airway response $\frac{R_{p,BASE}}{R_{p,CHAL}}$ in subjects without asthma (NA). We expected that regions of increased δ_{IC} should have an increased peripheral airway response (negative correlation). However, we found no significant negative correlation in any NA subjects. . .</p>	123
4-11	<p>Parenchymal distending capacity δ_{IC} and peripheral airway response $\frac{R_{p,BASE}}{R_{p,CHAL}}$ in subjects without asthma. We expected that regions of increased δ_{IC} should have an increased peripheral airway response (negative correlation). However, we found no significant negative correlation in any AS subjects.</p>	123
4-12	<p>Tidal distension δ_T and peripheral airway response $\frac{R_{p,BASE}}{R_{p,CHAL}}$ in subjects without asthma. There was no positive correlation between tidal distension and peripheral airway response in any subject.</p>	124

4-13 Tidal distension δ_T and peripheral airway response $\frac{R_{p,BASE}}{R_{p,CHAL}}$ in subjects with asthma. Similarly, there was no positive correlation between tidal distension and peripheral airway response in any subject. 124

4-14 Peak parenchymal distension δ_P and peripheral airway response $\frac{R_{p,BASE}}{R_{p,CHAL}}$ in subjects without asthma. In 6 out of 8 NA subjects, there was a strong positive correlation suggesting that regions with high peak parenchymal distension had smaller response to MCh ($R = 0.68 \pm 0.07$ SEM). 125

4-15 Peak parenchymal distension δ_P and peripheral airway response $\frac{R_{p,BASE}}{R_{p,CHAL}}$ in subjects with asthma. There was a significant positive correlation in two AS subjects with the least response to Mch challenge (highest PC20). 125

THIS PAGE INTENTIONALLY LEFT BLANK

List of Tables

3.1	Demographics of asthmatic and non-asthmatic subjects and PFT collected from screening in an upright position (mean \pm standard deviation). * Unpaired t-test comparison between asthmatic and non-asthmatic groups; * P<0.05, *** P<0.0001.	57
3.2	The statistical properties of $\%U_{total}$, $\%U_{area}$, and $\%U_{shape}$ in asthmatic and non-asthmatic subjects computed from 3 scans: baseline at MTLV, post MCh at MTLV and post MCh at TLC. *Values shown are medians \pm standard deviations with range in parentheses. Definition of abbreviations: $\%U_{total}$ = total underestimation of airway resistance due to ignoring the longitudinal heterogeneity; $\%U_{area}$ = the contribution to $\%U_{total}$ caused by longitudinal heterogeneity in the airway cross sectional area; $\%U_{shape}$ = the contribution to $\%U_{total}$ caused by a non-circular shape; BM = Baseline scan at mean lung volume (MLV); MM = post MCh scan at MLV; MT = post MCh scan at total lung capacity (TLC).	66
3.3	P-values and mean estimates of pairwise comparisons of the log-transformed $\%U_{total}$, $\%_{area}$, and $\%_{shape}$ within asthmatic and non-asthmatic subjects. . . .	66
3.4	P-values of the two-way analysis of variance (ANOVA) with repeated measurements of $\log(\%U_{total})$, $\log(\%U_{areal})$, and $\log(\%U_{shapel})$	67
3.5	The statistical measures of $CV^2(A)$ and ϵ . Definition of abbreviations: $CV^2(A)$ = Longitudinal heterogeneity of the airway cross sectional area; ϵ = eccentricity of the assumed-elliptical cross section.	70

4.1 Demographics and PFT collected from screening in an upright position of asthmatic and non-asthmatic subjects. Values are means \pm SD. Unpaired t-test comparison between asthmatic and non-asthmatic groups: *P < 0.0001. 96

Chapter 1

Introduction

1.1 Existence of Patchiness in Constricted Lungs

During an asthma attack, elevated resistance with heterogeneous airway narrowing leads to a non-uniform distribution in ventilation. Imaging studies have shown that in subjects with induced bronchoconstriction, the distribution of ventilation is patchy with contiguous regions of very low ventilation compared to the rest of the lung [35, 34, 101, 100].

Although previous research studies have focused on characterizing airway narrowing and heterogeneity in ventilation distribution, the link between changes in airway behavior during bronchoconstriction and the formation of patchiness requires further investigation. Because the heterogeneity in the distribution of ventilation can greatly impair the quality of gas exchange within the lung, such link is of particular importance. Moreover, understanding of mechanisms related to the emergence of patchiness during bronchoconstriction remain unclear.

Using both medical imaging technologies and computational modeling, I investigated the relationship between respiratory structure and function as well as the mechanism associated with the emergence of patchiness during bronchoconstriction.

Noninvasive imaging techniques such as Computed Tomography (CT) and Positron Emission Tomography (PET) were used to obtain measurements of the structure and geometry of

the airway tree and lung functions before and during bronchoconstriction. From these data, an approach to estimate resistance of peripheral airways at a level beyond the resolution of HRCT images was derived. Applying this approach, I tested hypotheses concerning various sources related to the preferential clustering of patchiness such as the gravity-oriented gradient of alveolar ventilation, airway distensibility, longitudinal heterogeneity of individual airways, central airway constriction, etc.

The application of this approach on our data set enables the quantification of the effect of the presence or absence of various previously postulated mechanisms of bronchoconstriction, i.e. dynamic stretch on airway smooth muscle (ASM) [23], the distribution of ASM activation, etc. on the modulation of patchiness in asthmatic and non-asthmatic lungs before and during a simulated asthma attack. The implication of this work can directly impact the selection of asthma treatment in a per individual basis.

1.2 Thesis Organization

This thesis is organized into three main sections exploring the effect of breathing patterns on the emergence of patchiness and catastrophic airway closure, the relationship between respiratory structure and function in central and peripheral airways, and identification of the mechanism that governs peripheral airway response.

In chapter 2, with complex system modeling of a network of airways, I investigated the effect of breathing patterns on the catastrophic closure of airways and the emergence of patchiness hypothesized to occur during an asthma attack.

In chapter 3, the effect of longitudinal heterogeneity on resistance to airflow within central airways was studied from High-Resolution Computed Tomography (HRCT) images of the lung. The latter half of the chapter dealt with the paradoxical dependency of airway distensibility on airway wall area.

The thesis concludes with chapter 4, the relationship between respiratory structure and function estimated from Positron Emission Tomography (PET) and HRCT images was examined. Responses of central airways to a simulated asthma attack was not able to explain

the observed ventilation, thus prompting for an estimation of peripheral airway resistance to be added such that the predicted ventilation matched the ventilation observed in PET scans. Three mechanisms hypothesized to be responsible for airway hyperresponsiveness in asthma and their influences on peripheral airway response were tested in our data set.

Future work and potential applications of the work in clinical settings were included at the end of each chapter.

THIS PAGE INTENTIONALLY LEFT BLANK

Chapter 2

Mechanical Ventilation and the Network Model of the Lung

The two common ventilatory modes are volume-controlled ventilation (VCV) and pressure-controlled ventilation (PCV). Interestingly, experimental data suggest that PCV may have advantages on gas exchanges over VCV, which is a traditional mode of ventilation for patients with severe asthma. Lopez-Herce et al. [54] reported two clinical cases showing significant and rapid improvements in blood gases of children with severe asthma when ventilatory mode was switched to PCV after ventilating with VCV for 6 h, during which Lopez-Herce et al. observed no improvement in blood gases. Sarnaik et al. [79] published a study of 40 patients with severe asthma who showed significant improvements in blood gases as a result of mechanical ventilation with PCV. Understanding the theoretical basis of the regional behavior of a constricted lung could be helpful to interpret results of those studies.

We postulate that the significant improvement in blood gases observed experimentally during PCV may have resulted from changes in the distribution of ventilation caused by modifications in the interaction between a short-range positive and long-range negative feedback mechanism within the lung [101]. A positive feedback takes place when a small increase in local airway constriction leads to further constriction of that airway and those distal to it. Central to this mechanism is the response of the airway smooth muscle (ASM) to dy-

dynamic conditions. When ASM is activated, the airway narrows, reducing the amount of airflow through that airway. The reduction in airflow leads to reductions in regional tidal ventilation and thus the dynamic forces on the airway wall from parenchymal tethering and the transmural pressures. A reduction in these forces leads to shortening of the ASM and therefore further enhances the constriction of the airway. This mechanism is short ranged because it involves local interactions between airway and surrounding parenchyma and interconnected airways.

A long-range negative feedback takes place when airway constriction in one airway leads to airway dilatation of others far away in the tree. Central to this feedback mechanism is the maintenance of total tidal volume (VT) such as in VCV. When an airway constricts, airflow through that airway is reduced. If total VT is kept constant, a decrease in airflow along that airway subsequently causes an increase in driving pressure and airflow to the rest of the lung, which leads to airway dilatation by the mechanism described above. This mechanism is long range because it involves the interaction of airways far from each other.

Because in PCV driving pressure does not change in response to increased airway resistance, the negative feedback will be absent. This should affect the patchiness in ventilation distribution, and the instability of an unopposed positive feedback should rapidly lead to catastrophic closure of airways. In this paper, we investigate the impact of ventilatory mode on the distribution of ventilation during bronchoconstriction. Using a computational network model embodying the above-mentioned feedback mechanisms [101], we 1) examine the differences in spatial distribution of ventilation, total delivered VT , and airway lumen in a bronchoconstricted lung between VCV and PCV, 2) investigate how these differences depend on the baseline ASM tone and ventilator settings, and 3) investigate whether the dynamic response of active ASM to tidal breathing is responsible for the differences in the ventilation distribution between VCV and PCV.

2.1 Network Model of the Lung

Simulations were run on the network model that was previously described in details [101, 109]. The model consisted of a 12-generation airway tree with symmetric dichotomous branching. Airway sizes were taken from the morphological data from the fourth generation to the terminal bronchi of a human airway tree estimated by Weibel [105]. The model of a single terminal airway published by Anafi and Wilson [3] was implemented for all airways. Flow through each airway driven by a pressure drop was assumed to be laminar [60], with negligible gas compressibility [75] and negligible entrance effect. Each terminal bronchiole was connected to an acinar unit of constant and linear compliance. The effects of pleural pressure, gravity, and chest wall mechanics were neglected. Additionally, we neglected the interdependence between neighboring acinar units, as well as the nonlinearities of parenchyma and chest walls. Airway length was independent of lung inflation, and the wall thickness was adjusted with changes in airway diameter to preserve the wall volume [87]. To break the model-imposed functional and structural symmetry, a small random variation in wall thickness (1% coefficient of variation) was added to all airways. In the model, the lumen of each airway was assumed to remain constant during the breath. However, in a breath-by-breath manner, airway luminal area was determined based on the airway wall area and the ASM length, which was assumed to be equal to the outer circumference of the airway. The ASM length was computed based on the transmural pressure across the airway wall and the dynamic properties of the ASM. To do this, transmural pressure as a function of time was estimated in time steps of 10 ms along the breath as the net sum of radial forces on the airway wall caused by the luminal pressure, tethering stress from the surrounding parenchyma, and average pressure within the subtended alveoli.

Dynamic Equilibrium of Active ASM For a given set of flow and pressure conditions within each breath, the ASM length expected for dynamic equilibrium was extrapolated from an empirical linear relationship between the peak ASM length and peak ASM tension for maximal ASM activation [3, 23, 28, 87]. Such a peak ASM tension was calculated as

that balancing the peak transmural pressure during the breathing cycle. We then compared the current ASM length of each airway with that expected for dynamic equilibrium, and, if different, ASM length was adjusted by a fraction of the difference. This algorithm, repeated over several breaths, led to steady-state conditions where ASM length of each airway was in dynamic equilibrium. This approach has been found to describe well the dynamic response of airways to a deep breath [11, 23] and is consistent with the force-velocity relationship [99] and the viscoelastic properties for active smooth muscle [102].

Relative level of ASM activation In the Anafi and Wilson model [3], the relationship between the peak ASM tension and peak ASM length at dynamic equilibrium was taken to be that for a maximally activated ASM. To simulate conditions with the ASM activation below maximum, the slope of that relationship was scaled by a factor of relative level of ASM activation Tr . This factor ranged from $Tr = 0$ for fully relaxed to $Tr = 1$ for maximally activated ASM.

Alveolar ventilation was estimated as the VT expansion of a terminal acinar unit during the breath as determined by the product of compliance and the alveolar pressure swing. Total lung VT was computed as the difference between maximum and minimum total lung volume during each breath.

2.2 Simulations

We numerically solved the set of recursive state equations using MATLAB (Mathworks, Natick, MA) to determine the flow along each airway and the pressure at each branch point of the network. The model was driven with a constant breathing frequency of 12 breaths per minute, with inspiratory-to-expiratory time ratio of 1:1 and a positive end-expiratory pressure of 5 cmH₂O. Our previous model [101] was modified so that a user could specify the ventilatory mode to VCV or PCV. For VCV, the model input function was a constant inspiratory flow providing a predefined VT , followed by a passive exhalation in which airway opening pressure was kept constant at the positive end-expiratory pressure value. For PCV,

the input function was a constant pressure during inspiration (P_I) followed also by a passive exhalation as in VCV. The mode of ventilation could be changed at the end of a given breath. For a transition from VCV to PCV, a specific value of P_I could be selected or a value estimated so that the VT delivered during the first breath at PCV was equal to that during VCV. The value of Tr was set to be uniform throughout the airway tree and constant during each breath but could be varied breath by breath in a predefined manner.

Simulation protocols All simulations started with VCV (constant VT of 650 ml) until a steady state was established at baseline (Tr_0). In simulation protocol 1, we maintained VCV at a constant $VT = VT_0$. In simulation protocol 2, a ventilatory mode was changed from VCV to PCV, keeping the respiratory frequency and inspiratory-to-expiratory time ratio. For PCV, the value of $P_I = P_{I,0}$ was defined such that the total VT for the first breath following the transition of ventilatory mode equaled VT_0 (Fig. 2-1). After a steady state was achieved, a ramp increase in Tr from Tr_0 to $Tr = 1$ with a slope of 0.0002 per breath was applied to simulate a slow and progressive exposure to a bronchoconstrictor stimulus (Fig. 2-1). The following three sets of simulations were run to investigate the three aims listed in the Introduction of Chapter 2.

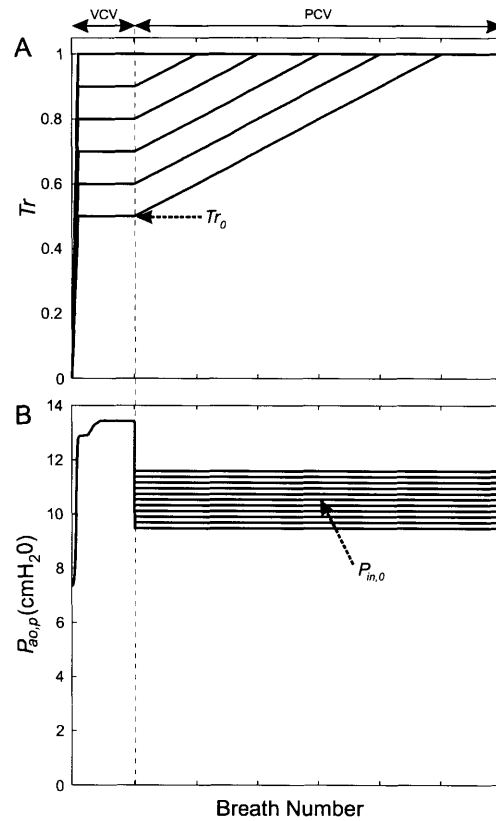


Figure 2-1: Simulation Protocols. **A**: relative smooth muscle activation (Tr) plotted breath by breath. **B**: response of peak airway opening pressure ($P_{ao,p}$) relative to positive end-expiratory pressure (PEEP). The dashed line divides the 2 simulation protocols (volume-controlled ventilation (VCV) and pressure-controlled ventilation (PCV) with the inspiratory pressure (P_I) set at a fraction of $P_{I,0}$). $P_{I,0}$ is the P_I that yields the tidal volume (VT) immediately after the transition equal to VT_0 during VCV.

Ventilatory Modes of Mechanical Ventilation Effects of ventilatory mode on airway lumen, delivered VT , and the distribution of ventilation. Both simulation protocols were run using $Tr_0 = 0.5$. This value was chosen to be 10% less than the estimated Tr_0 reported previously [109]. Two hundred fifty-six terminal airways were randomly selected, and their radii were normalized by the fully dilated respective radius at Tr_0 plotted as a function of time. The fraction of closed terminal airways, at a given time, was computed as the fraction of airways with radii less than 0.5% of their fully dilated radii. Values of P_I during PCV and VT/VT_0 and the peak airway opening pressure during VCV were plotted as a function of time. Finally, the distribution of ventilation was represented by a Mandelbrot-like tree, where ventilation to each terminal unit corresponded to a data point in the 64 x 64 grid. The color scale corresponded to the ventilation normalized by the average ventilation during VCV. Throughout this paper, this plot is referred to as a pseudo-ventilation image.

Influence of the baseline ASM activation and ventilator setting Both simulation protocols were conducted with Tr_0 set at a value ranging from 0.5 to 1.0 in increments of 0.1. In simulations with protocol 2, PCV was given with values of $P_I/P_{I,0}$ ranging from 0.90 to 1.10 in increments of 0.01. Differences in steady-state airway radii, steady-state VT (VT_{ss}), and the spatial distribution of ventilation were noted. The sensitivity of VT_{ss} to the selection of P_I was calculated as the slope of a plot between VT_{ss}/VT_0 and $P_I/P_{I,0}$. The spatial distributions of ventilation in steady state were plotted for VCV before the transition to PCV and in PCV for all P_I settings.

Contribution of the dynamic behavior of ASM to the distribution of ventilation in PCV Simulation protocol 2 was run with $Tr_0 = 1$ with a transition to PCV using $P_I/P_{I,0} = 1.031$. This number was derived iteratively so that VT during steady-state condition in PCV equaled VT_0 . Note that this value of P_I is not the same as that which gives a first-breath $VT = VT_0$. The simulation was then repeated, but this time with a model that did not include the dynamic properties of ASM; instead, airway radii during PCV were fixed to the values obtained during steady-state VCV. Ventilation histograms and pseudo-

ventilation images during steady state in PCV were generated for each simulation. The degree of ventilation heterogeneity was quantified by the coefficient of variation (equal to SD/mean) [67, 100, 101]. The simulations were also run with a value of $P_I/P_{I,0} = 1.04$, a condition where the effect of the ASM dynamic behavior on the distribution of ventilation was exaggerated.

2.3 Effects of Mechanical Ventilation

As observed before, in VCV, the constriction of airways was homogenous at low levels of ASM activation. A slow increase in Tr over time caused a reduction in airway radii and a concomitant increase in peak airway opening pressure. As Tr reached a critical point ($Tr < 0.8$), groups of airways rapidly constricted, whereas others expanded, resulting in a combination of airway constriction and dilation [101] and in patchy ventilation distribution characterized by large size ventilation defects [109] (Fig. 2-2). As Tr continued to increase above that critical point, ventilation defects continued to emerge with a concomitant redistribution of ventilation away from ventilation defects. During PCV, low levels of Tr resulted in a uniform airway constriction similar to that in VCV as long as VT remained unchanged (up to around 1,000 breaths in Fig. 2-3). However, as Tr continued to increase, we observed a progressive drop in VT and an accelerated airway constriction that led to full closure of all terminal airways (Fig. 2-3). Note that the timing for full airway closure was not uniform.

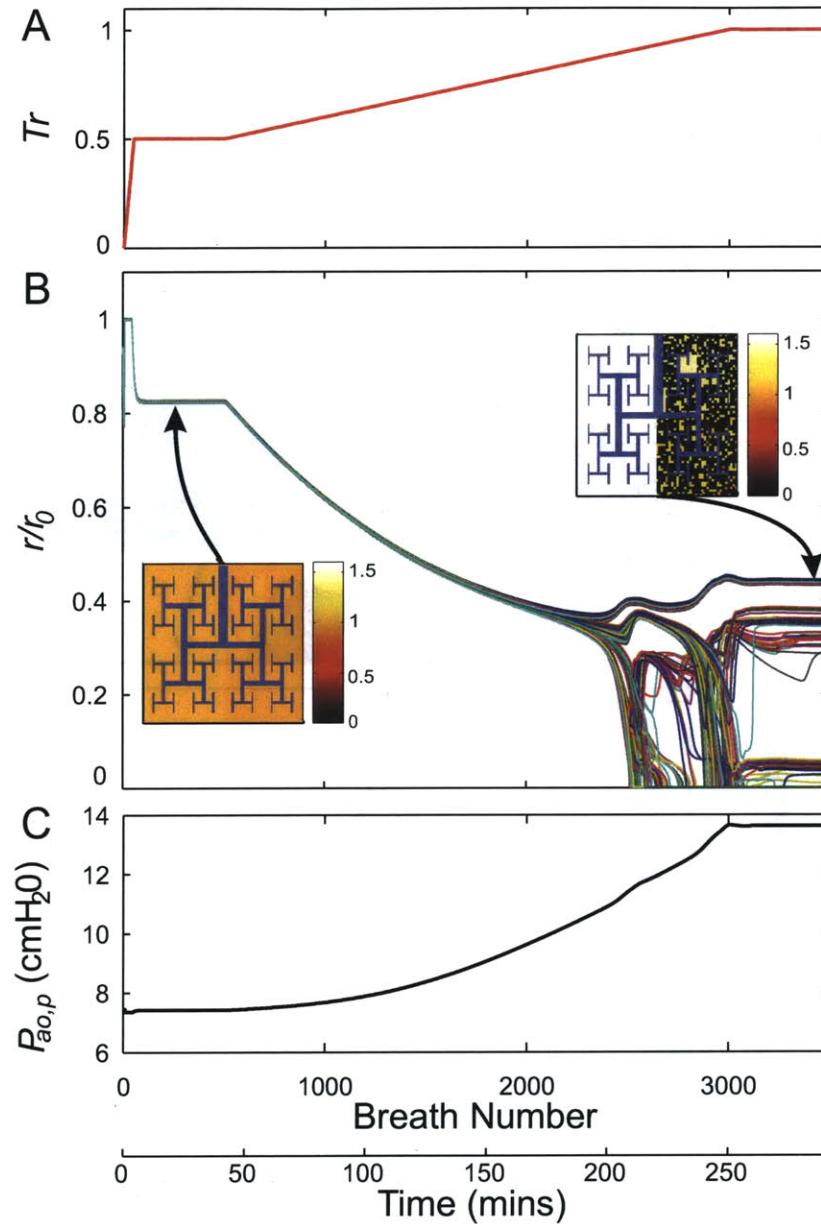


Figure 2-2: Airway response and changes in airway opening pressure with progressive bronchoconstriction during VCV. **A:** Tr plotted breath by breath. **B:** Response to the changes in Tr of lumen radii of terminal airways normalized by their corresponding fully dilated radii (r/r_0). Data from 256 representative airways are presented. In the pseudo-ventilation images at 2 steady conditions, the values of acinar ventilation normalized by total ventilation were represented in a color scale. **C:** Response of $P_{ao,p}$ relative to PEEP.

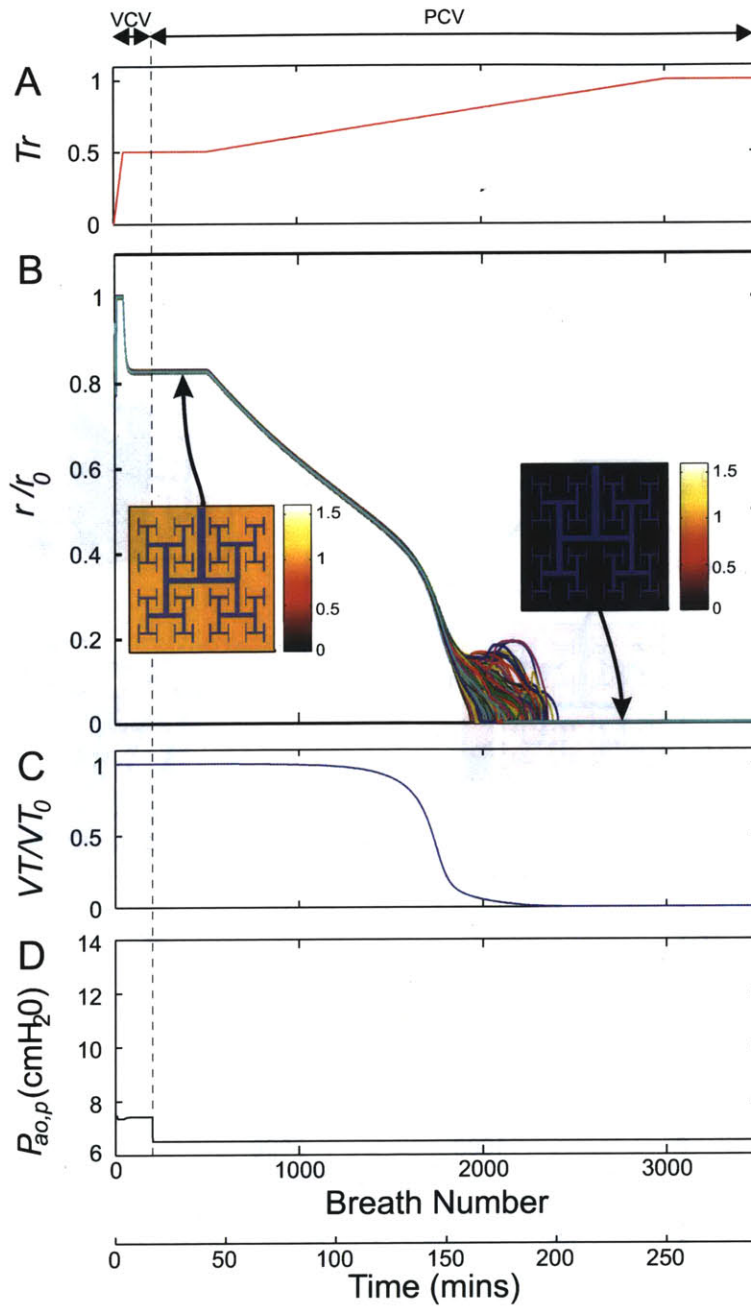


Figure 2-3: Airway response and changes in airway opening pressure during progressive bronchoconstriction with PCV with $Tr_0 = 0.5$. **A:** Tr plotted breath by breath. **B:** Response to the changes in Tr of lumen radii of terminal airways normalized by their corresponding fully dilated radii (r/r_0). Data from 256 representative airways are presented. In the pseudo-ventilation images at 2 steady conditions, the values of acinar ventilation normalized by total ventilation were represented in a color scale. **C:** Response of VT normalized by VT_0 . **D:** Response of $P_{ao,p}$ relative to PEEP

2.3.1 Transition from VCV to PCV

For transitions from VCV to PCV taking place with $Tr_0 \leq 0.8$, airway radii were uniformly constricted and remained constant before, during, and after the transition (Fig. 2-3). However, for $Tr_0 > 0.8$, i.e., 0.9 (Fig. 2-4) or 1.0 (Fig. 2-5), transitions from VCV to PCV led to P_I -dependent dynamic changes in radius and VT until a new steady state was reached. Note that even when P_I was set such that the firstbreath VT in PCV was equal to that during VCV ($VT = VT_0$), when distribution of ventilation was heterogeneous, the new steady state reached involved a substantially reduced VT with a ventilation distribution that was also heterogeneous but no longer patchy. Further increasing Tr during PCV led to rapid closure of most terminal airways (fraction of closed airways was 0.96) (Fig. 2-4).

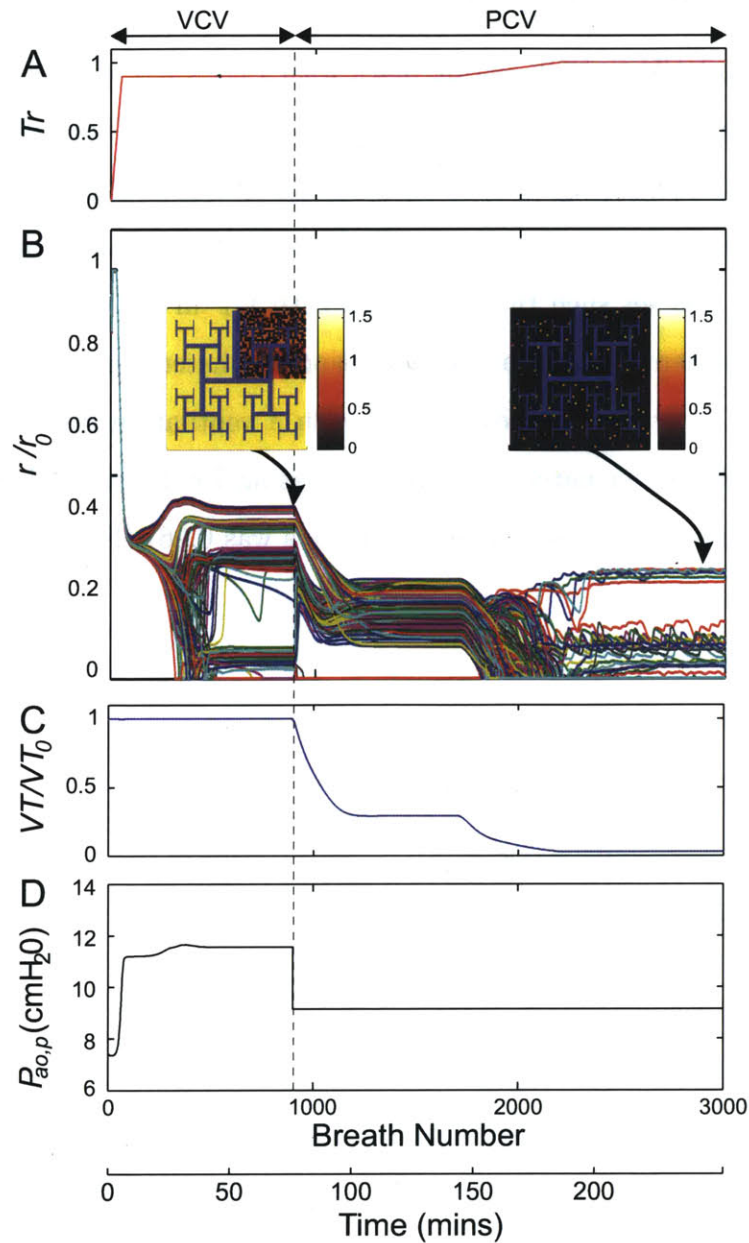


Figure 2-4: Airway response and changes in airway opening pressure during progressive bronchoconstriction with PCV with $Tr_0 = 0.9$. **A:** Tr plotted breath by breath. **B:** Response to the changes in Tr of lumen radii of terminal airways normalized by their corresponding fully dilated radii (r/r_0). Data from 256 representative airways are presented. In the pseudo-ventilation images at 2 steady conditions, the values of acinar ventilation normalized by total ventilation were represented in a color scale. **C:** Response of VT normalized by VT_0 . **D:** Response of $P_{ao,p}$ relative to PEEP.

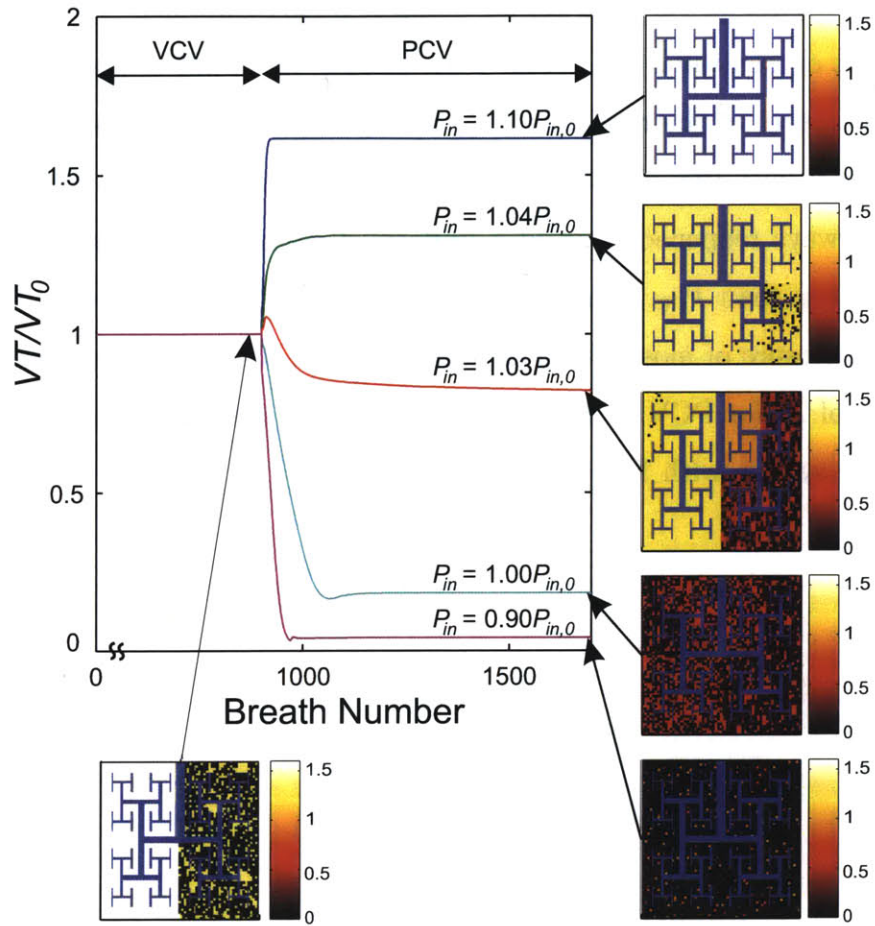


Figure 2-5: Effect of the setting of P_I during PCV on the VT normalized by VT_0 , the VT during VCV, and ventilation distribution during maximal ASM activation ($Tr_0 = 1$). Tr was initially increased to 1.0 and kept constant to ensure a steady state (until the 900th breath). At that point, the ventilatory mode was transitioned to PCV with P_I set at different values as a fraction of $P_{I,0}$. The pseudo-ventilation images illustrate the effect of different P_I on ventilation distribution.

2.3.2 Sensitivity of VT and regional ventilation to selection of P_I

After the transition from VCV to PCV in conditions of $Tr_0 \leq 0.8$, both VT and the regional distribution of ventilation remained steady, with VT_{ss} linearly related to P_I . However, for $Tr_0 > 0.8$, VT_{ss} and the distribution of ventilation at steady state were highly and nonlinearly dependent on the chosen value of P_I (Fig. 2-6). Indeed, small differences in the setting of P_I led to large differences in the resultant VT_{ss} and the distribution of ventilation (Fig. 2-5). For example, for P_I just 10% greater than $P_{I,0}$, VT_{ss} increased by 68% relative to VT_0 with PCV and all airways reopened to yield a uniform distribution of ventilation. Conversely, for P_I just 10% less than $P_{I,0}$, there was a reduction of VT_{ss} of more than 95% relative to VT_0 and virtual closure of most (78%) terminal airways. The maximum sensitivity of VT_{ss} to the selection of P_I for PCV at $Tr_0 = 1$ (Fig. 2-7) was almost 40 times greater than the sensitivity of the system with $Tr_0 \leq 0.8$.

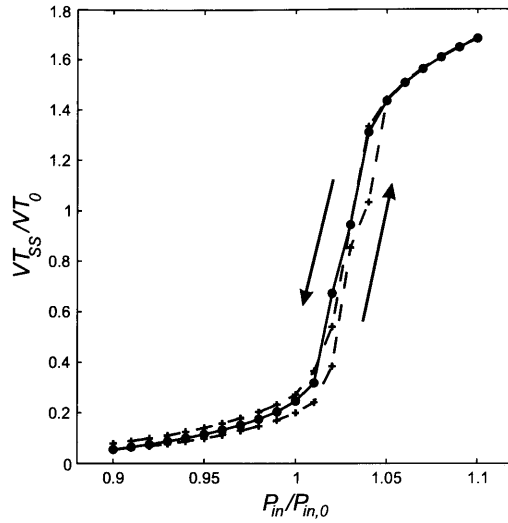


Figure 2-6: Steady state VT (VT_{ss}) during PCV as a function of P_I for simulations with maximal ASM activation ($Tr_0=1$). VT_{ss} was normalized by the VT during VCV (VT_0) and P_I by the P_I yielding a first-breath VT following the transition equal to VT_0 ($P_{I,0}$). The solid line connects data points obtained from different simulations that were run with different values of $P_I/P_{I,0}$. The dashed line connects data points obtained from a single simulation that was run with successive step increases in $P_I/P_{I,0}$ from 0.9 to 1.1 and successive step decreases from 1.1 back to 0.9 (the direction of change is indicated by arrows).

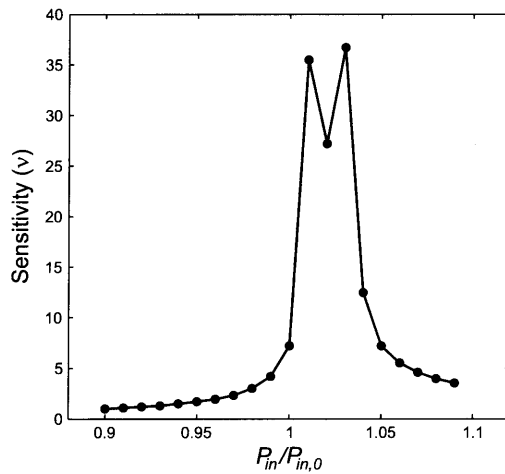


Figure 2-7: The sensitivity of VT_{ss} to the selection of P_I was estimated from multiple simulation runs with independent changes in P_I (solid line in Fig. 2-6). Note that the sensitivity of VT_{ss} to the values of P_I is exceptionally high around $P_I = 1.03 P_{I,0}$.

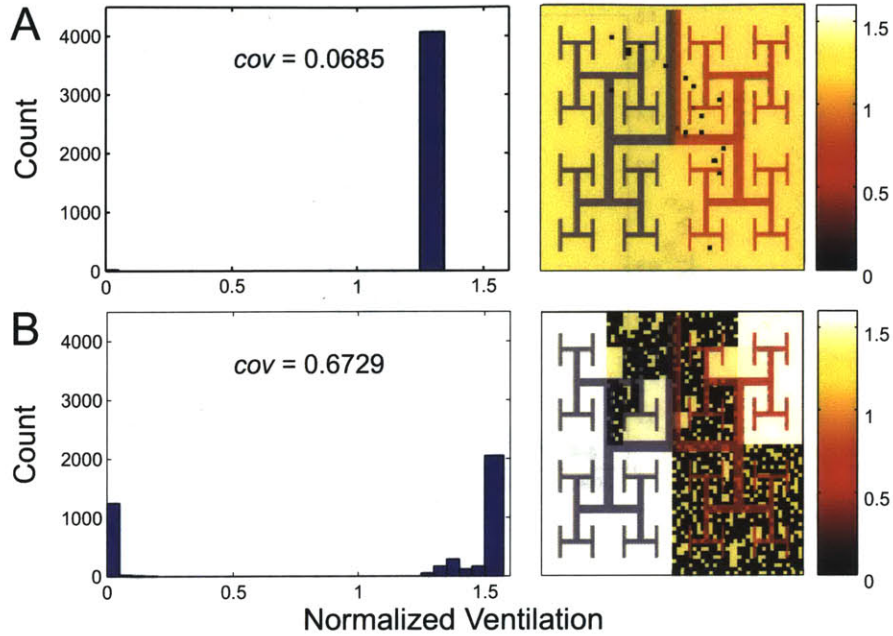


Figure 2-8: Histograms and spatial distributions of ventilation normalized by the average ventilation during VCV at maximal ASM activation ($Tr_0=1$). Histograms and pseudo-ventilation images from 3 simulations of the identical VT_{ss} were compared. Both data sets were during steady state after the transition from VCV to PCV with $P_I=1.04 P_{I,0}$. However, in **A**, the dynamic properties of active ASM were present, while **B** absent.

2.3.3 Ventilation heterogeneity and ASM dynamic behavior

When airway radii were allowed to change according to the dynamic properties of active ASM, the ventilation heterogeneity was higher during VCV (Fig. 2-9A) than during PCV with P_I selected for equivalent VT_{ss} ($P_I = 1.031 P_{I,0}$) (Fig. 2-9B). Indeed, the coefficient of variation of regional ventilation during PCV was reduced by 31.05% compared with VCV, and the ventilation to severely hypoventilating units substantially decreased lower in the model that included the dynamic properties of active ASM (Fig. 2-8).

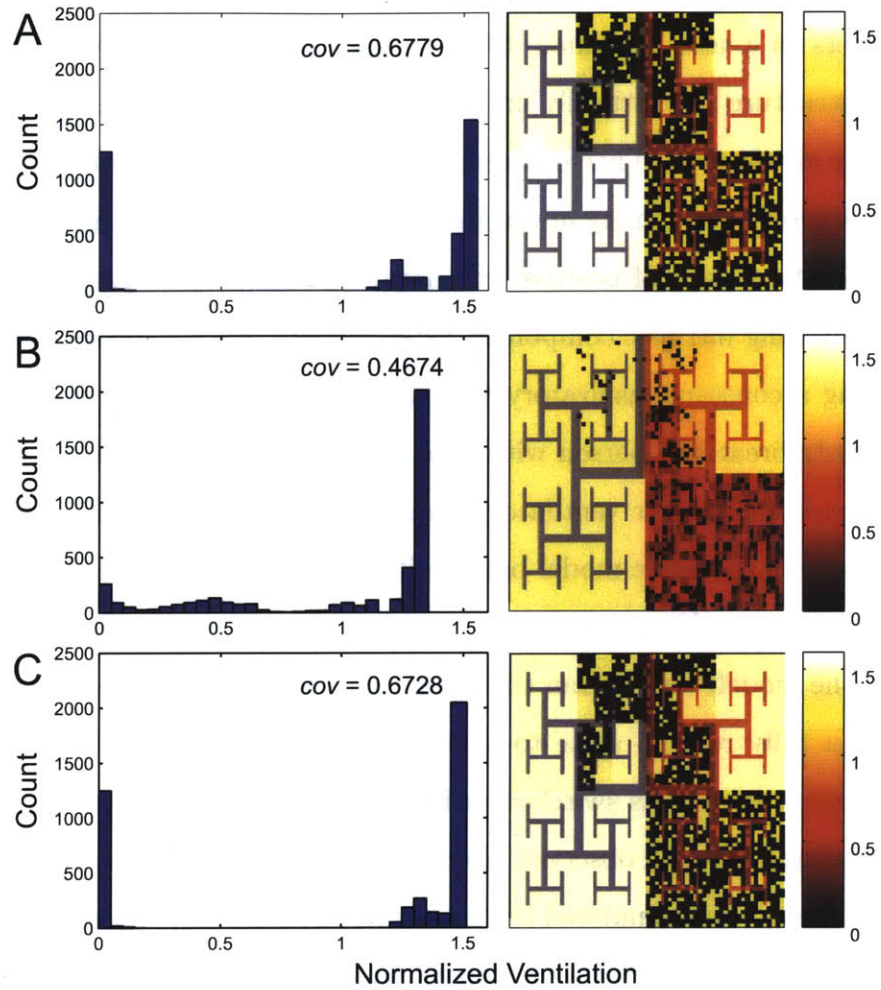


Figure 2-9: Histograms and spatial distributions of ventilation normalized by the average ventilation during VCV at maximal ASM activation ($Tr_0=1$). Histograms and pseudo-ventilation images from 3 simulations with identical VT_{ss} were compared. Each simulation was run under the following 3 conditions. **A:** During steady state, VCV before the transition to PCV. **B:** During steady state, after the transition from VCV to PCV with P_I selected so that VT_{ss} equaled VT_0 ($P_I=1.031 P_{I,0}$) and the dynamic properties of active ASM were present. **C:** During steady state after the transition from VCV to PCV with P_I selected so that VT_{ss} equaled VT_0 ($P_I=1.031 P_{I,0}$) and the dynamic properties of active ASM were absent.

2.4 Methodological considerations

We used a computational network model of the lung that used realistic anatomic and physiological parameters for a healthy human [101]. The model incorporated Weibels [105] symmetric airway tree structure and virtually uniform anatomic and functional parameters for each generation of the airway tree. This idealized structurefunction architecture served to demonstrate that the severe heterogeneity in ventilation during bronchoconstriction in asthma could be explained by interactions of positive and negative feedbacks among the systems components without invoking intrinsic component heterogeneity. Such a model was previously run with VCV, using a constant inspiratory flow and passive exhalation, to simulate an idealized spontaneously breathing person with enough respiratory drive and respiratory muscles capable of maintaining his/her ventilatory requirements during bronchoconstriction. Here, we took advantage of the same model but ran it with PCV to explore the sensitivity of the model when P_I , and not VT , was kept constant during bronchoconstriction. To establish an initial state in the model, we first ran the simulations with VCV while Tr was progressively increased from a fully relaxed state to a baseline muscle tone. Once a steady state was achieved, ventilatory mode was switched to PCV with P_I set to deliver the next breath VT equal to that during VCV and observed the dynamic changes in airway radii and ventilation to a new steady state. This simulated the case where P_I for PCV was set to keep ventilatory levels at transition equivalent to those with VCV. Transitioning to PCV such that VT was similar to that during VCV helped us to eliminate the possibility that the known effect of VT on bronchoconstriction and on the size of ventilation defects [101] was the cause of observed differences in airway behavior between ventilatory modes. However, note that because of the difference in the input function in both modes of ventilation, during heterogeneous conditions, VT and its regional distribution were not at steady state after the transition to PCV but underwent a transient period before settling into a new steady state at a substantially reduced value (Figs. 2-4 and 2-5).

For the smooth muscle activation beyond criticality ($Tr > 0.8$), a transition from VCV to PCV caused major changes in ventilation. Delivered VT during PCV could not be

maintained equal to that during VCV, even though P_I was selected to deliver equal VT in the breath immediately after the transition to PCV. In fact, a slightly larger value of P_I had to be chosen so that VT_{ss} during PCV would equal VT_0 .

2.5 Emergence of Patchiness, Catastrophic Airway Closure and Dynamics of Tidal Volume

Our simulations suggest that the total ventilation and spatial distribution during PCV could be substantially more sensitive to changes in smooth muscle activation level (Fig. 2-3) and P_I settings (Figs. 2-5 and 2-6) than previously anticipated. Such a high sensitivity was the result of the properties of the active ASM under dynamic forces and was much greater than that attributable to temporal differences predicted by models that ignore ASM dynamic properties. In practical terms, our findings imply that small changes in the settings of the mechanical ventilator or in the degree of bronchoconstrictive stimulus to the lung of asthmatic patients ventilated with PCV could result in unexpectedly large changes in the magnitude of the delivered VT (increase or decrease), in airway behavior (full reopening of closed airways or catastrophic closure), and in ventilation distribution (elimination of patchiness).

After the transition from VCV to PCV, the system behaved differently depending on the baseline level of smooth muscle activation (Tr_0). For $Tr_0 \leq 0.8$, the system started off constricting uniformly. After the transition from VCV to PCV, the system remained uniform with a stable VT . As Tr was further increased during PCV, airways continued to constrict uniformly with constant VT , and, at a certain point, VT rapidly dropped as accelerated airway constriction led to full airway closure (Fig. 2-3). This behavior can be explained based on the positive feedback mechanism implicit in the basic building block of our model [3]. To understand this behavior, let us consider first an equivalent lung model of parallel pathways where each path to a terminal unit is represented by resistance element connected to a compliant alveolar element. Assuming this model is driven at constant frequency (f),

the flow rate and volume delivered into each branch (i) at a given pressure amplitude depends on the magnitude of the pathway impedance $|Z_i|^2 = R_i^2 + \left(\frac{1}{2\pi f C_i}\right)^2$, where C_i and R_i are the equivalent compliance and resistance for each pathway, respectively.

For low levels of Tr and ventilation at normal f in this network, since $R_i < \omega l/2fC_i$, Z_i is mostly dependent on C_i , and thus VT and its distribution among branches are relatively independent of Tr . This behavior is apparent during the period of the breaths 5001,000 in Fig. 2-3. However, as Tr is further increased and airway caliber reduced, R_i becomes an increasingly important contribution to pathway impedance and VT begins to drop. As VT is reduced, the tidal tethering forces on the airways decreased, further constricting them, increasing R and reducing VT . Eventually, ventilation delivered to each of the branches in the network catastrophically collapses. This effect is manifested differently during VCV. In VCV, total VT is kept constant, and, as Tr is increased above a critical level, the reduction of flow to a slightly overconstricted branch results in an increase in pressure gradient and a redistribution of flow toward slightly less constricted branches. This shift in regional expansion affected both parent and daughter branches, resulting in the patchiness of ventilation shown in Fig. 2-2 as previously described [101].

In simulations with $Tr_0 > 0.8$, the system under VCV started in a highly heterogeneous state with a patchy distribution of ventilation. Under this condition, the transition to PCV was not stable and was highly dependent on the value of P_I selected for PCV (Figs. 2-4 and 2-5). Indeed, the total VT and the distribution of ventilation changed in the subsequent breaths following the transition, even though PCV was set to provide a first-breath VT equal to that during VCV and P_I was kept constant. This behavior is not entirely surprising since, in contrast to the case of $Tr_0 \leq 0.8$, the distribution of ventilation before the transition was not uniform and thus expected to change due to the difference in the driving signal [95]. PCV maintains airway opening pressure at a high constant level during inspiration, whereas in VCV airway pressure is initially low and increases progressively with lung volume inhalation. Therefore, the driving signal in PCV should promote more flow to regions with prolonged time constant (high $R_i C_i$) than that in VCV. Moreover, in contrast with VCV, in PCV

as some airways constricted, flow is not redirected to less constricted airways, potentially reducing ventilation heterogeneity relative to that during VCV (Fig. 2-5). However, the reasoning based exclusively on linear networks [27, 56, 70] failed to explain the magnitude of the response of our model. In fact, when airways were kept frozen in the model during the transition from VCV to PCV, the resulting reduction in ventilation heterogeneity was substantially less than that observed when airway dimensions were dynamically determined by the properties of active ASM (Figs. 2-9 and 2-8).

The simulation data also showed that the sensitivity of VT to P_I during PCV was almost 40 times greater in the model with the dynamic properties of ASM than in the model with no dynamic properties of ASM. As a result, differences in P_I of $\pm 10\%$ during PCV could lead to dramatic differences in both VT and the distribution of ventilation from severe hypoventilation to hyperventilation. Worth noticing was the fact that a change of only 1% in P_I (from $1.03 P_{I,0}$ to $1.04 P_{I,0}$) resulted not only in an elevation of 30% in VT but also in the virtual elimination of patchiness in ventilation (Fig. 2-5).

This model behavior could explain clinical observations by Lopez-Herce and colleagues [54, 79] of rapid and significant improvements in arterial PCO₂ and oxygenation during PCV. They found in two children with severe asthma, whose level of gas exchange had not improved during 6 h of VCV, that a change to PCV resulted in fast improvements in blood gases [54]. The results from our simulations might explain those improvements as resulting from an improvement in ventilation distribution. Motivated by that case report work, Sarnaik et al. studied 40 patients with severe asthma who were intubated and mechanically ventilated with PCV. They also found significant improvements in blood gases after an initiation of mechanical ventilation [79]. In both papers, the authors speculated that improvements in blood gases with PCV were due to the improvement in ventilation distribution expected from the enhanced pressure equilibration between alveolar units with heterogeneous time constants. As we discussed above, in a severely constricted network, pressure equilibration alone resulted in changes in ventilation heterogeneity much smaller than those seen when we incorporated the dynamic properties of active ASM in the network model. Switching from

VCV to PCV with airway dimensions unaffected by dynamic forces only minimally reduced the heterogeneity in ventilation. Therefore, we believe that clinical improvements seen in PCV may have resulted from the dilating effects of tidal breathing on the ASM, rather than from just pressure equilibration.

Increasing level of bronchoconstriction Inspiratory flow is generated by the difference between airway opening and pleural pressure, referred to as transpulmonary pressure. During mechanical ventilation with PCV, this is accomplished by specifying the ventilators driving pressure, P_I . Our model predicts that, in a severe asthma attack, if P_I is insufficient for maintaining VT , catastrophic airway closure may follow (Fig. 2-3). In a spontaneously breathing person, the increase in transpulmonary pressure is generated by a reduction in pleural pressure. Therefore, during severe airway constriction, a compensatory reduction in inspiratory pleural pressure by respiratory muscles is required to maintain ventilation. In our model, this is equivalent to the compensatory increase in driving pressure inherent to VCV, which leads to a redistribution of VT to regions of the lung with relatively less constriction. This redistribution can be thought of as a long-range negative feedback that causes airway dilatation of relatively well-ventilated airways. This long-range negative feedback combined with the short-range positive feedback results in a patchiness of ventilation distribution similar to that observed in several complex systems in nature [77]. It should be noted that, despite the patchiness if the respiratory muscles generate enough pressure, VT can be maintained and total closure of all airways can be prevented. However, during increased airway obstruction if respiratory muscles become fatigued and are unable to maintain ventilation, airflow will not be redistributed to ventilating regions. This will eliminate the long-range negative feedback and thus the compensatory airway dilation, eventually leading to catastrophic closure of all airways.

Ventilation heterogeneity and ASM dynamic behavior From our results, we conclude that the dynamic behavior of active ASM may play an important role in reducing heterogeneity of ventilation and magnifying the VT sensitivity to P_I during PCV. The sig-

nificant reduction in ventilation heterogeneity when active ASM behavior was included in our model reaffirmed our hypothesis that positive feedback might contribute to nonlinearity in airway response under PCV. The data also suggest that the sensitivity to P_I in PCV could be advantageously exploited to improve ventilation and its uniformity by judicious adjustments in the ventilator pressure settings.

Model assumptions The network model is structurally symmetric Tr could vary breath by breath but was set to be uniform throughout the airway tree. Symmetry breaking was achieved by adding a small random variation in wall thickness (1% coefficient of variation) to all airways. The purpose of this approach was to evaluate the effects caused purely by the dynamic behavior of the ASM independent of other preexisting heterogeneity. Variations of smooth muscle activation within the airway tree, regional differences in pleural pressure within the thorax, and the asymmetry of the airway tree were not included in our network model. We expect that these features, if incorporated into the model, would precipitate symmetry breaking and the formation of ventilation defects at lower values of Tr . Furthermore, they would promote the systematic localization of ventilation defects and magnify the patchiness in ventilation during VCV. As a result, to reduce ventilation heterogeneity during PCV, the setting of P_I may have to be increased relative to that predicted by this model. Also, the presence of structural or functional parameter heterogeneity could be expected to reduce the overall VT sensitivity of the system, which in the limit would behave as one with fixed obstructions and minimal dynamic effects of ASM.

Additional reasons that VT sensitivity to P_I in a real lung could be different from that predicted by this symmetric network model are discussed here. Although the model incorporates structural and functional features that are consistent with a human lung, it can be expected to exhibit general behaviors of a complex branching network in conditions within the physiological range. However, the effects of some assumptions on the models complex behavior are difficult to predict. For example, the model assumes linear chest wall and parenchyma compliances and ignores the passive characteristics of the airway wall. Non-linear mechanical properties of these elements could affect the magnitude of the predicted

sensitivity in different ways. On the one hand, it is well known that the passive properties of the respiratory system become stiffer at low and high lung volumes. This could result in an even greater sensitivity of VT to the P_I setting than those predicted for a constant compliant chest wall under physiological conditions. Likewise, nonlinear changes in parenchymal tethering forces with lung volume could result in higher than predicted VT sensitivity. Also, the potential formation of liquid bridging [29], not included in this model, could result in rapid airway closure without luminal cross-sectional area being reduced to zero. This phenomenon, ignored in our model, could further increase the VT sensitivity to changes in P_I by precipitating airway closure as P_I is reduced.

On the other hand, the passive nonlinear characteristics of the airway wall could tend to reduce the magnitude of the VT sensitivity by acting to stabilize drastic changes in airway lumen. This effect would be more likely prominent in central airways, which are protected by cartilaginous rings or plates, and less important in peripheral airways, which are simulated in this model (generations 4 to 16 of the human airway tree). Given the opposing effects of the different assumptions on the model, it is difficult to speculate whether the VT sensitivity to P_I , during PCV predicted for our bronchoconstricted model, could be an over- or an underestimation of the sensitivity in a real lung. Thus these predictions have to await experimental validations.

2.6 Summary

Our simulations with an integrative network model of the lung provide new insights into complex interactions among airways and explore the impact of ventilation mode, or breathing pattern, on the stability of ventilation and its spatial distribution within the asthmatic lung. In contrast to VCV, which ensures the total ventilation but results in a patchy distribution of regional ventilation during bronchoconstriction, PCV results in a more uniform distribution, but the total ventilation could be highly sensitive to minor changes in driving pressure. Although the simplifications inherent to a theoretical model limit its direct clinical application, the insights derived from these simulations may provide a theoretical foundation

to guide the selection of ventilation mode, the adjustment of ventilator settings for patients with asthma, and the interpretation of clinical observations.

THIS PAGE INTENTIONALLY LEFT BLANK

Chapter 3

Central Airways

Characteristics of central airways under normal and challenged conditions have been explored in the field of asthma research. Imaging techniques such as Computed Tomography or bronchoscopy have been widely used to assess the sizes of central airways and its change after an induced asthma attack. The following two studies explore the effect of heterogeneity along an airway on the estimated resistance, and distensibility of the central airways.

3.1 Function Effect of Longitudinal Heterogeneity in Constricted Airways Before and After Lung Expansion

3.1.1 Introduction

Heterogeneity in narrowing among airways is an essential feature of asthma and has been the object of many experimental and modeling studies [8, 9, 13, 27, 26, 32, 48, 56, 93, 94, 98, 100, 101, 109]. In most experimental studies, the luminal area was assessed at a single site of the airway [8, 9, 13, 48]. However, given the lack of knowledge on the degree of heterogeneity in the cross sectional area along airways and the extent to which airways narrow heterogeneously along their length, the precision of these measurements is unknown.

This longitudinal heterogeneity in the cross sectional area when ignored could affect the estimation of airway function, i.e. airway resistance (R_{aw}). This is due to the nonlinear relationship between the pressure drop and luminal area. For example, R_{aw} of an airway with a uniform cross sectional area along its length is always less than that of an airway of equivalent average area but with longitudinal heterogeneity in the cross sectional area. In addition, the shape of the cross sectional area may also be important in the estimation of R_{aw} . For example, R_{aw} of a tube with a circular cross section is lower than that of a conduit with the same cross sectional area but elliptical shape. Thus, disregarding these two factors, the non-circularity of the shape of the cross section, and the longitudinal heterogeneity in the cross sectional area, should result in an underestimation in the calculation of R_{aw} . It is also possible that the effect of these two factors on airway resistance calculation may be different between asthmatic (AS) airways and non-asthmatic (NA) ones. If the longitudinal heterogeneity in the cross sectional area under bronchoconstriction is greater in AS compared to NA airways, we expect that it would accentuate the differences in R_{aw} between AS and NA airways.

In this study, we evaluated the underestimation of R_{aw} resulting from ignoring the longitudinal heterogeneity in the cross sectional area and non-circularity of the shape at baseline, during bronchoconstriction and after an increase in lung volume to TLC. Airway dimensions were obtained from the analysis of High-Resolution Computed Tomography (HRCT) images using previously validated 3-D reconstruction algorithms [33, 53, 76, 96].

3.1.2 Methods

Subjects Images obtained from 8 mild-to-moderate asthmatic and 9 non-asthmatic adult volunteers were analyzed. Subject demographics and pulmonary function tests during screening visit, performed while subjects were in an upright position, are shown in Table 3.1. Subjects with mild-to-moderate asthma were selected according to the NIH Global Initiative for Asthma with forced exhaled volume within 1 sec (FEV1), or forced vital capacity (FVC), $\geq 80\%$ predicted, less than daily symptoms, and peak flow or FEV1 variability of $\leq 30\%$. Ex-

clusion criteria were the use of tobacco (current smokers, and those with > 10 pack-years), or oral steroids, symptoms of upper and lower respiratory tract infection, or emergency visits or hospitalizations for asthma in the past month, history of cardiopulmonary disease other than asthma. No systemic or inhaled corticosteroids had been used within 1 wk prior to enrollment. The study protocol was approved by the Massachusetts General Hospital-Institutional Review Board. All subjects gave their written informed consent.

Prior to the study date, all subjects underwent a Methacholine (MCh) challenge to determine their PC20: the concentration of inhaled MCh aerosol that caused a 20% reduction in FEV1. PC20 was determined based on the method published by Crapo [18]. The maximum dose given to asthmatics was 8 mg/ml and all non-asthmatic subjects were given 25 mg/ml. Spirometry during the initial screening of subjects was performed while subjects were in an upright position.

Group	Asthmatic subjects	Non-asthmatic subjects
Age, years	30.9 ± 10.9	31.7 ± 10.3
Gender (F/M)	(2/6)	(5/4)
Height, cm	174.5 ± 7.4*	165.7 ± 6.4
Weight, kg	77.8 ± 13.3	64.9 ± 7.8
FEV1, L(%Predicted)	3.5 ± .47 (86.7±12.2)	3.26 ± .74 (91.1 ± 10.5)
FVC, L (%Predicted)	4.39 ± .56 (93.5 ± 11.2)	3.79 ± .86 (89.8 ± 10.3)
PC20, mg/ml	1.7 ± 1.3***	> 25

Table 3.1: Demographics of asthmatic and non-asthmatic subjects and PFT collected from screening in an upright position (mean ± standard deviation). * Unpaired t-test comparison between asthmatic and non-asthmatic groups; * P<0.05, *** P<0.0001.

Study Protocol HRCT images were obtained with a Siemens Biograph 64 PET-CT tomograph with the subject in the supine position. In this report, we analyzed HRCT images obtained with the scanner in a helical mode with 64 slices per rotation, 0.6 mm collimation, a pitch of 1, 120 kV peak, and 80 mA. The image reconstruction was done using the B31 kernel with a 0.75 mm slice thickness, 0.5 mm slice increment and 0.25mm overlap. Images were

acquired during a short breath hold (20 secs) at a lung volume equal to the mean lung volume (MLV) averaged over a 30-second stable breathing period prior to each scan. To guide the breath-hold maneuver, impedance plethysmography (SomnoStarPT, SensorMedics Corp, Yorba Linda, CA) was used and a signal of instantaneous lung volume during breathing and a reference line corresponding the MLV were presented to the subject via a head mount display. The first and second scans were acquired at baseline and after MCh challenge during a breath hold at MLV. A third scan was then acquired during at total lung capacity (TLC). We referred to the first, second and third scan as BM (Baseline-MLV), MM (MCh-MLV) and MT (MCh-TLC) scan, respectively.

Data Analysis Pulmonary Workstation 2.0 (PW2) software (VIDA Diagnostics, Iowa City, IA) was used to analyze all HRCT scans, obtain 3D rendered airway trees, and derive airway dimensions. From each scan, we analyzed 35 defined central airways (0-6th generation) with diameter > 2 mm (Fig. 3-1A). Airways with cross sections that were not perpendicular to its centerline due to the segmentation error in PW2 were excluded in our analysis by inspection (on average around 1-2 airways per subject). We used measurements from the middle half of the airways in order to minimize potential systematic errors that could have been caused if measurements near bifurcations were used. For each airway, the following parameters were imported into MATLAB (Mathworks, Natick, MA): 1) the major and minor radii (a_i and b_i) for 5 airway lumen cross sections (i) equally spaced over the middle half of each airway (Fig. 3-1B), 2) the average luminal area (A_{avg}), assumed as the average of the 5 elliptical sections of radii a_i and b_i , and 3) the airway length (L). Estimation of Airway Resistance to Flow. Using HRCT images, for each airway we computed the resistance of three airway models (Fig. 3-2) assuming laminar flow as follows,

1. R_{avg} : the resistance of a cylindrical airway with the average radius (r_{avg}) and length (L) was computed as,

$$R_{avg} = \frac{8\mu L}{\pi r_{avg}^4} \quad (3.1)$$

where μ is the viscosity of air and,

$$r_{avg} = \sqrt{\frac{A_{avg}}{\pi}} = \sqrt{\frac{1}{5} \sum_{i=1}^5 a_i b_i} \quad (3.2)$$

2. R_T : the total resistance of an airway made of 5 segments ($i = 1, 2, , 5$) each of which had the length $l_i = L/5$ and elliptical cross section with major and minor radii of a_i and b_i . Note that a_i and b_i varied along the airway length. R_T was computed as the sum of resistances of each elliptical segment as follows,

$$R_T = \sum_{i=1}^5 \frac{4\mu l_i [(a_i/b_i)^2 + 1]}{\pi a_i^3 b_i} \quad (3.3)$$

3. R_A : the resistance of an airway made of 5 segments ($i = 1, 2, , 5$) each of which had the length $l_i = L/5$ and circular cross section with radius of r_i that could vary along the length. To ensure that the circular cross sectional area was equal to that of the elliptical one, r_i was set to,

$$r_i = \sqrt{a_i b_i} \quad (3.4)$$

R_A was computed as,

$$R_A = \sum_{i=1}^5 \frac{8\mu l_i}{\pi r_i^4} \quad (3.5)$$

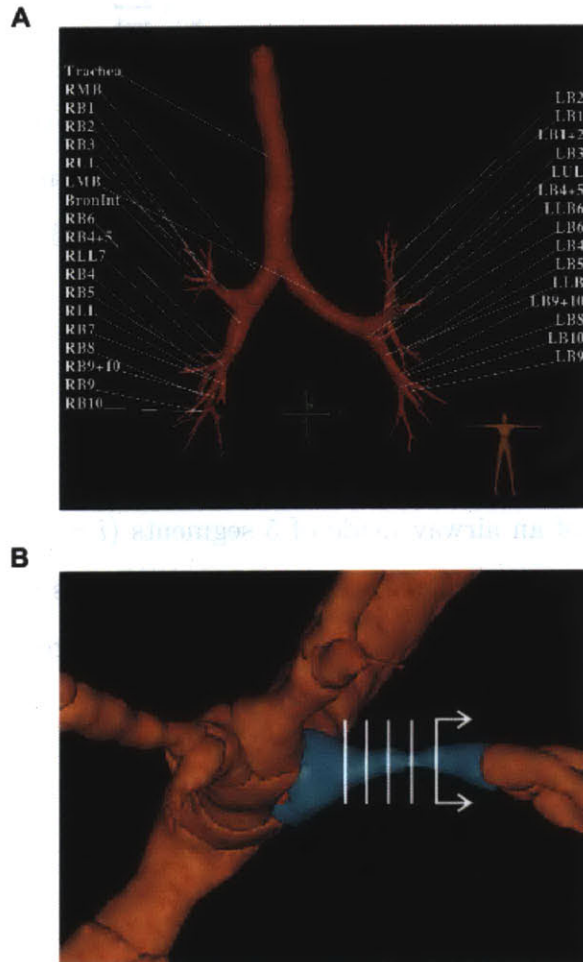


Figure 3-1: 3D rendered airway tree of an asthmatic subject after MCh challenge imaged at mean lung volume (MLV). A: Labels of all 35 defined central airways (0 – 6th generation) that were included in our analysis. B: A close-up of an airway (colored in blue) illustrating the presence of large longitudinal heterogeneity in the cross sectional area. To calculate the resistance of three airway models (See text and Fig. 3-2), dimensions of the five luminal cross sections (marked in white) equally spaced over the middle half of each airway were used. See text for an explanation.

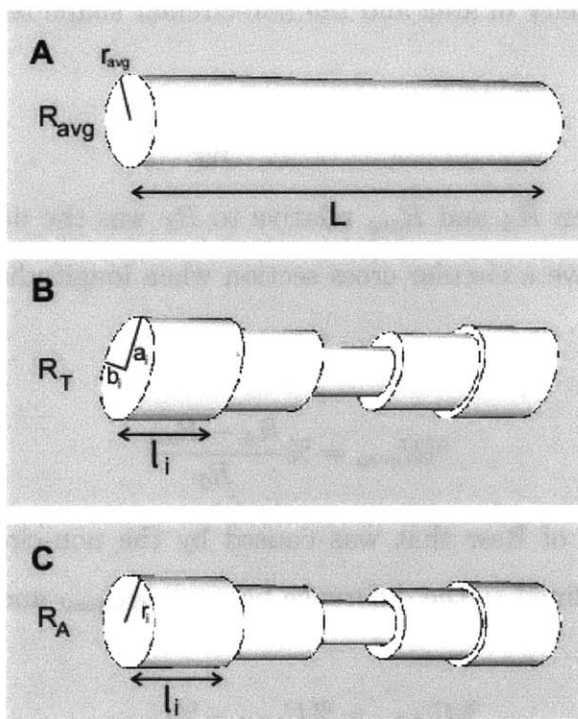


Figure 3-2: Three models of the airway used for calculating three airway resistances (R_{avg} , R_T and R_A). A: Model of a cylindrical airway with a constant radius of r_{avg} and total length of L used for computing R_{avg} . B: Model of an airway with both longitudinal variability in the cross sectional area and non-circularity of the cross sectional shape used for computing R_T . The cross section was assumed elliptical with a major and minor radius of a_i and b_i , and the segmental length of l_i . C: Model of an airway with circular cross sections with the radius r_i and the longitudinal variability in the cross sectional area used for computing R_A .

Quantifying the Functional Effect of Longitudinal Heterogeneity The underestimation of R_{aw} could result from the longitudinal heterogeneity in the area and the non-circularity of the shape of its cross section. The relative difference between R_T and R_{avg} was an estimated error when the airway was assumed cylindrical with an average airway luminal area. This relative difference was defined as the total underestimation of R_{aw} due to longitudinal heterogeneity in area and the non-circular shape termed $\%U_{total}$.

$$\%U_{total} = \% \frac{R_T - R_{avg}}{R_T} \quad (3.6)$$

The difference between R_A and R_{avg} relative to R_T was the underestimation of R_{aw} of an airway assumed to have a circular cross section when longitudinal heterogeneity in area was ignored ($\%U_{area}$).

$$\%U_{area} = \% \frac{R_A - R_{avg}}{R_T} \quad (3.7)$$

The underestimation of R_{aw} that was caused by the non-circular shape of the cross section ($\%U_{shape}$) was defined as the difference between $\%U_{total}$ and $\%U_{area}$.

$$\%U_{shape} = \%U_{total} - \%U_{area} \quad (3.8)$$

Factors Affecting the Underestimation of Airway Resistance We evaluated the contribution of two physical factors to the underestimations of R_{aw} : 1) The longitudinal heterogeneity in the cross sectional area quantified by the square of the coefficient of variation in cross sectional area ($CV^2(A)$), and 2) The non-circularity of the cross section, quantified by the average eccentricity (ϵ) of 5 elliptical cross sections.

$$\epsilon = \frac{1}{5} \sum_{i=1}^5 \sqrt{1 - \left(\frac{b_i}{a_i}\right)^2} \quad (3.9)$$

Because of the quadratic dependence of R_{aw} on the inverse of the cross sectional area, if R_{aw} is estimated assuming a constant average area, it should underestimate the true R_{aw} in

proportion to $CV^2(A)$. Because that the distributions of $\%U_{area}$ on $CV^2(A)$ did not follow normal distributions, we evaluated the dependence between the log-transformed variables as the goodness of fit coefficient (R^2) of the a linear regression model:

$$\log(\%U_{area}) = k_0 + k_1 \cdot \log(CV^2(A)) \quad (3.10)$$

The shear stress resisting fluid flow through a highly non-circular cross section (ϵ close to 1) is larger than that through a circular cross section of the same cross sectional area ($\epsilon=0$) and thus, the resistance to flow through a tube with non-circular cross section must be higher than that through a tube with circular cross section. Since followed the normal distribution while $\%U_{shape}$ did not, we evaluated the dependence of $\log(\%U_{shape})$ on ϵ in terms of the goodness of fit coefficient of the simple linear regression model to the data:

$$\log(\%U_{shape}) = k_2 + k_3 \cdot \epsilon \quad (3.11)$$

Statistical Analysis $\%U_{total}$, $\%U_{area}$, and $\%U_{shape}$ from 3 scans for each subject were reported as the median \pm standard deviation (range: minimum maximum). All statistical analyses were performed using the statistical software package SAS 9.2 (SAS Institute, Cary, NC). Since distributions of $\%U_{total}$, $\%U_{area}$, and $\%U_{shape}$ were not normal and better resembled lognormal distributions, we analyzed effects of the group and imaging condition on the log-transformed $\%U_{total}$, $\%U_{area}$, and $\%U_{shape}$ using a two-way analysis of variance (ANOVA) with an interaction term and repeated measurements. Pairwise comparisons between BM, MM and MT were made within each group based on the two-way ANOVA model for $\log(\%U_{total})$, $\log(\%U_{area})$, and $\log(\%U_{shape})$. The two-way ANOVA model yielded an estimate of the mean of the $\log(\%\tilde{U}_{total})$, $\log(\%\tilde{U}_{area})$, and $\log(\%\tilde{U}_{shape})$ distributions for each scan per group, which were then used to compute Δ_r , the relative change in the log-transformed data, between any two scans. To quantify the change in caused by MCh challenge, and by the lung volume increase to TLC, Δ_r was defined as $\log(\%\tilde{U}_{MM}/\%\tilde{U}_{BM})$, and as $\log(\%\tilde{U}_{MT}/\%\tilde{U}_{MM})$, respectively. Moreover, we investigated whether the effect of

lung volume on $CV^2(A)$ could be different for airways of different sizes. For each subject, airways were sorted by their average inner cross sectional area at baseline (ABM) and divided into 4 quartiles. Using SAS, the log of the ratio of $CV^2(A)$ before and after TLC in each quartile was compared with 0 to determine if the change in $CV^2(A)$ caused by the increase in lung volume to TLC was statistically significant. For all statistical analyses, $P < 0.05$ was considered significant.

3.1.3 Results

The Total Underestimation of Resistance ($\%U_{total}$) was highly variable among airways and could be substantial in some (Table 3.2). The median of $\%U_{total}$ was relatively small ($< 6\%$) (Table 3.2) and not significantly different between the asthmatic (AS) and non-asthmatic (NA) group in any of the three conditions imaged (Table 3.4). However, there was a significant effect of imaging condition on $\%U_{total}$ ($P < 0.01$) (Table 3.4). This can be illustrated by a left shift of the cumulative distribution function (CDF) of $\%U_{total}$ caused by the increase in lung volume to TLC (Fig. 3-3A). The left shift observed was more noticeable in the NA than in AS group (Fig. 3-3A). As a result of the increase in lung volume to TLC, $\%U_{total}$ significantly decreased in both the NA group ($P < 0.0001$) and the AS group ($P < 0.01$) (Table 3.3 and Fig. 3-3A). However, the change in $\%U_{total}$ caused by MCh challenge was not significant in either group (Table 3.3).

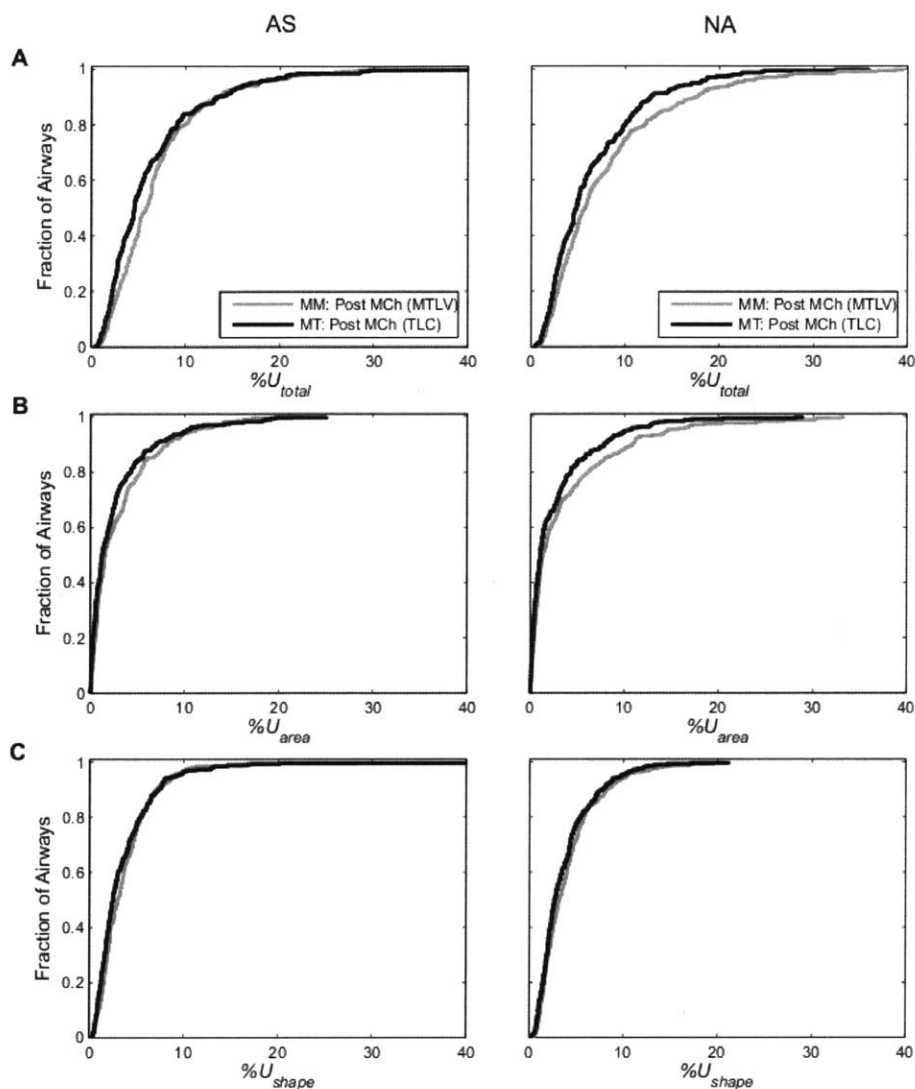


Figure 3-3: Cumulative distribution functions (CDF) of underestimations of airway resistance grouped for all airways of all asthmatic subjects (AS, left) and of non-asthmatic subjects (NA, right) after MCh challenge at mean lung volume (grey) and TLC (black). A: CDF of the total underestimation of airway resistance due to ignoring all longitudinal heterogeneity ($\%U_{total}$). B: CDF of the contribution to $\%U_{total}$ caused by longitudinal heterogeneity in the airway cross sectional area ($\%U_{area}$). C: CDF of the contribution to $\%U_{total}$ caused by a non-circular shape ($\%U_{shape}$). See text for explanation.

	Asthmatic	Non-asthmatic
$\%U_{total}$		
BM	5.61 \pm 5.50 (0.58 - 32.37)	5.48 \pm 5.79 (0.77 - 33.06)
MM	5.81 \pm 5.15 (0.67 - 29.54)	5.73 \pm 6.84 (0.53 - 39.45)
MT	4.55 \pm 5.90 (0.45 - 52.99)	4.87 \pm 5.34 (0.44 - 35.88)
$\%U_{area}$		
BM	1.53 \pm 4.39 (0.02 - 28.38)	1.33 \pm 4.43 (0.02 - 26.36)
MM	1.55 \pm 3.78 (0 - 22.36)	1.37 \pm 5.67 (0 - 33.22)
MT	1.23 \pm 3.76 (0.01 - 24.97)	1.09 \pm 4.02 (0.02 - 28.86)
$\%U_{shape}$		
BM	3.17 \pm 3.00 (0.31 - 21.91)	3.29 \pm 3.20 (0.50 - 21.15)
MM	3.01 \pm 3.08 (0.36 - 28.22)	3.20 \pm 3.27 (0.49 - 20.79)
MT	2.48 \pm 4.15 (0.31 - 51.09)	2.66 \pm 2.99 (0.22 - 21.18)

Table 3.2: The statistical properties of $\%U_{total}$, $\%U_{area}$, and $\%U_{shape}$ in asthmatic and non-asthmatic subjects computed from 3 scans: baseline at MTLV, post MCh at MTLV and post MCh at TLC. *Values shown are medians \pm standard deviations with range in parentheses. Definition of abbreviations: $\%U_{total}$ = total underestimation of airway resistance due to ignoring the longitudinal heterogeneity; $\%U_{area}$ = the contribution to $\%U_{total}$ caused by longitudinal heterogeneity in the airway cross sectional area; $\%U_{shape}$ = the contribution to $\%U_{total}$ caused by a non-circular shape; BM = Baseline scan at mean lung volume (MLV); MM = post MCh scan at MLV; MT = post MCh scan at total lung capacity (TLC).

	Asthmatic		Non-asthmatic	
	P-value	Δ_r	P-value	Δ_r
$\log(\%U_{total})$				
BM \rightarrow MM	0.6085	1.014	0.2519	1.021
MM \rightarrow MT	0.0067	0.898	<0.0001	0.884
$\log(\%U_{area})$				
BM \rightarrow MM	0.0075	1.885	0.0059	1.497
MM \rightarrow MT	<0.0001	0.297	<0.0001	0.151
$\log(\%U_{shape})$				
BM \rightarrow MM	0.4510	0.967	0.2825	0.971
MM \rightarrow MT	0.0858	0.888	0.0048	0.890

Table 3.3: P-values and mean estimates of pairwise comparisons of the log-transformed $\%U_{total}$, $\%U_{area}$, and $\%U_{shape}$ within asthmatic and non-asthmatic subjects.

	$\log(\%U_{total})$	$\log(\%U_{area})$	$\log(\%U_{shape})$
Effect of group	0.3128	0.7063	0.1226
Effect of imaging condition	0.0052	0.0024	0.0478

Table 3.4: P-values of the two-way analysis of variance (ANOVA) with repeated measurements of $\log(\%U_{total})$, $\log(\%U_{areal})$, and $\log(\%U_{shapel})$.

Contributions of $\%U_{area}$ and $\%U_{shape}$ to $\%U_{total}$ On average, $\%U_{area}$ contributed to 36% of $\%U_{total}$ with the rest contributed by $\%U_{shape}$. Neither $\%U_{area}$ nor $\%U_{shape}$ was, on average, different between the AS and NA group at any of the three conditions studied (Table 3.4). Additionally, the two-way ANOVA showed significant effects of the imaging condition on $\%U_{area}$ and $\%U_{shape}$ in both AS and NA groups (Table 3.4). The increase in lung volume to TLC resulted in a systematic left shift in the CDF of $\%U_{area}$ in both AS and NA (Fig. 3-3B). However, there were only minimal changes caused by the increase in lung volume to TLC in the CDF of $\%U_{shape}$ from the AS group (Fig. 3-3C). The reduction in the mean of the log-transformed $\%U_{shape}$ after the lung volume increase to TLC was significant only in the NA group ($P < 0.005$ with $\Delta_r = 0.89$) from the two-way ANOVA model (Table 4 and Fig. 3-4C). No significant effect of MCh on $\%U_{shape}$ in any group was observed.

A significant reduction in mean $\log(\%U_{area})$ was observed with the increase in lung volume to TLC in both groups ($P < 0.0001$) ($\Delta_r = 0.2965$ for AS and 0.1511 for NA) (Table 4 and Fig. 3-4B). A significant increase in the mean $\log(\%U_{area})$ was observed in both AS ($P < 0.01$ with $\Delta_r = 1.8845$) and NA group ($P < 0.01$ with $\Delta_r = 1.4966$) (Table 3.3) and Fig. 3-4B).

Longitudinal Heterogeneity in the Cross Sectional Area and the Non-Circular Shape Figure 3-5A and 3-5B shows the probability distribution of $CV^2(A)$ and that of eccentricity (ϵ) of all airways in all subjects under 3 conditions. The first four moments (mean, variance, skewness, and kurtosis) of these distributions are presented in Table 3.5.

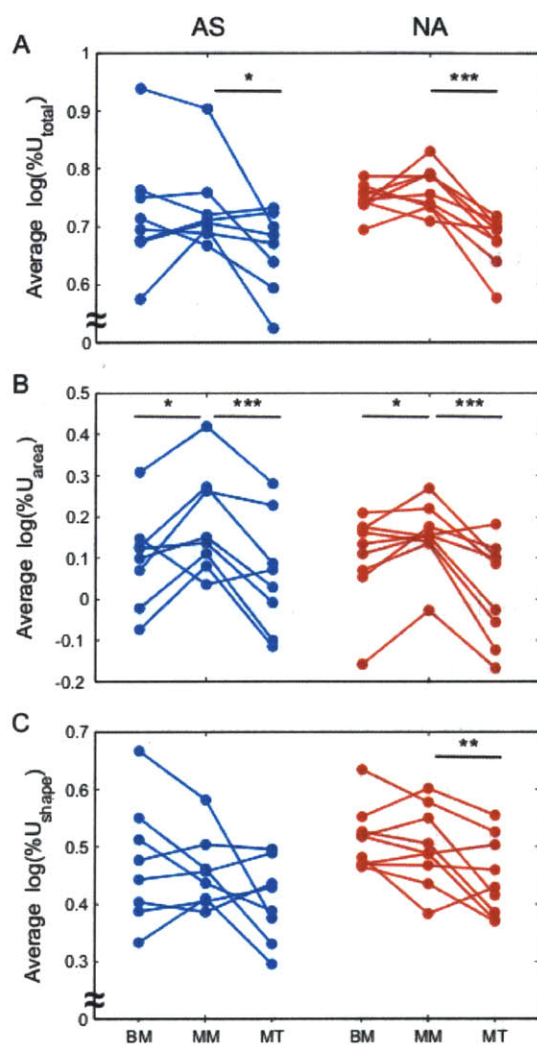


Figure 3-4: Changes in average underestimations of airway resistance caused by MCh challenge and an increase of lung volume to TLC. Each point represents the average of all airways for each asthmatic (AS, left) and non-asthmatic (NA, right) subject. A: Average underestimation of resistance caused by ignoring longitudinal heterogeneity in the airway cross sectional area and the non-circularity of the cross sectional shape ($\%U_{total}$). B: Average contribution to $\%U_{total}$ caused by longitudinal heterogeneity in the cross sectional area ($\%U_{area}$). C: Average contribution to $\%U_{total}$ caused by a non-circular shape ($\%U_{shape}$). BM denotes the image taken at baseline during breath-hold at mean lung volume (MLV). MM denotes the image taken post MCh challenge at MLV. MT denotes the image taken post MCh challenge at total lung capacity (TLC). Pairwise comparison based on the two-way ANOVA model with repeated measurements: * $P < 0.05$, ** $P < 0.005$, and *** $P < 0.0001$.

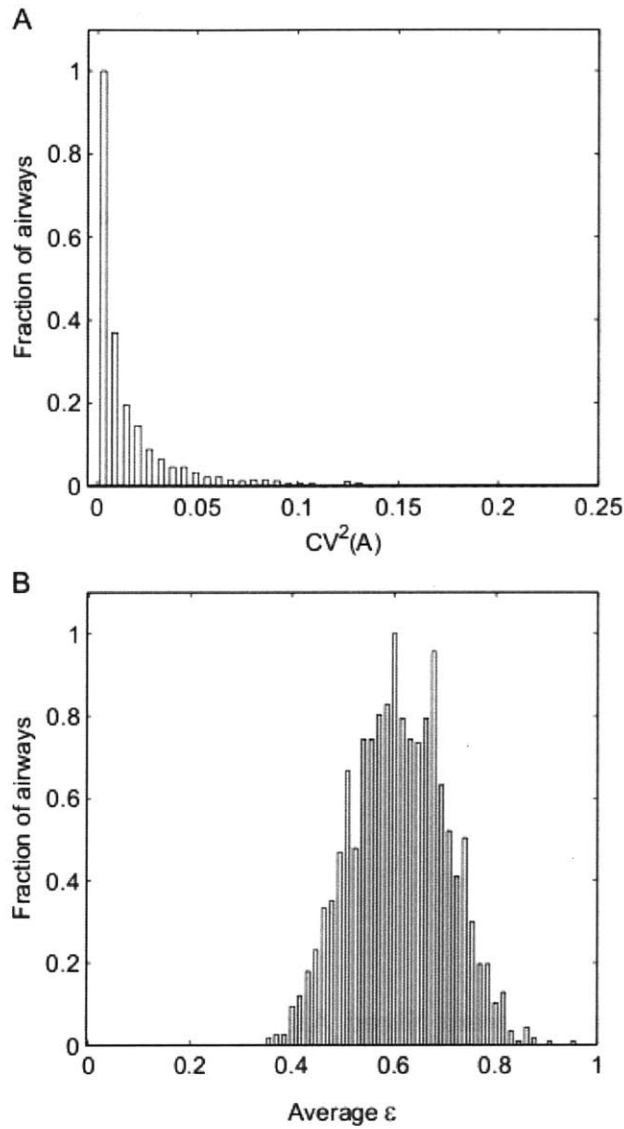


Figure 3-5: The distribution of the longitudinal heterogeneity in the cross sectional area quantified by $CV^2(A)$ and the non-circularity of the shape of the airway cross section (ϵ). A: The distribution of $CV^2(A)$ in all airways of all subjects under 3 conditions. Skewness of this distribution was measured using statistical software, SAS, to be 3.24 with the median of 0.009. B: The distribution of eccentricity of the assumed-elliptical cross section (ϵ). The average ϵ was 0.611.

	Mean	Variance	Skewness	Kurtosis
$CV^2(A)$	0.016	0.001	3.235	14.264
ϵ	0.611	0.009	0.054	-0.312

Table 3.5: The statistical measures of $CV^2(A)$ and ϵ . Definition of abbreviations: $CV^2(A)$ = Longitudinal heterogeneity of the airway cross sectional area; ϵ = eccentricity of the assumed-elliptical cross section.

Correlations between Longitudinal Variability in Cross Sectional Area and Shape

$\log(\%U_{area})$ was linearly related to $\log(CV^2(A))$ yielding $k_0 = 2.29$, and $k_1 = 0.97$ in Eq. 10 ($R^2=0.997$) (Fig. 3-6). Similarly, $\log(\%U_{shape})$ was linearly related to ϵ yielding $k_2 = -1.67$, and $k_3 = 3.50$ for Eq. 3.11 ($R^2=0.966$) (Fig. 3-7).

Changes in $CV^2(A)$ for Different Sized Airways When the lung volume was increased to TLC, the average $CV^2(A)$ was significantly reduced in all but the largest airways quartile (airways with average ABM > 29 mm²) ($P<0.05$) (Fig. 3-8). However, the reduction in $\%U_{area}$ or in $CV^2(A)$ after the lung volume increase to TLC was not correlated with airway size or with the change in airway size (data not shown).

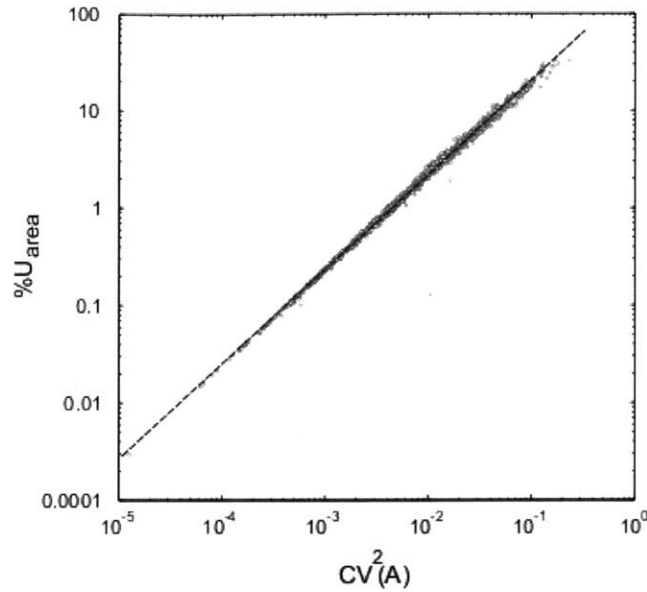


Figure 3-6: Correlation between the contribution to $\%U_{total}$ caused by longitudinal heterogeneity in the airway cross sectional area ($\%U_{area}$) and $CV^2(A)$ (the square of the coefficient of variation in the cross sectional area along that airway). Data are taken from all airways in all subjects in all three imaging conditions. A least-square linear regression of the log-transformed data shows high correlation between $\log(\%U_{area})$ and $\log(CV^2(A))$ had a goodness of fit $R^2 = 0.997$.

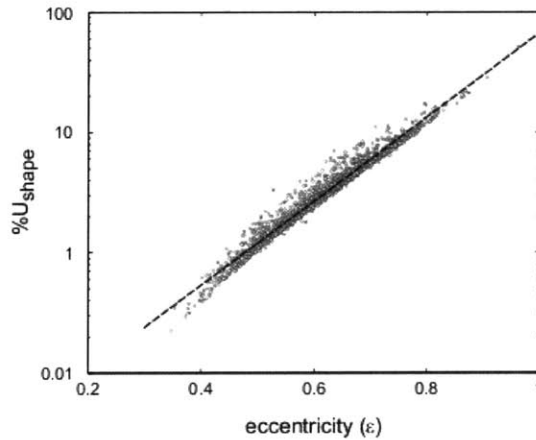


Figure 3-7: Correlation between the contribution to $\%U_{total}$ caused by the non-circular shape ($\%U_{shape}$) and ϵ (the eccentricity of the assumed-elliptical cross section). Data are taken from all airways in all subjects in all three imaging conditions. A least-square linear regression of $\log(\%U_{shape})$ and ϵ had a goodness of fit $R^2 = 0.966$.

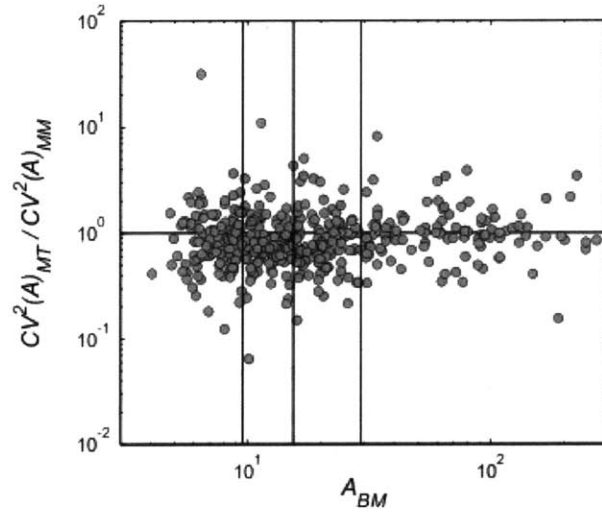


Figure 3-8: Changes in longitudinal heterogeneity in the cross sectional area caused by the lung volume increase to TLC in airways of various sizes. The average luminal area of an airway at baseline (A_{BM}) was plotted against the ratio in longitudinal heterogeneity in the cross sectional area ($CV^2(A)$) at TLC over that at mean lung volume (MLV) of the same airway. The plot includes all airways of all subjects. A_{BM} was imaged at MLV. The subscript MM denotes the image taken after MCh challenge at MLV; MT after MCh challenge at TLC. Airways with reduction in $CV^2(A)$ after the increase in lung volume to TLC would be below the unity line. Airways were binned into 4 quartiles with an equal number of airways (indicated by vertical lines). Note that in airways with the largest A_{BM} the increase in lung volume to TLC did not significantly change the longitudinal heterogeneity.

3.1.4 Discussion

This study demonstrated that neglecting the longitudinal variability in the luminal area and the non-circularity of the cross sectional shape results in an underestimation of Raw. The effect was highly variable with $\%U_{total}$ being as high as 53% (AS) and 36% (NA) after MCh challenge at TLC. However, the median values were less than 5% and similar in AS and NA subjects. On average, the longitudinal heterogeneity in the cross sectional area contributed to 1/3 of $\%U_{total}$, while the non-circular shape contributed to 2/3 of $\%U_{total}$. In both AS and NA subjects, the mean values of $\%U_{total}$ and $\%U_{area}$ increased after MCh challenge and reduced by elevating lung volume to TLC. After lung volume was increased to TLC, $\%U_{shape}$ significantly decreased in non-asthmatic subjects, but not in asthmatic subjects.

It is worth noting that, in contradiction to our initial expectation, longitudinal heterogeneity in these central airways was not higher in AS compared to NA. Indeed, we found no difference between AS and NA in the longitudinal heterogeneity in the area and/or the non-circularity of the shape. Interestingly, the effect of elevating lung volume to TLC was different in both groups in that it made the cross section more circular only in NA.

Methodology Limitations The methodology used by PW2 was previously validated in Plexiglas phantoms of airways with diameters ranging from 1.98 to 19.25 mm (inner cross sectional area (A) ranging from 3.08–291.04 mm²) [53]. In the smallest tube, the contribution of imaging error to CV^2 in the area estimation was 0.0021. Based on those results, and given that airways analyzed in our study ranged from 4.0 mm² to 271.3 mm², the largest expected contribution of measurement errors to $CV^2(A)$ should be less than 0.0013, which corresponds to 1/13 of the observed average value $CV^2(A)$ in the smallest 25% of the airways analyzed and much lower for the larger airways. Given the complexity of the airway tree airway structure in vivo, the contribution of measurement errors to $CV^2(A)$ could be somewhat higher. Nonetheless, the error was not of enough magnitude to obscure the small but significant effects of MCh or lung inflation observed.

Model Assumptions Assumptions for estimating R_{aw} were: steady and fully developed laminar flow, negligible gravity, incompressible fluid, and constant viscosity. In addition, we assumed the airway walls shape and luminal area were approximately elliptical and changed smoothly along the airway, such that inertial effects or secondary flows due to these effects would be negligible. Depending on the flow rate, the airflow through trachea and large airways could be turbulent (Reynolds number > 2000). Pedley estimated that flow at 100 L/min through airways from the first 4 generations of a symmetric airway model would be turbulent [74]. Therefore, in high flow conditions such as during exercise, the pressure drop in large airways would be greater than that calculated assuming laminar flow, thus yielding an even greater underestimation of R_{aw} . However, during spontaneous breathing in adults, the flow rate is typically around 12 L/min [81]. Hence, a laminar flow assumption would be reasonable. Effects of the unsteady developing flow through the complex tree structure should result in even greater pressure drops and underestimations of R_{aw} . Nonetheless, independent of the flow conditions, since R_{aw} is a function of the cross sectional area elevated to an exponent ≥ 2 , results obtained from this study can be seen as a lower bound of the effect, and the pairwise comparisons should remain qualitatively valid.

Physical Parameters Determining $\%U_{area}$ and $\%U_{shape}$ The longitudinal heterogeneity in the cross sectional area, taken as its mean-normalized variance ($CV^2(A)$), was highly correlated to the underestimation of resistance attributed to changes in cross-sectional area ($\%U_{area}$). The two parameters were not identical, or expected to be so a priori, but $CV^2(A)$ explained almost all (99.7 %) variance in $\%U_{area}$.

Also, shear stress is known to be higher in an elliptical cross section compared to a circular one. Therefore, it can be expected that if the non-circularity of the cross section is ignored, airway resistance should be underestimated. Our result showed that $\%U_{shape}$ was highly correlated with 103.5ϵ . Given these high levels of correlation, it can be concluded that results and conclusions presented in terms $\%U_{area}$ or $\%U_{shape}$ can also be applicable in terms $CV^2(A)$ and ϵ .

Bronchoconstriction Methacholine challenge caused an increase in the longitudinal heterogeneity in the area and $\%U_{area}$ in both AS and NA subjects with a higher increase in AS. We speculated that such difference in airway response between AS and NA could be due to local differences in airway responsiveness that might be larger in subjects with asthma leading to a higher increase in longitudinal heterogeneity in the cross sectional area after MCh challenge.

Effects of Lung Expansion from MLV to TLC In both AS and NA groups, an increase in lung volume to TLC during bronchoconstriction reduced $\%U_{total}$. In NA, the reduction in $\%U_{total}$ at TLC was the result of reductions in $\%U_{area}$ and $\%U_{shape}$. In contrast, in asthmatics, the reduction in $\%U_{total}$ during the TLC maneuver was only due to the reduced $\%U_{area}$ but not in $\%U_{shape}$. This suggested that the cross sectional shape of a non-asthmatic airway once the lung volume increased to TLC became more circular, while that of an asthmatic airway did not. We speculate that parenchymal tethering forces acting on the airway wall could be more heterogeneous along the wall in asthmatic airways compared to non-asthmatics. If parenchymal tethering forces were homogeneous along the perimeter of the airway after lung inflation, one could expect that the airway wall would be distended symmetrically in the radial direction making the cross-section more circular, and thus with a lowered eccentricity as we observed in non-asthmatic airways, but not in asthmatic ones. Therefore, our results might suggest that the lack of reduction in $\%U_{shape}$ and e observed in asthmatic subjects might be due to a less homogeneous lung expansion in asthmatics particularly during bronchoconstriction.

Another explanation for this difference could be related to the reduced elastic recoil in asthmatic patients. Based on results from a computational model of airway narrowing [108] with parameters taken from actual lung tissues from AS and NA patients, Wiggs et al. concluded that airway narrowing was enhanced in the presence of the reduced elastic recoil [107]. Elastic recoil may be reduced in asthmatic patients after asthma attacks [111], during a stable period [63], or even 6 weeks following successful treatments of acute attacks [22]. This reduction in the elastic recoil in AS could imply a reduced magnitude of the parenchy-

mal stress increase upon the increase in lung volume, potentially making the reduction in eccentricity of the cross sectional shape under ASM tension more difficult in AS compared to NA airways. The reduced sensitivity of the non-circular shape to lung volume increase in AS may also be compatible with differences in the behavior of airway smooth muscle postulated to explain the reduced or absent response of asthmatic lungs to a deep inhalation [24, 57, 91].

Despite observing the trend in the change in underestimations of resistance caused by the increase in lung volume to TLC, individual airways in fact behaved heterogeneously. In a large fraction of the airways (54% of AS airways and 57% of NA airways), the increase in lung volume to TLC caused a decrease in $\%U_{area}$ ($>5\%$ decrease), but an increase in $\%U_{area}$ in a substantial number of airways (33% of AS airways and 32% of NA airways with an increase in $\%U_{area}$ of $>5\%$). Originally, we had expected that the high distensibility airway should have a large decrease in longitudinal heterogeneity in cross sectional area. Surprisingly, we found no correlation between the change in the cross sectional area caused by the lung volume increase to TLC and the change in $\%U_{area}$. Therefore, the variability in the change of $\%U_{area}$ was not attributable to differences in airway distensibility per se and the mechanism responsible for these effects remains illusive. Nevertheless, interesting results emerged as we investigated the reduction in the average longitudinal heterogeneity in the cross sectional area in airways of different sizes. We found that the average longitudinal heterogeneity in the cross sectional area was only reduced in the smallest 75% of the airways. It is possible that in the largest 25% of the airways, the relative effect of pleural pressure change or parenchymal tethering could have been small compared to the effects of stiff cartilage plates [69], which are more prevalent in large airways.

In conclusion, we demonstrated that neglecting the longitudinal heterogeneity in airway luminal area, and assuming a circular cross section led to underestimations in airway resistance, which could be considerable (50%) in some airways, but small on average (median $<6\%$). We estimated the magnitude of the two sources responsible for the underestimation of R_{aw} : the variability in the cross sectional area and the non-circularity of its shape. These sources contributed on average to 1/3 and 2/3 of the total underestimation, respectively.

We found that an increase in lung volume to TLC during bronchoconstriction reduced on average the longitudinal heterogeneity in the cross sectional area in both AS and NA airways. However, the magnitude of that effect was variable among airways and the average reduction was smaller and less consistent in AS compared to NA subjects. We speculated that loss of lung recoil, increased wall stiffness, remodeling of the airway wall, or reduced airway-parenchymal interdependence in asthmatic airways might be the cause of the lack of reduction in the non-circularity of the cross section by inhalation to TLC observed in AS subjects.

3.2 Paradoxical Dependency of Airway Distensibility on Airway Wall Area in Asthma

3.2.1 Introduction

Lung expansion has been thought as a potential mechanism for reducing excessive airway narrowing in bronchoconstricted patients. However, it has been shown that this does not apply to asthmatic patients. Many research studies have therefore focused on understanding the mechanism of lung inflation and its effect on airway expansion. To do this, understanding the mechanics of airway narrowing becomes very important.

Due to the potential benefit of lung expansion on the reduction and/or prevention of excessive airway narrowing in non-asthmatic subjects, many recent research studies have focused on the mechanism of lung inflation and its effect on airway expansion [14, 17, 83, 84, 82, 85, 91]. To understand the effect of lung inflation on airway expansion, it becomes essential to study the mechanics of airway narrowing.

Many researchers suggested that excessive airway narrowing could be related to thickening of airway wall [41, 58, 65, 72, 80]. Moreno et al. investigated how airway narrowing could be affected by the changes in the airway structure and airway smooth muscle [65]. They suggested that airway narrowing should increase with mechanical factors such as thickening of airway wall, increased ASM proportion to the airway cross section [65]. Based on the

measurements from postmortem specimens of asthmatic lungs, James et al. concluded that thickening of airway wall could be an important determinant of airway hyperresponsiveness [41]. In addition, Macklem claimed that thickening of airway wall could lead to uncoupling of airway-parenchymal interdependence [58], unloading the airway smooth muscle and eventually resulting in excessive airway narrowing [72]. Moreover, Sasaki et al. proposed that thinning of airway wall could reduce airway narrowing [80].

Based on these studies, we would expect that under the same increase in lung volume, airways with thick walls should expand less than those with thin walls. To investigate this hypothesis, we compared airway dimensions analyzed from High-Resolution Computed Tomography (HRCT) images taken during Methacholine-induced bronchoconstriction in asthmatic and non-asthmatic subjects at mid-tidal lung volume and total lung capacity.

3.2.2 Methods

Subjects Selection We studied High-Resolution Computed Tomography (HRCT) images from 8 mild-to-moderate asthmatics and 9 non-asthmatic adult volunteers. Based on NIH guidelines, individuals with the forced exhaled volume in 1 sec (FEV1) or forced vital capacity (FVC) $\geq 80\%$ predicted, and peak flow or FEV1 variability of $\leq 30\%$ in daily symptoms were qualified as a mild-to-moderate asthmatic patient. Subjects that were either non-smokers, or ex-smokers of ≤ 10 pack-year history were not included in the study. All asthmatic subjects had no chronic respiratory symptoms or cardiopulmonary disease other than asthma. Prior to the study date, the concentration of inhaled MCh aerosol that causes a 20% reduction in FEV1 (PC20) was determined for each subject after a Methacholine (MCh) challenge test done in an upright position. The maximum PC20 dose for normal subjects without hyperresponsiveness is 25 mg/ml.

Study Protocol HRCT images were acquired during a short breath hold (around 20 secs) at a lung volume equal to that averaged over a stable breathing period prior to each scan. Impedance plethysmography (RespiraceTM) was used to aid the breath-hold maneuver.

Through a head mount display, subjects were able to view their instantaneous lung volume during breathing, as well as a reference line at its mean value. The total of 3 HRCT images of the whole lung were taken during a breath hold in the following order: 1) BM: at baseline before MCh challenge at mean lung volume (MLV), 2) MM: after MCh challenge (with a PC20 dose) at MLV, and 3) MT: after MCh challenge at total lung capacity (TLC).

Imaging The subjects were imaged in supine positions with a Siemens Biograph 64 PET-CT tomograph. The scanner was used in a helical mode with 64 slices per rotation, 0.6 mm collimation, a pitch of 1, 120 kV peak, and 8 mA. The image reconstruction was done using the B31 kernel with a slice thickness of 0.75mm, 0.5mm slice increment and 0.25 mm overlap.

Data Analysis In this paper, we exclusively used Pulmonary Workstation 2.0 software (VIDA Diagnostics, Iowa City, IA) to analyze all HRCT images obtained as part of the study and obtain airway measurements. For each image, for 35 specific central airways (up to the 6th generation), we imported the following measurements into MATLABTM: the average outer airway cross sectional area (A_o), average inner airway cross sectional area (A_i), total lung volume (VL). On average 1 airway per subject was removed from the analysis because its cross section was, by inspection, clearly not perpendicular to the centerline.

The cross sectional area of the airway wall (WA), and apparent wall area (ω) were calculated as $WA = A_o A_i$, and $\omega = WA/A_i$. The relative distensibility (Δ) was computed using the following equation:

$$\Delta = \frac{\frac{A_{iMT} - A_{iMM}}{A_{oMT}}}{\frac{VL_{MT}^{2/3} - VL_{MM}^{2/3}}{VL_{MT}^{2/3}}} \quad (3.12)$$

where the subscript MM indicates that the data was from the image taken after MCh challenge at MLV, and the subscript MT indicates that the data was from the image taken after MCh challenge at TLC.

Using MATLAB, we generated a linear least-square regression between the apparent wall

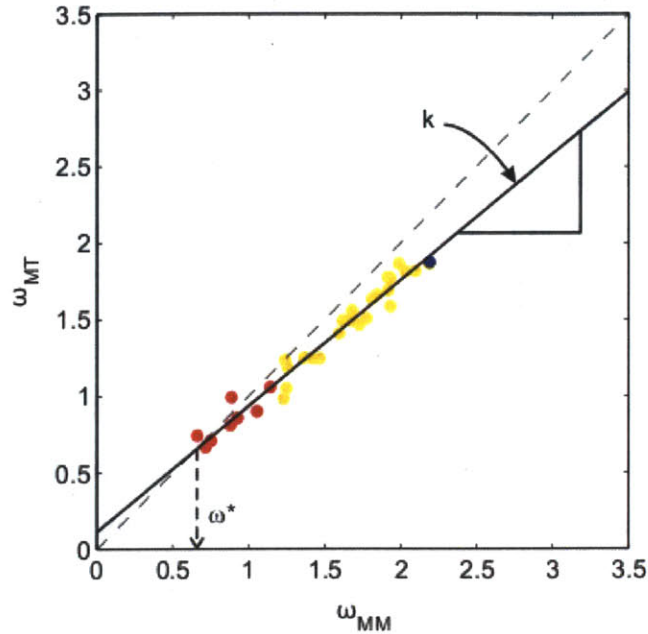


Figure 3-9: The apparent wall area during bronchoconstriction at the mean lung volume (MLV), ω and the apparent wall area during bronchoconstriction at total lung capacity (TLC), ω_T , belonging to one asthmatic subject. The least-square linear regression line was drawn in the solid black line. k is the slope of the regression line. ω^* is the apparent wall area where the predicted $\omega =$ the predicted ω_T based on the linear regression.

area before and after lung expansion to TLC for each subject. Then, for each regression (See Fig 3-9) we obtained 3 following parameters: the slope of the regression line (k), ω along the regression line where $\omega = \omega_T(\omega^*)$, and R^2 of the regression line. Additionally, we speculated that the higher the change in lung volume from MLV to TLC is, the more the regression line should deviate from the 45deg line. Hence, k should be positively correlated with the relative change in lung volume from MLV to TLC. A linear least-square regression of k and $(VL_{MM}/VL_{MT})^{2/3}$ was generated such that the regression line was constrained to pass through.

Statistical analysis Data are expressed as means \pm standard deviation. Using the statistical software package SAS (SAS Institute, Cary, NC), we analyzed the data with a 2-way analysis of variance (ANOVA) model with repeated measurements (same subject imaged at different times). Pairwise comparisons of WA , ω , Δ and VL within each group based on the 2-way ANOVA model from baseline at MLV to post MCh at MLV, and post MCh at MLV to post MCh at TLC were made. For all statistical analyses, $P < 0.05$ was considered significant.

3.2.3 Results

A lung volume increase to TLC during bronchoconstriction (BC) resulted in a statistically significant increase in the airway wall area (WA) in both asthmatic (AS) and non-asthmatic (NA) subjects ($P < 0.0001$) (Fig 3-10). The statistically significant difference in the change of WA between AS and NA subjects following the lung volume increase to TLC was observed only in large airways ($P < 0.05$) (Fig 3-11).

Despite the increase in WA , the apparent wall area (ω) in both AS and NA airways significantly decreased after the lung volume increased to TLC ($P < 0.0001$) (Fig 3-10). After the lung volume was increased to TLC, ω of small airways reduced to a greater extent than ω of large airways in both AS and NA subjects (Fig 3-12 and 3-13). The reduction in ω of each individual airway within each subject scaled linearly with the apparent wall area of an airway imaged at MLV post MCh challenge (ω_{MM}). The relationship between ω_{MM} and ω_{MT} was approximated to be linear with R^2 value ranging from 0.83 to 0.97 (0.91 ± 0.05) in AS, and 0.75 to 0.92 (0.87 ± 0.05) in NA subjects. The slope of the regression (k) was less than 1 in all AS and NA subjects and was positively correlated with the lung volume at TLC relative to that at MLV (Fig 3-14). When the increase lung volume from MLV to TLC was small, k was also small. Forcing the regression line to pass through $k=1$ when the lung volume did not change from MLV to TLC, the least square linear regression was described by the following equation: $k = 0.9052 * (VL_{MM}/VL_{MT})^{2/3}$ ($R = 0.53$).

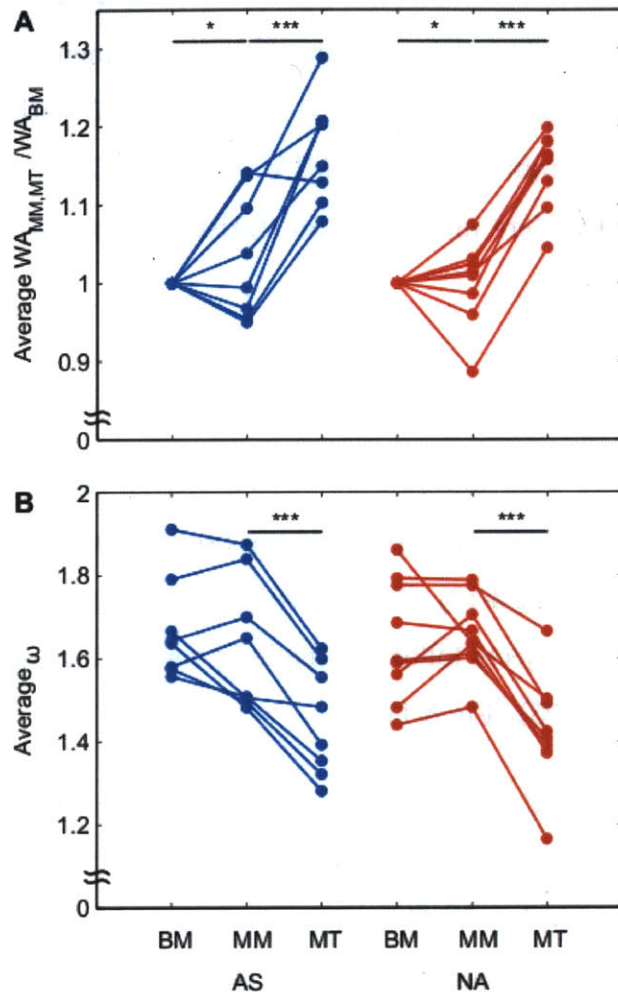


Figure 3-10: The intra-subject change in the measured wall area (WA) and the intra-subject average apparent wall area (ω). The data were taken from 3 images taken at: (1) BM: baseline at mean lung volume (MLV), (2) MM: post MCh challenge at MLV, and (3) MT: post MCh challenge at total lung capacity (TLC). The left column (blue) represents data from asthmatic (AS) subjects. The right column (red) represents data from non-asthmatic (NA) subjects. A: The intra-subject average of the WA_{MM} or WA_{MT} relative to WA_{BM} . In both AS and NA subjects, WA increased after MCh challenge ($P < 0.05$) and following the lung volume increase to TLC during bronchoconstriction ($P < 0.0001$). B: The intra-subject average ω . Following the lung volume increase to TLC during bronchoconstriction, the apparent wall area decreased in both AS and NA subjects ($P < 0.0001$).

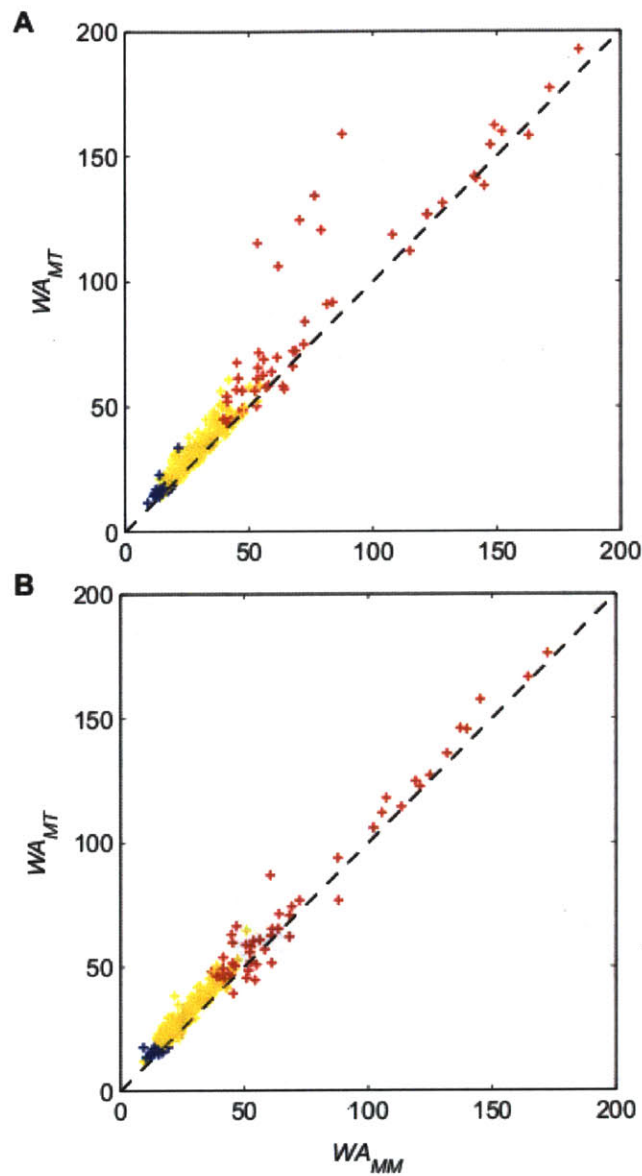


Figure 3-11: The change in the airway wall area (WA) before and after lung expansion to TLC during bronchoconstriction. Data from all airways in all asthmatic (AS) and non-asthmatic (NA) subjects were plotted in A and B, respectively. WA of each airway are colored according to their airway type: small (blue), medium (yellow), and large (red). The significant difference of the change in WA between AS and NA subjects was observed only in large airways. The extent to which WA increased in large airways of AS subjects is higher than that in large airways of NA subjects following lung expansion to TLC.

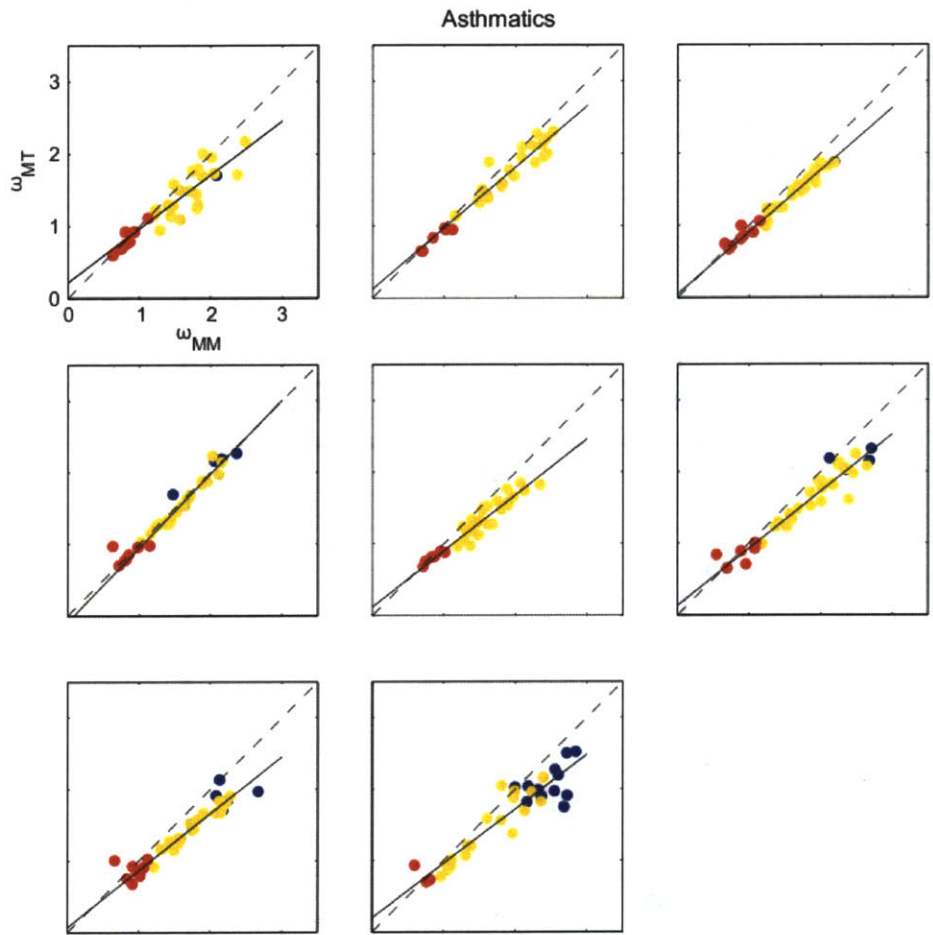


Figure 3-12: The apparent wall area before and after lung expansion to TLC in 8 asthmatic subjects. The apparent wall area during bronchoconstriction at MTLV (ω_{MM}) and at TLC (ω_{MT}) from small, medium, and large airways were plotted in blue, yellow, and red, respectively. A least-square linear regression was generated for each subject and drawn in the solid black line. See text for explanation.

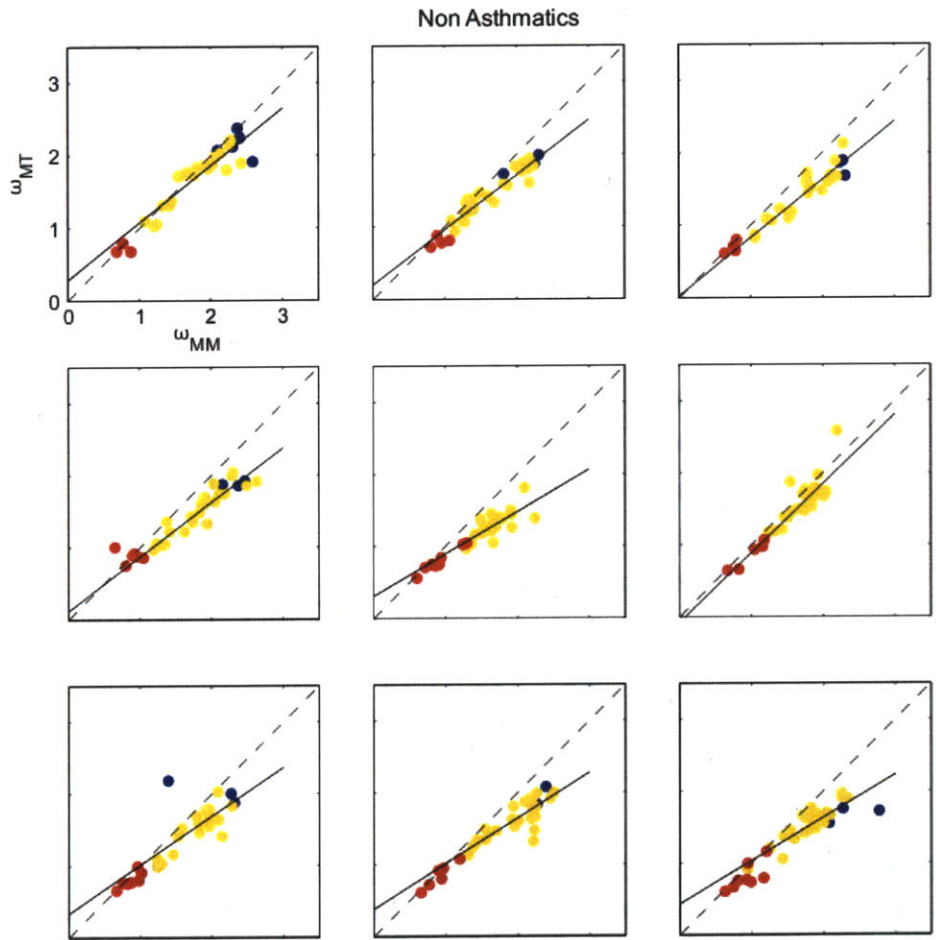


Figure 3-13: The apparent wall area before and after lung expansion to TLC in 9 non-asthmatic subjects. The WA during bronchoconstriction at MTLV (ω_{MM}) and at TLC (ω_{MT}) from small, medium, and large airways were plotted in blue, yellow, and red, respectively. A least-square linear regression was generated for each subject and drawn in the solid black line. See text for explanation.

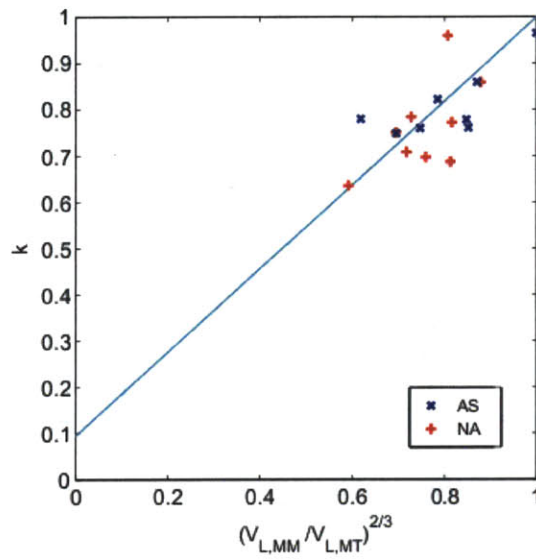


Figure 3-14: The slope of the linear regression (k) and relative change in lung volume $(V_{LMM}/V_{LMT})^{2/3}$. Data from each of the 8 asthmatic (AS) subjects (colored in blue) and 9 non-asthmatic (NA) subjects (colored in red) were plotted with a least-square linear regression line (colored in light blue) that was forced to go through (1,1) ($R = 0.53$). See text for explanation.

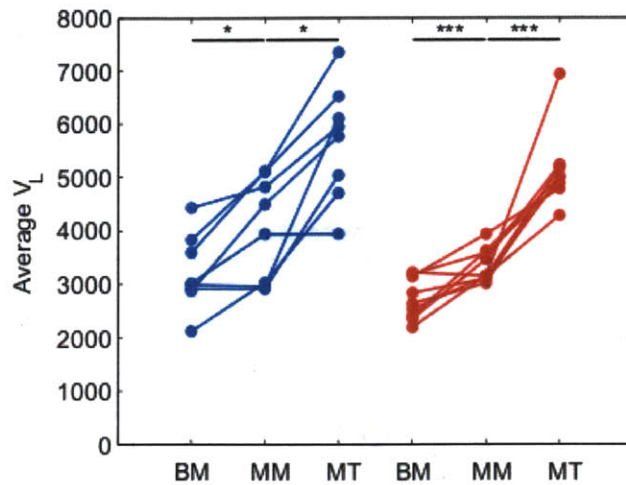


Figure 3-15: The estimated lung volume (V_L) at three imaging conditions of all asthmatic (AS) and non-asthmatic subjects (NA). The lung volume were taken from 3 images taken at: 1) BM: baseline at mean lung volume (MLV), 2) MM: post MCh challenge at MLV, and 3) MT: post MCh challenge at total lung capacity (TLC). The left column (colored in blue) represents data from AS subjects. The right column (colored in red) represents data from NA subjects. In AS subjects, V_L increased both following the MCh challenge ($P < 0.05$) and lung expansion to TLC ($P < 0.05$). In NA subjects, V_L increased both following the MCh challenge ($P < 0.0001$) and lung expansion to TLC ($P < 0.0001$).

The lung volume varied across 3 imaging conditions. After MCh challenge, lung volume increased in both AS subjects ($P < 0.05$) and NA subjects ($P < 0.0001$) (Fig 3-15). The lung volumes after MCh challenge at MTLV and TLC in AS subjects were higher than that in NA subjects ($P < 0.05$). However, there was no statistical difference in lung volume between AS and NA subjects before the challenge at MLV.

In both AS and NA subjects, WA increased after MCh challenge ($P < 0.05$), but the increase in less than that observed after the lung volume was increased to TLC (Fig 3-10). After MCh challenge, there was no statistical difference in ω in neither AS nor NA subjects (Fig 3-10). Fig 3-16 and 3-17 illustrated no systematic response of ω in individual airways of all AS and NA subjects after MCh challenge.

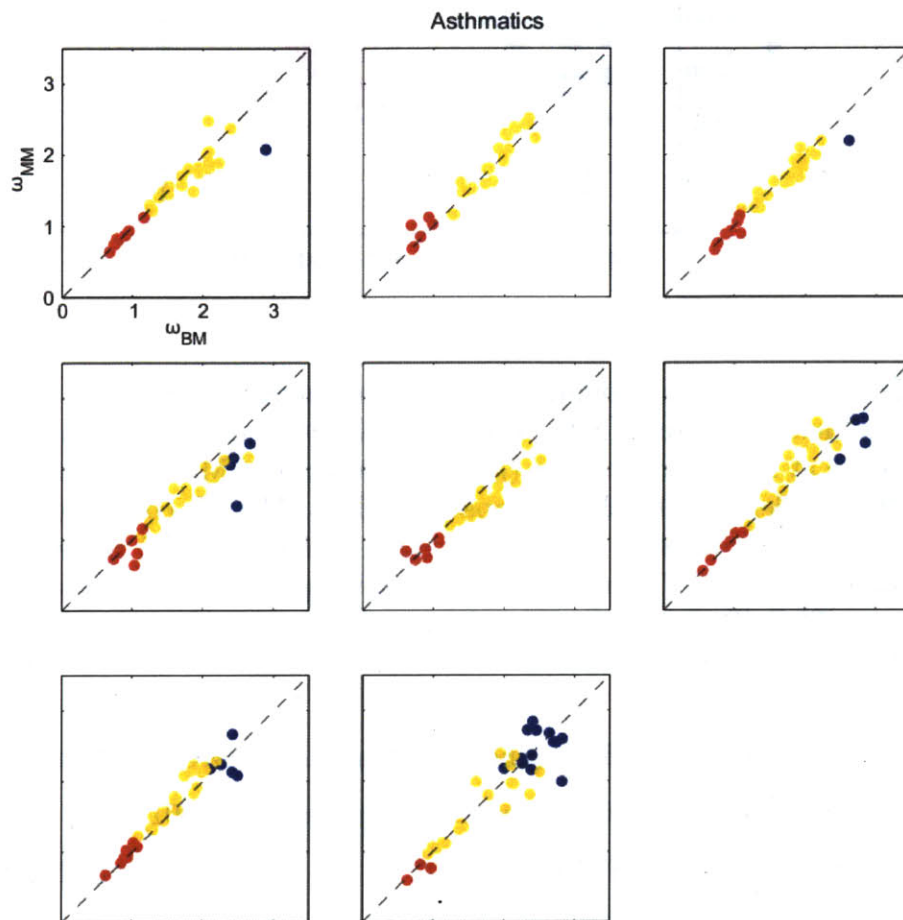


Figure 3-16: The apparent wall area at mean lung volume (MLV) before and after MCh challenge in 8 asthmatic subjects. The apparent wall area at MLV before MCh challenge (ω_{BM}) and after MCh challenge (ω_{MM}) from small, medium, and large airways were plotted in blue, yellow, and red, respectively. See text for explanation.

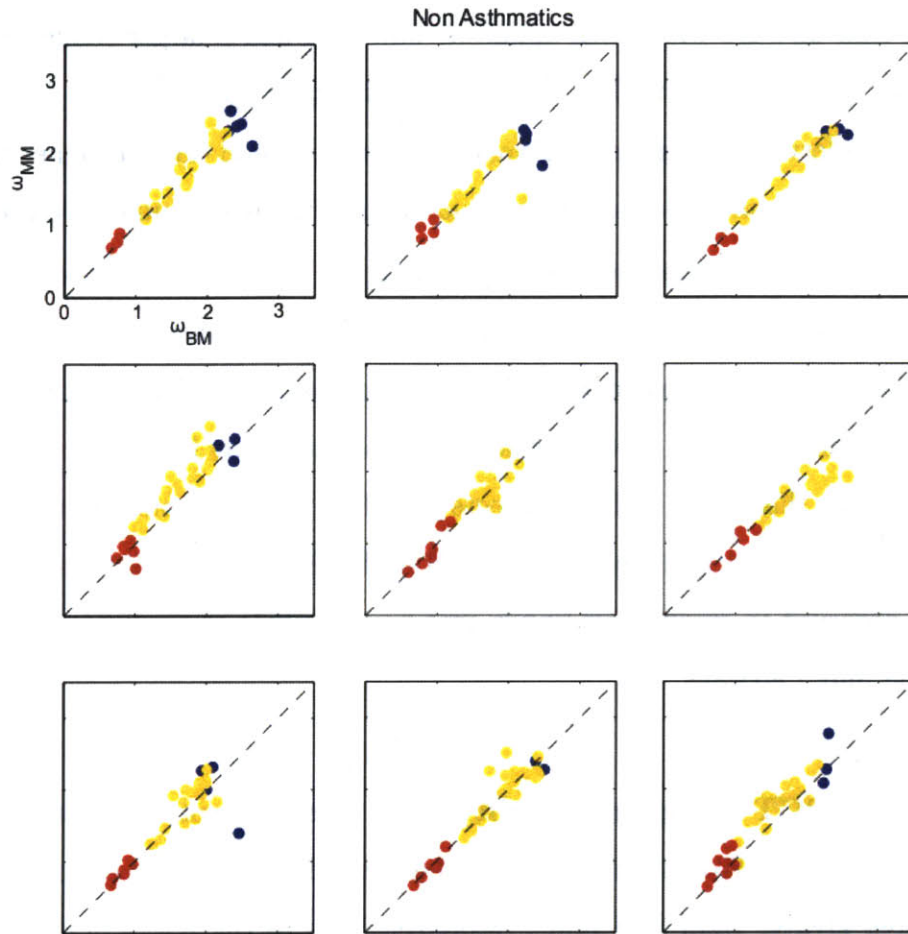


Figure 3-17: The apparent wall area at mean lung volume (MLV) before and after MCh challenge in 9 non-asthmatic subjects. The apparent wall area at MLV before MCh challenge (ω_{BM}) and after MCh challenge (ω_{MM}) from small, medium, and large airways were plotted in blue, yellow, and red, respectively. See text for explanation.

3.2.4 Discussion

The results of this study show that the lung expansion to TLC caused a reduction in the apparent wall area (ω) of central airways in both asthmatic (AS) and non-asthmatic (NA) subjects during bronchoconstriction. This reduction was systematic in both AS and NA subjects, such that airways with thick apparent wall area had a larger reduction in ω after the lung volume was increased to TLC than those with thin apparent wall area. Moreover, an airway that underwent a higher lung volume increase would have a higher reduction in ω , even though the two airways had the same ω before the lung volume increase.

Despite the reduction in the apparent wall area, we observed that the measured wall area (WA) increased both after MCh challenge and lung expansion to TLC. Note that the increase in WA after lung expansion to TLC was significantly different between AS and NA subjects, but only in large airways whose inner area was at least 38 mm². WA in AS subjects was higher than that in NA subjects for all 3 imaging conditions. Interestingly, the difference between the increased WA in AS and NA subjects after lung expansion to TLC was not observed in small-sized (inner area is < 7 mm²) or medium-sized (inner area is between 7-38 mm²) airways.

Limitations of HRCT Imaging Modality The measurements estimated from HRCT images using Pulmonary Workstation 2.0 have been validated only for central airways with the luminal area greater than 3.08 mm². Moreover, due to the restriction on the allowed radiation exposure, only static images were acquired. This imaging modality could not capture the time-dependent responses, which would be helpful in understanding the mechanics of airway narrowing, a process that was highly dynamic.

In our analysis of airway response to MCh challenge, the difference in the MCh concentration (PC20 dose) between subjects was not accounted for. Note that depending on the degree of airway hyperresponsiveness in each subject, the PC20 dose could be different. PC20 dose in AS subjects is lower than that in NA subjects because of the hyperresponsiveness is higher in AS than NA subjects.

Simultaneous Lung Expansion during Bronchoconstriction We found that after the MCh challenge, when airways were constricted, the lung volume also increased. This made the effect of bronchoconstriction difficult to be separated from that of the lung expansion to TLC on airway dimensions. Therefore, a definite conclusion cannot be made as to either the bronchoconstriction and/or lung expansion to TLC influence the change in airway dimensions following the MCh challenge.

Change in the Measured Wall Area The response in the change of WA during bronchoconstriction reported in previous literature was contradictory. In the studies published by James et al., they found that the inner WA remained relatively unchanged both during bronchoconstriction and after the change in the lung volume [39, 40]. However, Sasaki et al. reported no change in the inner WA during bronchoconstriction and a decrease in the outer WA [80]. Interestingly, however, our results indicate that during bronchoconstriction and after the increase in lung volume, WA increased.

Note that in the studies published by James et al. and Sasaki et al., the airway wall area was measured from the postmortem sample taken from the lung that had been mechanically ventilated before dissection. In contrast, our airway measurements were estimated from in vivo images. Additionally, during our study, subjects were breathing spontaneously, while the animals in the studies conducted by James et al. and Sasaki et al. were mechanically ventilated. Thus, we speculated that the discrepancy between our results and those published by James et al. and Sasaki et al. might have come from differences in the experimental procedure and method for acquiring airway measurements.

The increase in WA during bronchoconstriction observed in our study could have resulted from the shifting of blood volume into the bronchial venous plexus in the airway wall as a result of an induced bronchoconstriction. The induced bronchoconstriction can cause the pulmonary blood flow to increase [86]. Due to the increased blood flow in pulmonary circulation and the close communication between pulmonary circulation and the bronchial venous plexus as shown in the study by Murata et al. [66], we expected that the blood flow into the bronchial venous plexus could increase, and therefore, lead to the increase in WA

during induced bronchoconstriction.

Similarly, the observed increase in WA after the increase in lung volume to TLC could have resulted from the increase in blood flow in the bronchial venous plexus. However, we expected that the mechanism might be different. The increase in lung volume leading to the increased parenchymal expansion should reduce the interstitial pressure. When the interstitial pressure was lowered, the vessels outside the influence of alveolar pressure were minimally affected, leading to the increase in blood flow [37]. Due to this increase in pulmonary blood flow and its close communication with the bronchial venous plexus, we expected that after the increase in lung volume to TLC, WA could increase. The amount of blood volume within the lung may not be insignificant as studies in sheep have shown that the bronchial blood volume comprises as much as 20% of the total tissue volume [4, 62].

Changes in the Apparent Wall Area Based on the interdependence of airways and parenchyma, it should follow that airways with thicker wall when subjected to an increase in lung volume should not dilate as much as those with thinner wall. Hence, we expect airways with large apparent wall area when subjected to the increase in lung volume to not have an increase in its apparent wall area (due to smaller increase in the luminal area). However, we found the opposite to be true in our data set, that is, small airways (large apparent wall area) are more distensible, i.e. have larger decrease in its apparent wall area (large increase in its luminal area) after lung expansion to TLC.

A larger reduction in apparent wall area in small airways after TLC expansion could be because during bronchoconstriction, small airways had larger constriction and thus for the same increase in luminal pressure due to TLC expansion, there was more dilatation of the airway lumen than in large airways. This agrees with findings in the literature showing high distensibility in small airways [46].

Studying the measured and apparent wall area helps guide our understanding of the relevance of parenchymal interdependence in asthma.

Chapter 4

Peripheral Airways

Although peripheral airways have not been extensively studied due to the limitation in image resolution and imaging techniques, published data in the literature have suggested that asthma pathogenesis could be highly affected by changes in peripheral airways (diameter <2 mm). In this chapter, an approach for estimating resistance of peripheral airways was presented along with the application of this approach on experimental data. Later in the chapter, we applied this approach on the data to study three mechanisms of bronchoconstriction and evaluate their correlation with peripheral airway responses.

4.1 Image-Based Modeling Approach for Estimating Peripheral Airway Constriction in Human Lungs

4.1.1 Introduction

Airway hyperresponsiveness and ventilation heterogeneity are important characteristics of asthma. Underlying both of these characteristics is the complex relationship between airway structure and lung function. To study this relationship during bronchoconstriction, recent research has focused on developing morphometric models of the lung [2, 27, 92] or inverse models for estimating lumped parameters of the respiratory system from global measure-

ments, i.e. from data obtained from forced oscillation techniques [30, 44].

Advancements in medical imaging technologies have provided increasingly more detailed images of the in vivo lung, and led to development of novel insights into the relationship between airway structure and lung function. Noninvasive measurements of airway dimensions during bronchoconstriction using High Resolution Computed Tomography (HRCT) has led to better understanding of heterogeneity in airway narrowing [48], the site of airway narrowing caused by bronchoconstriction in asthma [71], the effect of longitudinal heterogeneity on airway resistance [110], and structural changes in asthmatic airways [12]. A pulmonary imaging technique to quantify regional specific ventilation from dynamic Positron Emission Tomography (PET) scans [103] has been used to investigate the emergence of patchiness in asthma [101], the characteristics of ventilation distribution [100], and patterns of airway constriction [94]. Magnetic Resonance Imaging had also been used to quantify the extent of ventilation defects [15, 21], as well as parameters of lung microstructure such as number of alveoli per unit lung volume and acinar airway radii-parameters [112].

However, despite these advances in imaging technologies, there has not been any method to quantify the resistance of peripheral airways within anatomically defined regions in humans. The fact that the majority of airways within the bronchial tree have diameters too small to be measured by HRCT in vivo poses a major challenge for measurements of peripheral airway resistance within anatomical regions.

Here we describe an approach that combines measurements from two imaging modalities (PET and HRCT) to estimate the resistance of peripheral airways (≤ 2 mm in diameter) within anatomically defined regions of the lung and their changes during bronchoconstriction. This approach was applied to data from 7 asthmatic (AS) and 8 non-asthmatic (NA) subjects at baseline and during bronchoconstriction and used to evaluate changes in resistance of airways smaller than those measurable with HRCT.

4.1.2 Methods

Data from our PET-HRCT studies were collected (See Data Acquisitions and Study Protocol) and used to estimate subject-specific parameters in asthmatic and non-asthmatic subjects at baseline and during bronchoconstriction (See Derivations of Subject Specific Parameters). These parameters were then used as inputs to a lumped parameter network model (LPN) of the lung to provide estimates of regional peripheral resistance (See Equivalent Network Analysis).

Data Acquisition and Study Protocol

Subjects Images were obtained from 7 mild-to-moderate asthmatic and 8 healthy adult volunteers (demographics shown in Table 4.1). Subjects with mild-to-moderate asthma were selected according to the criteria of the NIH Global Initiative for Asthma with forced exhaled volume within 1 sec (FEV1) or forced vital capacity (FVC) $\geq 80\%$ predicted, less than daily symptoms, and peak flow or FEV1 variability of $\leq 30\%$. We excluded subjects that were current smokers, and those with > 10 pack-years). Other exclusion criteria were the use of oral steroids, symptoms of upper and lower respiratory tract infection, or a history of hospitalizations for asthma in the past month, or history of cardiopulmonary disease other than asthma. No systemic or inhaled corticosteroids could be used within 1 week prior to enrollment. The study protocol was approved by the Massachusetts General Hospital Institutional Review Board. All subjects gave their written informed consent.

Prior to the study date, all subjects underwent a methacholine (MCh) challenge to determine their PC20: the provocative concentration of inhaled MCh aerosol that caused a 20% reduction in FEV1. PC20 was determined based on the method published by Crapo [18]. The maximum dose given to asthmatics was 8 mg/ml and all non-asthmatic subjects were given 25 mg/ml, a dose that by protocol was less than their PC20. Spirometry during the initial screening of subjects was performed while subjects were in an upright position.

	Non-asthmatic subject (n = 8)	Asthmatic subjects (n = 7)
Age, yr	32.1 ± 10.9	31.4 ± 11.7
Sex (F/M)	(5/3)	(2/5)
Height, cm	166.4 ± 6.5	173.3 ± 7.1
Weight, kg	65.4 ± 8.2	76.3 ± 13.6
FEV1, L (%Predicted)	3.3 ± 0.8 (93.8 ± 10.3)	3.6 ± 0.5 (88.0 ± 7.9)
FVC, L (%Predicted)	4.0 ± 1.0 (93.6 ± 13.2)	4.6 ± 0.8 (93.2 ± 8.2)
PC20, mg/ml	> 25	2.4 ± 1.8*

Table 4.1: Demographics and PFT collected from screening in an upright position of asthmatic and non-asthmatic subjects. Values are means ± SD. Unpaired t-test comparison between asthmatic and non-asthmatic groups: *P < 0.0001.

Study Protocol A Siemens Biograph 64 PET-CT tomography scanner was used in a helical mode to acquire 64 slices per rotation. The scanner setting was 0.6 mm collimation, and a pitch of 1. The energy settings were 120 kV peak, and 80 mA. Image reconstruction was done using the B31 kernel with a 0.75 mm slice thickness, 0.5 mm slice increment and 0.25 mm overlap. With the subjects in the supine position, HRCT images were acquired during a short breath hold (around 12 secs) under 3 consecutive conditions: 1) at baseline and imaged at mean lung volume (MLV) (BASE), 2) following a five breaths of PC20 dose of MCh and imaged at the subject determined MLV (POST) and 3) post MCh and imaged at total lung capacity (PostTLC). Dynamic PET emission scans of tracer gas $^{13}\text{N}_2$ were acquired following the first and second CT scans. The kinetics of $^{13}\text{N}_2$ was used to assess regional specific ventilation within the lung. Prior to each HRCT or PET scan, MLV was determined over the 30-second period of stable breathing. To guide the breath hold maneuver, the instantaneous lung volume and a line indicating MLV from an impedance plethysmograph (SomnoStarPT, SensorMedics Corp, Yorba Linda, CA) were displayed to each subject by means of video glasses. Breathing frequency (f) was calculated for each subject at each condition as the dominant frequency of a Fast Fourier Transform of the lung volume signal from the impedance plethysmography during the $^{13}\text{N}_2$ washout period [38].

Data Analysis Pulmonary Workstation 2.0 (PW2) software (VIDA Diagnostics, Iowa City, IA) was used to analyze and obtain airway dimensions of 35 defined central airways

($0^{th} - 6^{th}$ generation) for each condition (Fig. 4-1A). The following parameters from PW2 were imported into MATLAB (Mathworks, Natick, MA): 1) the average luminal area (A), 2) airway length (L), and 3) generation number (starting with 0 for the trachea). From HRCT images, using PW2 19 sublobar regions subtended by 19 of the most distal airways were identified (Fig. 4-1B). For each region and imaging condition, the following parameters were gathered:

- d : relative distance of each sublobar regions geometric center from the most ventral point in the lung normalized by the total lung height (from ventral to dorsal),
- V_{tis} : tissue volume defined as the volume of the sublobar region not occupied by air.
- F_{gas} : fraction of the regions volume occupied by gas.

Lumped Parameter Network Analysis

For each subject at a given condition (BASE or POST), the 35 defined central airways, each with individual conductance of G_c , or resistance (G_c^{-1}), were interconnected in a network with a subject-specific airway tree structure (e.g. Fig. 4-1A). Each of the 19 most distal airways (colored in blue in Fig. 4-1B) was connected to a peripheral resistance (R_p), then to an elastic element with apparent compliance of C_a , and then a common pleural pressure (P_{pl}) (Fig. 4-1C). Airflow (\dot{V}) through each branch of the airway tree is assumed to be equal to the sum of flow of its daughter branches. Values of G_c and C_a were estimated from HRCT and PET images (See 4.1.2). Three network models were considered: 1) a network model where pressure drops across both resistive elements (and R_p) were neglected, 2) network model where only pressure drops across R_p , but not G_c^{-1} was neglected, and 3) a network model where pressure drops across neither G_c^{-1} nor R_p was neglected. \tilde{G}_c^{-1} was defined as the airflow through each of the 19 most distal airways divided by the sum of pressure drops across all central airways leading to each sublobar region (Fig. 4-1C and Appendix A). For Model 3, total pathway resistance (R_T) was defined as $\tilde{G}_c^{-1} + R_p$.

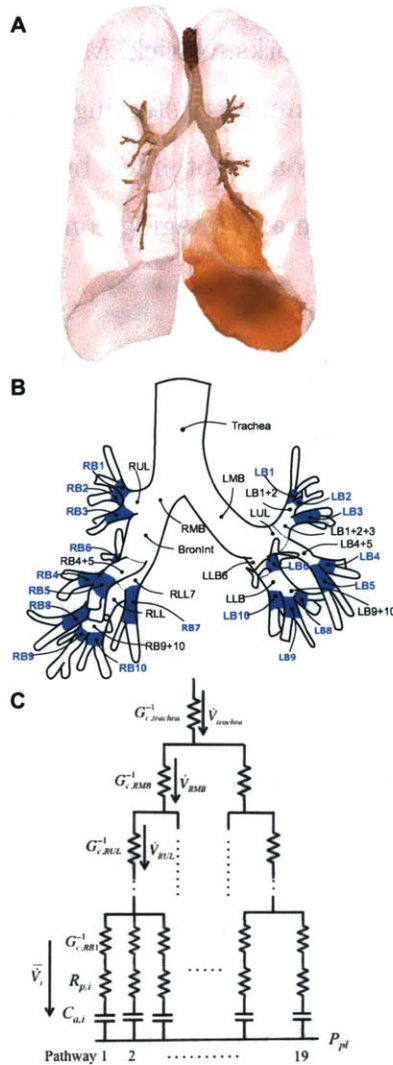


Figure 4-1: A: 3D volume rendering of an airway tree, lung, and a sublobar region imaged at TLC. B: Diagram of 35 defined central airways and their labels used in our analysis. Of these, the 19 most distal airways, colored in blue, were used to define respective sublobar regions each airway subtended. C: Diagram of the lumped parameter network model of the airway tree consisting of 35 defined central airways with individual conductance of G_c . For each of the 19 most distal airways, a resistive element (R_p) representing resistance of peripheral airways within each sublobar region and elastic element with apparent compliance of C_a were appended in series. These model parameters were estimated from airway tree morphometry quantified from HRCT images, and the distribution of ventilation among sublobar regions (\dot{V}) estimated from dynamic PET scans. Each pathway was connected to a common pleural pressure (P_{pl}).

Derivations of Subject-Specific Parameters

Regional gas volume (V_{gas}) Regional tissue volume (V_{tis}) measured from PW2 was found to be quite variable among three imaging conditions for each region in all subjects. For example, the mean and standard deviation (Mean \pm SD) of regional $\frac{V_{tis_i,BASE}}{V_{tis_i,POST}}$ for all subjects was 1.01 ± 0.32 compared with the average and SD of whole lung $\frac{V_{tisBASE}}{V_{tisPOST}}$ of 0.99 ± 0.04 for all subjects. This suggested that the variability in V_{tis_i} was likely due to an inconsistent segmentation among scansan observation that was confirmed by visual inspection. Given that parenchymal segmentation appeared to be most accurate at TLC and that V_{tis} of the lung did not significantly change with imaging condition, for each sublobar region V_{tis} was assumed to be equal to that measured at TLC for the other two conditions (BASE and POST). Moreover, since regional F_{gas} is a parameter normalized by the sublobar regions total volume, it should be less sensitive to the inaccuracy in sublobar segmentation than V_{gas} . Hence, we estimated V_{gas} of each sublobar region i from its regional F_{gas} (F_{gas_i}) and V_{tis_i} at TLC as,

$$V_{gas} = \frac{F_{gas_i}}{1 - F_{gas_i}} \cdot V_{tis_i,PostTLC} \quad (4.1)$$

Subtended Gas Volume (V_{sub}) was computed for each central airway as the sum of gas volumes of all regions subtended by that airway.

Alveolar Ventilation per Unit Volume ($s\dot{V}_A$) Within each sublobar region, the activity of ^{13}N during washout measured with PET was averaged and used to estimate alveolar ventilations per unit of gas volume assuming a two-compartment model [103]. Sublobar region $s\dot{V}_A$ was then computed as the blood flow weighted $s\dot{V}_A$ of the two compartments.

Total Ventilation ($\dot{V}_{T,i}$) of a sublobar region, i , was defined as the sum of its alveolar ($\dot{V}_{A,i}$) and dead space ($\dot{V}_{D,i}$) ventilations. Since specific ventilation ($s\dot{V}_A$) was the total ventilation per gas volume within each subtended region, $\dot{V}_{A,i}$ was the product of $s\dot{V}_A$ and V_{gas_i} . $\dot{V}_{D,i}$ was assumed to be 1/3 of $\dot{V}_{T,i}$. An average airflow through each airway was computed from

the sum of $\dot{V}_{T,i}$ to its subtended regions. $s\dot{V}^*$ was defined as the mean-normalized $s\dot{V}$ of all sublobar regions weighted by their corresponding $Vgas_i$.

Regional Apparent Compliance (C_a) Assuming that P_{pl} was constant throughout the pleural space, we estimated an apparent compliance of a sublobar region ($C_{a,i}$) as the change between MLV and TLC of its regional gas volume (ΔV_i) divided by the change in transpulmonary pressure (ΔP_{tp}). For both BASE and POST, we computed $C_{a,i}$ as,

$$C_{a,i} \equiv \frac{\Delta V_i}{\Delta P_{tp}} = \frac{Vgas_{i,TLC} - Vgas_{i,MLV}}{\frac{Vgas_{L,TLC} - Vgas_{L,MLV}}{sC \cdot FRC}} \quad (4.2)$$

where $Vgas_i$ and $Vgas_L$ were the gas volumes in the sublobar region and the whole lung, respectively; the subscript MLV and TLC denoted the lung volume state at which $Vgas$ was calculated; sC was the specific compliance of the lung and assumed to be 0.1 L/cmH_2O per 1L of FRC [47, 90]. We estimated each subjects FRC from their TLC and body mass index using the empirical table by Jones *et al.* [42] (See Appendix B). Fig. 4-2B shows a plot $\frac{Vgas_i}{Vgas_{i,TLC}}$ vs. whole lung $Vgas_L/Vgas_{L,TLC}$ for all sublobar regions of a subject at BASE (in black) and POST (in red). In this plot, the data from a sublobar region whose specific compliance is equal to that of the lung would follow the identity line, and the variation of the sublobar apparent compliance is reflected by differences in the slope in Fig. 4-2B.

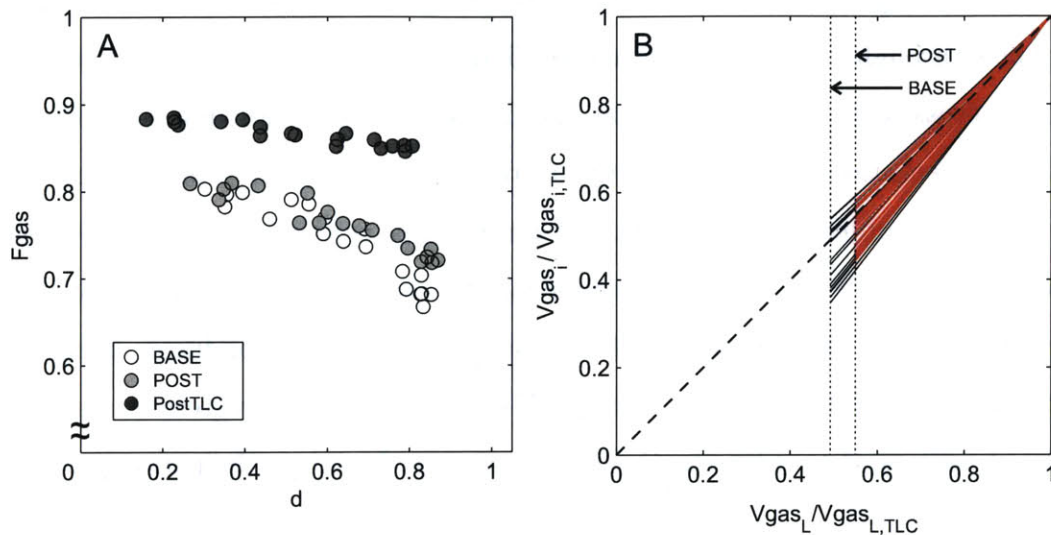


Figure 4-2: A: Fraction of gas content (F_{gas}) within each sublobar region located at a normalized distance d from the most ventral part of the lung ($d = 0$ most ventral, 1 most dorsal) taken at baseline (BASE), after MCh challenge (POST), and at TLC (PostTLC). F_{gas} was highest at TLC the top (supine position) and decreased toward dependent regions of the lung with increasing dependency on d as lung volume deviated from TLC. B: Regional gas volume (V_{gas_i}) normalized by its TLC value vs. gas volume of the lung (V_{gas_L}) normalized by TLC. Slopes of these lines (belonging to each sublobar region) represented specific compliance of a sublobar region relative to that of the lung (blackBASE, redPOST).

Conductance of Individual Airways (G_c) was defined as the ratio of airflow to pressure loss along each of the 35 anatomically defined airways. The pressure loss along each airway was computed as the sum of major and minor losses based on the work by Katz *et al.* that accounted for the local characteristics of flow in the human airway tree [45]. Major and minor losses were estimated based on a local Reynolds number, average airway diameter, length, average flow velocity, and empirical table of minor loss coefficients. That table provides constants for each generation number based on computational modeling and experimental results of flow through a bifurcating structure. This method was applied to all airways except those whose cross sections, by inspection, did not appear perpendicular to their centerlines due to the segmentation error in PW2. On average, this amounted to one, but no more than two, airways per subject. Conductance of erroneously segmented airways was estimated based on the observed correlation between $\log(G_c)$ and $\log(V_{subPostTLC})$ for all airways measured within each individual (Fig. 4-3). For BASE or POST condition, linear regression was applied to the plot of $\log(G_c)$ and $\log(V_{subPostTLC})$. The regression parameters for each subject were used to estimate G_c of those airways based on their measured subtended volume, $V_{subPostTLC}$.

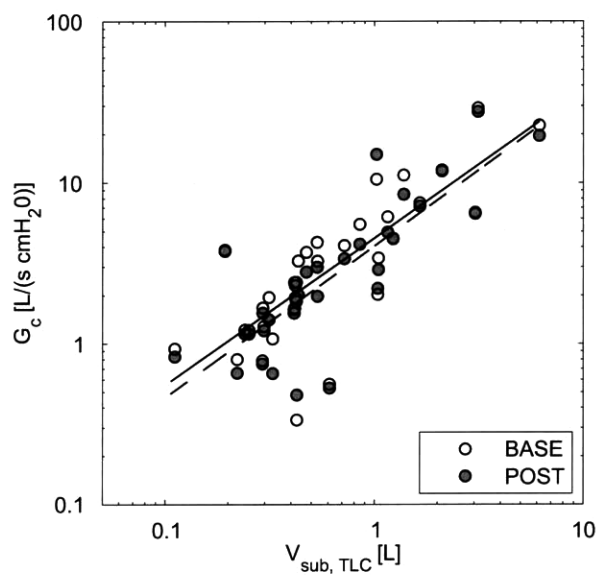


Figure 4-3: Individual conductance (G_c) of 35 defined central airways in a representative non-asthmatic subject at baseline (BASE: open circles) and post MCh challenge (POST: filled circles) and gas volumes of regions that each airway subtended (V_{sub}) estimated from the PostTLC image. $\log(G_c)$ scaled linearly with $\log(V_{sub})$ at PostTLC.

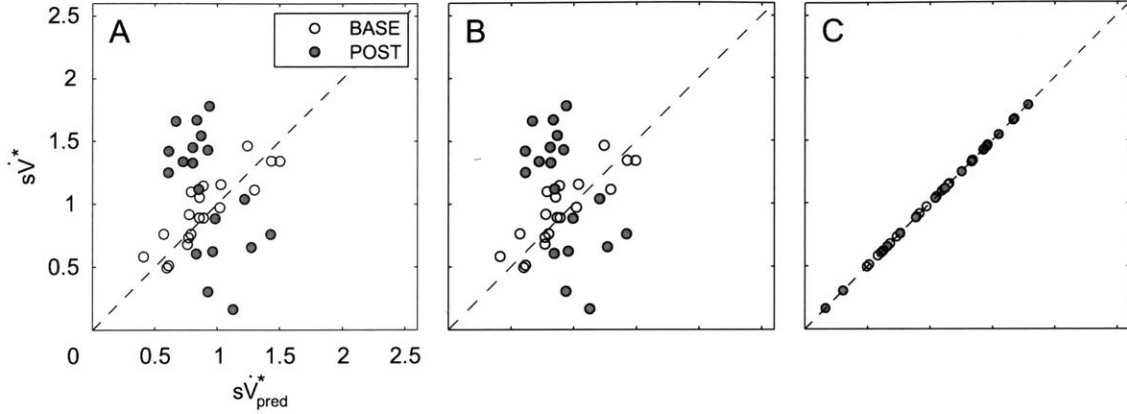


Figure 4-4: Mean-normalized data of specific ventilation measured from PET scans ($s\dot{V}^*$) and specific ventilation predicted from the lumped parameter network model ($s\dot{V}_{pred}^*$) for each pathway in a representative non-asthmatic subjects at baseline (BASE: open circles) and post MCh challenge (POST: filled circles). Data for $s\dot{V}_{pred}^*$ computed from Model 1, 2 and 3 are shown in A, B and C, respectively. In Model 1 and 2, the prediction of were reasonable at baseline, but not after the challenge. In Model 3, we were able to match with by adding the appropriate estimates of R_p with less 1% prediction error.

Peripheral resistance (R_p) In a plot of model-predicted ($s\dot{V}_{pred,i}^*$) vs. measured mean-normalized ($s\dot{V}_i^*$) specific ventilations of sublobar regions, deviations from the identity line of the data for Model 1 and Model 2 (Fig. 4-4A and Fig. 4-4B) imply that nonzero values of regional R_p need to be included to the network to account for the distribution of $s\dot{V}_i^*$ measured from PET scans. To estimate R_p for each pathway, we used the following algorithm. First, assuming a known oscillatory driving pressure and in-phase flow throughout the tree, we obtained approximate values of sublobar R_p such that the magnitude criteria in the following equation was satisfied,

$$-P_{pl} = \left(\sum_{k \in w_i} \frac{1}{G_{c,k}} \dot{V}_k + R_{p,i} \dot{V}_i \right) - j \left(\frac{1}{C_{a,i}} \frac{\dot{V}_i}{2\pi f} \right) \quad (4.3)$$

where k is an index defining specific airways along a pathway, i .

Values of estimated R_p entered into Model 3 allow airflow to be calculated for each sublobar region i (including both phase and magnitude). These airflows were used to calculate

$s\dot{V}_{pred,i}$ and compare them against the corresponding PET measured $s\dot{V}_i$. This yielded a prediction error of less than 1% for the initial estimate, and was rapidly reduced by iterative estimation of R_p .

Pleural Pressure (P_{pl}) was not directly measured during this study, and thus had to be estimated. First, for baseline conditions, we started with a fixed value of P_{pl} for all subjects. Although we found that values of $sG_{p,i}$ for each subject fell within a range, there was usually an outlier whose value was an order of magnitude higher than the average $sG_{p,i}$. This outlier was identified to be from the pathway with the highest the total pressure drop given by Model 2.

We chose to apply the following approach to select P_{pl} based on the assumption that the variance of the distribution of $sG_{p,i}$ at baseline should not be greatly affected by the exclusion of one of its pathways. For each subject, we began by identifying the smallest value of P_{pl} that yielded nonzero R_p as the pressure drop across the pathway j with the highest total pressure drop in Model 2. Then we calculated the values of $sG_{p,i}$ for incrementally increasing values of P_{pl} until the exclusion of $sG_{p,j}$ did not reduce the mean-normalized variance of sG_p by more than 20%. This value of P_{pl} was the final estimate used in our analysis. For the condition after MCh challenge, P_{pl} was assumed to double relative to P_{pl} at BASE.

Pathway Specific Conductance Peripheral airway component of pathway specific conductance ($sG_{p,i}$), and central airway component of pathway specific conductance ($s\tilde{G}_{c,i}$) were defined as $\frac{R_{p,i}^{-1}}{Vgas_i}$ and $\frac{\tilde{G}_{c,i}}{Vgas_i}$, respectively.

Statistical Analysis All reported measurements were the mean \pm standard error (range: minimum maximum). Statistical analyses were performed using SAS 9.2 (SAS Institute, Cary, NC). One-way ANOVA was used to determine the effect of MCh challenge on C_a . When the normality test failed, the Wilcoxon Rank Sum Test was used instead of the one-way ANOVA. Two-way ANOVA with repeated measurements was used to determine the effect of MCh challenge and the effect of asthma. If the normality test failed, two-way

ANOVA was reapplied to the log-transformed data. For all statistical analyses, $P < 0.05$ was considered significant.

4.1.3 Results

Fractional Gas Content (F_{gas}) F_{gas} within each subject increased after MCh challenge ($P < 0.0001$) reflecting an increase in total lung volume ($P < 0.001$). Lung volume increased after the challenge on average by $24.8 \pm 7.0\%$ in NA and $26 \pm 8.8\%$ in AS subjects, but were not significantly different between the two groups. F_{gas} measured at MLV had a vertical dependency that was reduced when lung volume increased after MCh challenge ($P < 0.05$). F_{gas} at PostTLC had a small but significant vertical dependency ($P < 0.001$) as illustrated in Fig. 4-2A. During inflation from MLV to TLC, sublobar gas volume (V_{gas_i}) increased differently among regions with some expanding more and others expanding less than the average expansion of the lung (Fig. 4-2B). Sublobar apparent compliance ($C_{a,i}$) derived from these regional changes in V_{gas} between MLV and TLC did not significantly change after MCh challenge in neither the NA, nor AS group (Wilcoxon Rank Sum test).

Conductance of Individual Central Airway (G_c) $\log(G_c)$ varied linearly with $\log V_{sub}$ at TLC in both NA and AS subjects at BASE and POST (Fig. 4-3). Linear regression parameters for that relationship had an average correlation coefficient of 0.85 (SE of 0.01) and average regression slope of 1.12 (SE of 0.05). Two-way ANOVA with repeated measurements performed on these correlation coefficients and slopes showed no significant effect of MCh challenge or the presence of asthma.

Central Component of Pathway Specific Conductance ($s\tilde{G}_{c,i}$) The data taken from all pathways in all subjects of each group show that $s\tilde{G}_{c,i}$ was highly variable as seen in the broad cumulative distributions both at BASE and POST. In addition, MCh challenge caused a left shift in these distributions in both groups reflecting a systematic reduction in median of $s\tilde{G}_{c,i}$ from $3.22 [\text{cmH}_2\text{O} \cdot \text{s}]^{-1}$ to $2.42 [\text{cmH}_2\text{O} \cdot \text{s}]^{-1}$ (Fig. 4-5A). Analysis by individual subject shows a significant, but small, reduction of the individual geometric mean (μ_g) of

$s\tilde{G}_{c,i}$ after MCh challenge for both groups ($P < 0.05$) (average reduction of 20.2 ± 0.1 SE) (Fig. 4-6A). The heterogeneity of $s\tilde{G}_{c,i}$ within subjects, measured by the geometric variance (σ_g^2), was not different between NA and AS subjects. Although there was an increase in σ_g^2 of $s\tilde{G}_{c,i}$ after MCh challenge in NA subjects, the increase did not reach significance ($P = 0.058$) (Fig. 4-6C). In the AS group, the response of σ_g^2 ($s\tilde{G}_{c,i}$) to MCh challenge was highly variable between subjects.

Peripheral Component of Pathway Specific Conductance ($sG_{p,i}$) The broad cumulative distributions of $sG_{p,i}$, pooled for all pathways in all subjects of each group, illustrates a large variability in peripheral pathway conductance in both groups at BASE and POST. MCh challenge also caused a left shift in these distributions of $sG_{p,i}$ in both groups reflecting a substantial reduction in the median of $sG_{p,i}$ from 0.12 [$\text{cmH}_2\text{O} \cdot \text{s}$] $^{-1}$ to 0.03 [$\text{cmH}_2\text{O} \cdot \text{s}$] $^{-1}$ (Fig. 4-5B). Analysis by individual showed that MCh challenge caused a significant and substantial reduction in μ_g of $sG_{p,i}$ in both groups ($P < 0.001$) (average reduction of 69.8 ± 0.1 SE), but μ_g of $sG_{p,i}$ was not different between groups (Fig. 4-6B). The geometric variance (σ_g^2) of $sG_{p,i}$ was not different between NA and AS subjects and was not affected by MCh challenge in a systematic manner (Fig. 4-6D).

The peripheral component of specific conductance was more than an order of magnitude smaller than the central component in both groups for both conditions (Fig. 4-6A and Fig. 4-6B). This large contribution of peripheral airways to mechanical obstruction can best be presented in terms of the ratio between peripheral resistance ($R_{p,i}$) and total resistance ($R_{T,i}$) of each pathway. The right shift in the cumulative distributions of $R_{p,i}/R_{T,i}$, pooled for all pathways in all subjects of each group, shows that at baseline $R_{p,i}/R_{T,i}$ was moderately higher in AS than NA subjects ($P < 0.005$), and increased substantially after MCh challenge ($P < 0.0001$) with no difference between NA and AS for POST condition (Fig. 4-7). Baseline values of $R_{p,i}/R_{T,i}$ ranged from 0.79 – 0.99 in NA (median of 0.96) and 0.75 – 0.99 in AS subjects (median of 0.97). For POST, values of $R_{p,i}/R_{T,i}$ were greater than 0.95 for all pathways with a median of 0.993 .

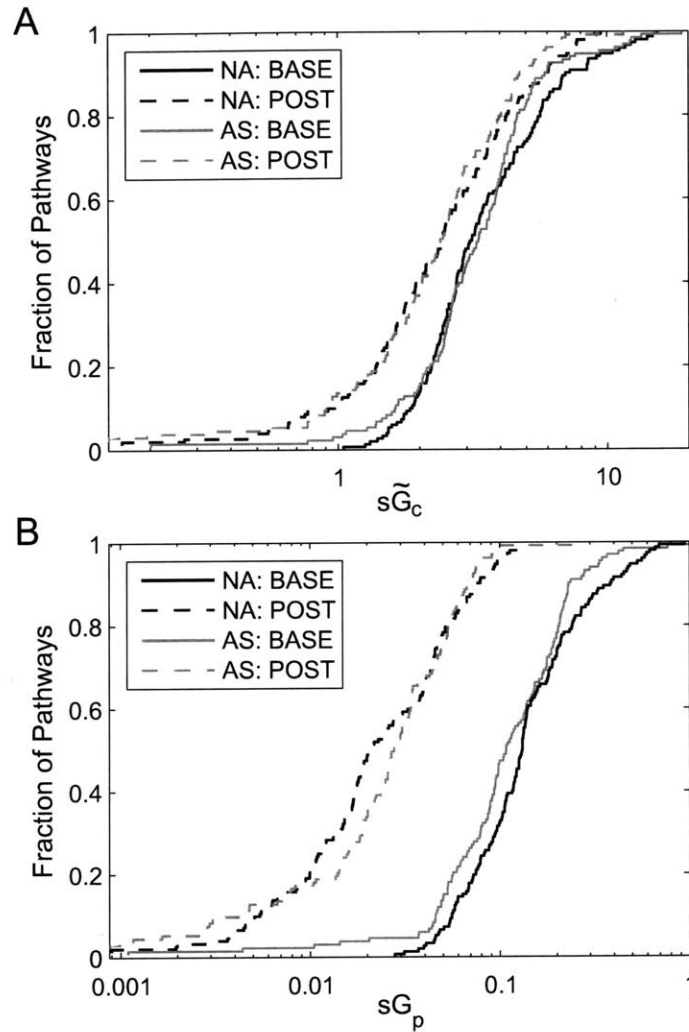


Figure 4-5: Cumulative distributions of the central component of specific pathway conductance ($s\tilde{G}_c$) at baseline (BASEsolid line) and post MCh challenge (POSTdashed line) in 19 pathways for A) all non-asthmatic (NA), and B) all asthmatic (AS) subjects. MCh challenge caused a significant reduction in $s\tilde{G}_c$ in both groups ($P < 0.01$). Peripheral component of specific pathway conductance (sG_p) at baseline (BASEsolid line) and post MCh challenge (POSTdashed line) in 19 pathways were plotted for C) all NA, and D) all AS subjects. In both groups, we found a significant reduction in sG_p after MCh challenge ($P < 0.001$).

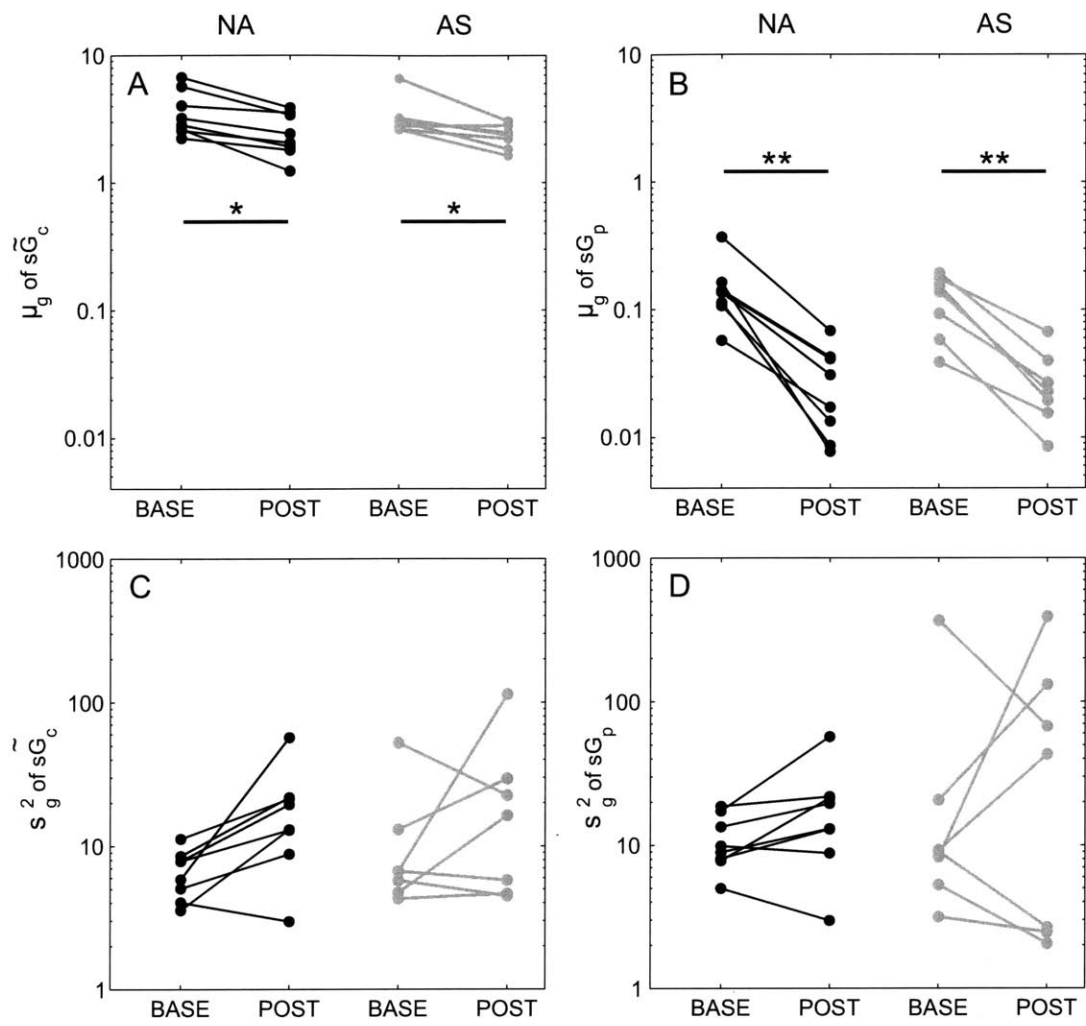


Figure 4-6: Geometric mean (μ_g) and variance (σ_g^2) of the central and peripheral component of specific pathway conductance ($s\tilde{G}_c$ and sG_p , respectively). Individual μ_g of $s\tilde{G}_c$ and sG_p are shown in Fig. A and B. σ_g^2 of $s\tilde{G}_c$ and sG_p within each individual are shown in Fig. C and D. Bronchoconstriction (POST) caused a reduction in μ_g of $s\tilde{G}_c$ in both non-asthmatic (NA) and asthmatic (AS) subjects ($P < 0.05$) and a substantial reduction in μ_g of sG_p in both groups ($P < 0.005$). The geometric mean of $s\tilde{G}_c$ were at least an order of magnitude higher than that of sG_p . The change in geometric variance was not systematic in either group. See text for further explanation.

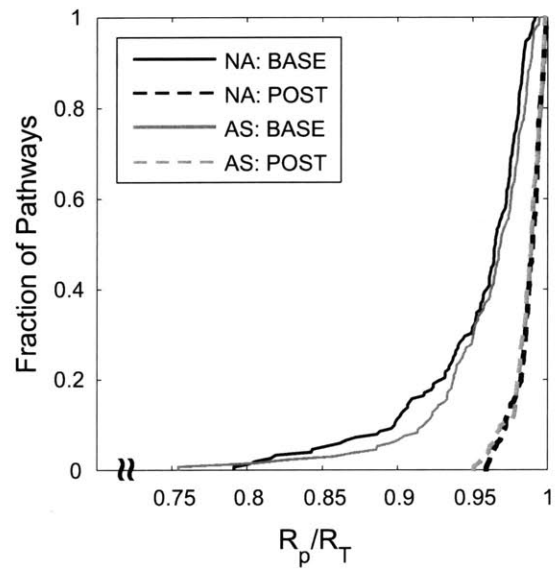


Figure 4-7: Cumulative distributions of peripheral resistance (R_p) relative to the total pathway resistance (R_T). The plot includes data from 19 pathways of all non-asthmatic (NA) and asthmatic (AS) subjects at baseline (BASE) and post MCh challenge (POST). At BASE, R_p/R_T was elevated in AS compared to NA subjects ($P < 0.005$). R_p/R_T significantly increased in both groups after MCh challenge ($P < 0.0001$).

4.1.4 Discussion

This paper presents a novel image-based, subject-specific modeling approach to estimate the resistance of central and peripheral airways, and the compliance of anatomically defined sublobar regions. Applying this approach to imaging data from asthmatic (AS) and non-asthmatic (NA) subjects, we found that the relative contribution of peripheral airway resistance (R_p) was elevated in AS compared to NA subjects at baseline (BASE) and substantially increased during bronchoconstriction (BC) in both groups. Moreover, R_p was highly heterogeneous within and among subjects. R_p represented a large fraction ($>75\%$) of the total resistance of any pathway (R_T) at BASE, and increased to account for $>95\%$ of R_T during BC. These results demonstrate that airway constriction during induced bronchoconstriction occurs mostly in peripheral airways (<2 mm in diameter).

We will discuss and compare advantages of our approach with existing modeling approaches in two categories.

1. Models of Regional Lung Mechanics. Distributed inverse models applied to frequency response data have been widely used to investigate mechanical responses during bronchoconstriction [43, 44, 92, 113]. Parameters such as resistance and elastance from the distributed model are estimated from whole organ measurements. They may provide measurements of functional heterogeneity within the lung but not for anatomically defined regions. In contrast, the modeling approach proposed in this paper provides estimates of regional mechanics within anatomically defined regions of interest. Moreover, the proposed approach not only allows for the quantification of functional impairment, but also links the source of functional impairment to anatomical structures.
2. Morphometric Models. Morphometric models of a human lung such as those developed by Weibel *et al.* [105] and Horsfield *et al.* [36] have been used to estimate the contribution of airway generations to the total pressure losses during breathing [74]. In Weibel and Horsfield models, assumptions about the airway tree were made to generalize its morphometry within a population, disregarding branching asymmetry and differences in airway morphometry among individuals, which may influence the regional distri-

bution of ventilation. Rather than a population-based model, the described approach allowed us to build a subject-specific model for the lung based on each individual's anatomical information.

Another morphometric model recently developed by Tawhai *et al.* [92] used lobar geometry obtained from the segmentation of subject-specific CT scan as an input to an algorithm to grow distal generations of the airway tree. This model uses a volume-filling algorithm to generate a tree structure that closely resembles that of the human lung. Although the model creates an airway tree using subject-specific constraints, it has many degrees of freedom to define the geometry of specific airways, which may or may not represent *in vivo* airway functions at baseline or during bronchoconstriction. In contrast, our estimation of peripheral resistance within sublobar regions can yield a solution where the predicted ventilation closely matched the measured regional ventilation. Nevertheless, the Tawhai model could be combined with our approach to investigate functional changes at smaller length scales within sublobar regions.

Tgavalekos and colleagues combined data from PET imaging, oscillatory ventilation mechanics, and the Tawhai model to identify potential patterns of airway constriction that could explain the observed size and location of ventilation defects during bronchoconstriction [94]. Such statistical modeling tested assumptions about the distribution of constriction at different levels of the tree to match global oscillatory mechanics, but were not necessarily consistent with quantitative measurements of regional ventilation. However, in our modeling approach without making an assumption about constriction patterns, we can estimate values of peripheral resistance for airways with diameter $<2\text{mm}$ within anatomically defined sublobar regions.

Model Assumptions Assumptions about unmeasured variables had to be made in our model to derive estimates of peripheral resistance. Here, we discuss the potential implications that these assumptions may have on our results and, when possible, how they can be avoided in the future.

Breathing Flow Waveform was assumed to be sinusoidal at a frequency equal to the dominant frequency evaluated from Fourier analysis of the lung volume signal recorded from impedance plethysmography during PET scan used to measure regional ventilation distribution. Therefore, this estimated flow waveform is a first order approximation of the actual flow, and it should not result in substantial differences in estimates of peripheral resistance. Deviations from the actual flow waveform can be represented by additional sinusoids of lower amplitude at frequencies other than the dominant frequency, which should result in a small effect on the estimated pressure losses.

Regional Lung Compliance was estimated from total lung compliance and regional changes in sublobar gas volumes derived from HRCT images. Total lung compliance was not measured, but was estimated for each subject based on their lung volume assuming a population-based specific compliance (sC) and an FRC-to-TLC ratio, determined from the subjects body mass index (BMI) [42]. This method allowed us to arrive at a first order approximation of a subject-specific total lung compliance, which can be measured in future studies.

Dead Space Ventilation In order to compute total flow along airways from alveolar ventilation per unit of gas volume ($s\dot{V}_A$), we need an estimate of dead space ventilation (\dot{V}_D). Hardman *et al.* showed in a modeling analysis that maximum VD/VT under normal physiological conditions was approximately 1/3 [31]. Therefore, we assumed VD/VT ratio to be 1/3 and equal for all sublobar regions. In reality, regional dead space ventilation is difficult to estimate and may differ between regions depending on several factors. For example, intraregional gas mixing, anatomical volumes of airway feeding sublobar regions, characteristics of regional airflow, or incomplete gas mixing between inhaled and alveolar gas can affect the efficiency of gas exchange, and thus our estimates of regional airflow from PET scans. Although studies by Wellman *et al.* [106] and Simon *et al.* [89] demonstrated a high degree of correlation between $s\dot{V}_A$ and specific alveolar volume change during breathing in animals, the effect of this assumption on our estimates has to be further investigated in

humans.

Pleural Pressure (P_{pl}) When either the pleural pressure (P_{pl}) or total lung resistance is known, the problem of determining peripheral resistance is well-defined and has a unique solution. Unfortunately, neither parameter was available in our data set suggesting that there could be infinite numbers of solutions for R_p s that can predict the observed regional distribution of ventilation. Hence, to evaluate regional R_p s with certainty using our approach, P_{pl} or total lung resistance needs to be measured or specified. Despite such limitation, we investigated whether using a fixed value of P_{pl} within a physiological range for all subjects could offer reasonable estimations of R_p . Although we found that, for each subject, most of the values of $sG_{p,i}$ from the 19 pathways fell within a bounded range, there was usually an outlier with either a negative or a very high positive value of $sG_{p,i}$ (more than an order of magnitude higher than the population mean). This outlier was identified to be from the pathway with the highest total pressure drop predicted by the model that ignored the presence of peripheral resistance (Model 2). Values of P_{pl} less than that pressure would give unrealistic negative values of R_p , and values above that pressure but too low would yield exaggerated values of $sG_{p,i}$ for that pathway compared with the rest. In retrospective, it is clear that because different people were breathing with different tidal volumes and frequencies, P_{pl} could not have been the same for all subjects.

Guided by this insight, we tested another method of selecting P_{pl} based on the assumption that the variance of the distribution of $sG_{p,i}$ at baseline for a given subject should not be greatly affected with the exclusion or inclusion of any one pathway. As P_{pl} was incrementally raised above the minimum value yielding nonzero $sG_{p,i}$, the mean-normalized variance (CV^2) of the distribution of $sG_{p,i}$ decreased and eventually converged to that of the distribution without the outlier. We chose the P_{pl} at which CV^2 fell within 20% of that excluding the outlying pathway. 20% was the typical change of CV^2 observed after excluding any other pathway from the distribution. This assumption allows the variability of $sG_{p,i}$ within pathways but implies a distribution without a single outlier.

In addition, we assumed MCh challenge resulted in a doubling of P_{pl} in both groups. For

a constant flow rate, this corresponds to a doubling in the magnitude of lung impedance, observed in studies of similar protocols conducted in our research lab. However, the increase in P_{pl} may have been different among individuals. In fact, if bronchoconstriction caused an increase in P_{pl} that was higher in AS than NA subjects, the values of R_p in AS would have been higher than those reported in this paper. Although we cannot prove that these assumptions are valid and, for that matter, that the selected P_{pl} represented the actual P_{pl} value on a given subject, the following results suggest that our selected P_{pl} is reasonable.

First, global values of lung specific conductance measured in humans with ages ranging from 4 to 87 years of age are around $0.2 \text{ [cmH}_2\text{O s]}^{-1}$ [7]. This compares extremely well with the values of the lung specific conductance calculated from our model as the volume-normalized inverse of the real component of total lung impedance without upper airways (average of 0.10 ± 0.05 SD for NA and 0.08 ± 0.04 for AS at baseline).

A second set of data suggesting that our estimates of R_p are reasonable was from the estimated values of R_p/R_T derived from theoretical calculations of airway resistance per generation by Pedley [74] in a Weibel symmetric tree. The sum of the resistances of the 4th generation and beyond in that model accounted for 0.86 of the total sum of resistances for the full tree assuming laminar flow or 0.63 for the case with a flow rate of 10 L/min. Our estimates of R_p/R_T at baseline ranged from 0.75–0.99 (median of 0.97). Although these estimates are larger than those from Pedley's model, they are not unrealistic because they came from imaging in vivo airways that had a baseline smooth muscle tone. In contrast, airway geometry for Pedley's model was derived from cadaver castings of airways without any smooth muscle tone and likely having lower peripheral resistance.

Techniques using a retrograde catheter, alveolar capsules, and wedged bronchoscope have been used to measure resistance of peripheral airways in human lungs [97, 104], rabbits [78], and dogs [52]. Values of peripheral resistance obtained from these techniques are also consistent with ours. For example, using the wedged bronchoscope technique, Wagner and colleagues [104] measured peripheral resistance in asymptomatic asthmatic subjects at baseline and after histamine challenge. They found that R_p of asthmatic subjects at baseline

was higher than that of normal subjects (the average baseline R_p in asthmatic was at least 3 times that in normal subjects) and R_p increased significantly after the challenge. Romero and Ludwig [78] used alveolar capsules glued to the pleura in rabbit lungs to measure tissue viscance, which was thought to, in part, include peripheral resistance. They found that the contribution of tissue viscance to total lung resistance was $65\% \pm 15\%$ at baseline and increased to $84\% \pm 12\%$ after challenge with MCh aerosols. These data sets give additional support to our estimates of P_{pl} and R_p s. Clearly, measurements of P_{pl} (using esophageal balloon techniques) or total lung specific conductance are necessary in order to obtain unique estimates of R_p . Furthermore, future studies can greatly benefit from direct measurements of sC and dead space (using the Fowler technique).

In summary, this paper presents an image-based, subject-specific modeling approach including PET and HRCT imaging to estimate structural and functional parameters of subjects at baseline and during bronchoconstriction. Measurements of central airway morphometry, derived from HRCT images, and ventilation distribution, derived from PET scans, were combined to yield estimates of peripheral resistance of anatomically defined sublobar regions. This method may aid in evaluating and understanding of regional differences in the constriction of peripheral airways in vivo. Data obtained from this approach may also help in identifying mechanisms responsible for the location and strength of peripheral airway obstruction in a subject-specific manner without requiring in vivo measurements of small airways, which are limited by imaging spatial resolution. It may also offer insights into the regional physiology of distal airways in other lung diseases.

4.2 Topographic Modulation of Peripheral Airway Response in Asthma

4.2.1 Introduction

Studying the effect of regional differences in respiratory function on the distribution of ventilation during bronchoconstriction may help identify a mechanism related to excessive air-

way response in asthma. During quiet breathing, the distribution of ventilation in normal lungs was known to be determined by differences in regional compliance of the expanding parenchyma [64], which varied based on gravitational dependency. However, from imaging studies during a simulated asthma attack, it is clear that the distribution of ventilation is patchy with contiguous regions of very low ventilation compared with the rest of the lung [100, 101, 1, 21]. The existence of patchiness was likely due to elevated airway resistance with heterogeneous airway narrowing. Modeling studies have provided insights that complex interactions between airways and their surrounding parenchyma in an interlinked branching structure can lead to the emergence of severe heterogeneity without existing asymmetries between branches [109].

In addition, the presence of structural heterogeneity should initiate and exaggerate the emergence of patchiness and define the anatomical location of ventilation defects. For example, during breathing, airway caliber is determined by a dynamic equilibrium of forces acting on the airway smooth muscle (ASM). Based on experiments on ex vivo ASM strips, it was observed that dynamic stretch of activated muscles reduced its average constrictive force. Similarly, application of dynamic forces on activated muscles increased its length. Given that the parenchymal tethering forces resulted in the dynamic stretch of the airway wall during breathing, one could expect that regions experiencing lower tidal distensions of the parenchyma could preferentially constrict compared to those subjected to higher tidal parenchymal distension. One could postulate that asymmetry caused by gravity-oriented gradients in lung expansion could contribute to the preferential clustering of constricted airways in less expanded, gravity-dependent regions of the lung. The anatomical location of patchiness could also be driven by the heterogeneity in the activation of ASM caused by the heterogeneous responsiveness of ASM or uneven distribution of allergens. In a simulated asthma attack, this would correspond to an uneven dosing of airway walls by an aerosolized agonist such as Methacholine (MCh), whereby regions with high agonist doses would drive the local formation of patchiness.

Here we explore the extent to which these sources of asymmetry may modulate the topo-

graphical distribution of peripheral airway constriction. To accomplish this, we developed a multi-modality image-based (PET-CT), patient-specific modeling approach. This was used to study subjects with and without asthma ($n=7$, $n=8$) as follows: HRCT images of their lungs and dynamic PET scans of ^{13}NN gas washout were obtained before and during a simulated asthma attack by inhalation of aerosolized MCh.

Dynamic lung volume was monitored by impedance plethysmography (SomnoStarPT, SensorMedics Corp, Yorba Linda, CA). HRCT images were obtained during breath hold at their mean lung volume during breathing before each PET scan, and at maximal inhalation during the simulated asthma attack. For each HRCT image, airway tree morphometry was defined and tissue and gas volumes of sublobar regions ($n = 19$) were obtained using Pulmonary Workstation 2.0 software (VIDA diagnostics, Iowa City, IA (Fig. 4-8A)). From each PET scan, specific ventilation ($s\dot{V}$) of each sublobar region was estimated from the ^{13}NN washout rate [103].

A lumped parameter network model of lung mechanics was created based on the patient-specific airway tree topology (Fig. 4-8B). Model characteristics G_c (conductance of each central airway ($n = 35$)), C_a (apparent compliance), Δ_P (driving pressure) and \dot{V} (airflow) were derived from the scans. Airflow through the trachea at the beginning of subjects airway tree was assumed to be sinusoidal at a frequency (f_b) measured by impedance plethysmography. From this model, elastic admittance (Y_E), peripheral airway resistance (R_p), and corner frequency (f_c) of the pathway leading to each sublobar region were derived for conditions before and during bronchoconstriction caused by the simulated asthma attack. Regional gas volume per unit tissue of each sublobar region parenchymal distension was characterized by its peak (δ_P), tidal amplitude (δ_T), and inspiratory distending capacity (δ_{IC}) (Fig. 4-8B).

Our study aims were to:

- Evaluate the extent to which compliance/elastance and central airway conductance may determine the topographic distribution of ventilation,

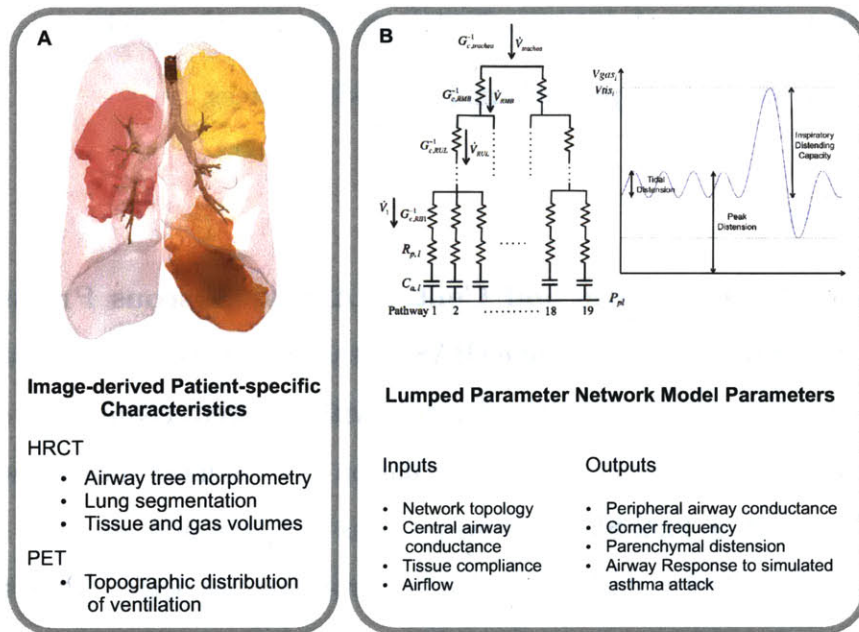


Figure 4-8: **A** 3D volume renders of the lung, airway tree and 3 representative sublobar regions and patient-specific parameters derived from HRCT and PET images. **B** Structure of the lumped parameters network model of the lung, corresponding lumped elements in each pathway, and regional parenchymal distension ($V_{gas,i}/V_{tis,i}$). Input and output parameters of the lumped parameter network model previously presented in section 4.1 are listed below 4-8.

- Estimate the value of peripheral airway resistance necessary to fully explain such ventilation distribution, and
- Compute the correlation between the regional response of peripheral airways to induced bronchoconstriction and the following sources of heterogeneity:
 1. δ_{IC} , as a surrogate of airway dosing of MCh.
 2. δ_T , as a surrogate of dynamic stretch on the smooth muscle,
 3. δ_P , as a surrogate of parenchymal distending forces,

4.2.2 Results

Contribution of Tissue Elastic and Central Airway Viscous Pressure Drops to Ventilation Distribution At baseline (BASE), the specific ventilation predicted ($s\dot{V}_{pred}$) from a network consisting only of elastic elements with apparent compliance of C_a was positively correlated with the regional specific ventilation ($s\dot{V}$) in most subjects without asthma (NA) ($n = 7$; $R = 0.79 \pm 0.02$ SEM). However, this was true only in a few asthmatic subjects (AS) ($n = 3$; $R = 0.80 \pm 0.01$ SEM). During bronchoconstriction (BC), this correlation disappeared for most subjects except for 2 NA and 2 AS subjects. Example plots of $s\dot{V}$ vs. $s\dot{V}_{pred}$ are shown in Fig. 4-9A and 4-9B. The sum of square (SS) defined as the relative difference between the mean normalized $s\dot{V}$ and $s\dot{V}_{pred}$ from the network consisting only of C_a increased after Mch challenge in NA ($P=0.003$, paired t -test), but not in AS subjects. During BC, SS of the model that included G_c was significantly lower than SS of the previous model ($P<0.05$). No difference in SS of the two models was found at BASE.

Lack of prediction of the elastic model was related to heterogeneity Values of peripheral resistance (R_p) were computed so that values of $s\dot{V}$ vs. $s\dot{V}_{pred}$ would be identical. To investigate the reason the model consisting only of elastic elements could not predict the ventilation well during BC, SS of the elastic model was correlated with the corner frequency (f_c) normalized by breathing frequency (f_b) (f_c/f_b). Note that f_c/f_b in each pathway was

identical to the ratio of elastic to resistive pressure drops in that pathway. Interestingly, we found that the heterogeneity, not the magnitude, of f_c/f_b was highly correlated with SS of model consisting only of elastic elements ($R=0.88$) (Fig. 4-9).

Sources of Heterogeneity and Regional Response of Peripheral Airways First, to study the relationship between the airway dosing of Mch agonists and responses in peripheral airways caused by BC, we correlated δ_{IC} with $\frac{R_{p,BASE}}{R_{p,CHAL}}$, a parameter that ranged from 0 (maximal constriction) to 1 (no response). Even though a negative correlation was expected, it was not found in any subject (See Fig. 4-10 and 4-11).

The second source of heterogeneity investigated that could affect the peripheral airway response was dynamic stretch on airway smooth muscle. We correlated δ_T with $\frac{R_{p,BASE}}{R_{p,CHAL}}$. To our surprise, we found that δ_T and $\frac{R_{p,BASE}}{R_{p,CHAL}}$ were not positively correlated as expected (Fig. 4-12 and 4-13).

Lastly, we studied another source of heterogeneity that could affect the peripheral airway response related to parenchymal tethering using δ_P as a surrogate for parenchymal distending forces. We found that in most NA subjects ($n = 6$), $\frac{R_{p,BASE}}{R_{p,CHAL}}$ and δ_P were positively correlated as expected ($R = 0.68 \pm 0.07$ SEM) (Fig. 4-14). This positive correlation was significant only in two AS subjects with highest PC20 (least response to Mch challenge) (Fig. 4-15).

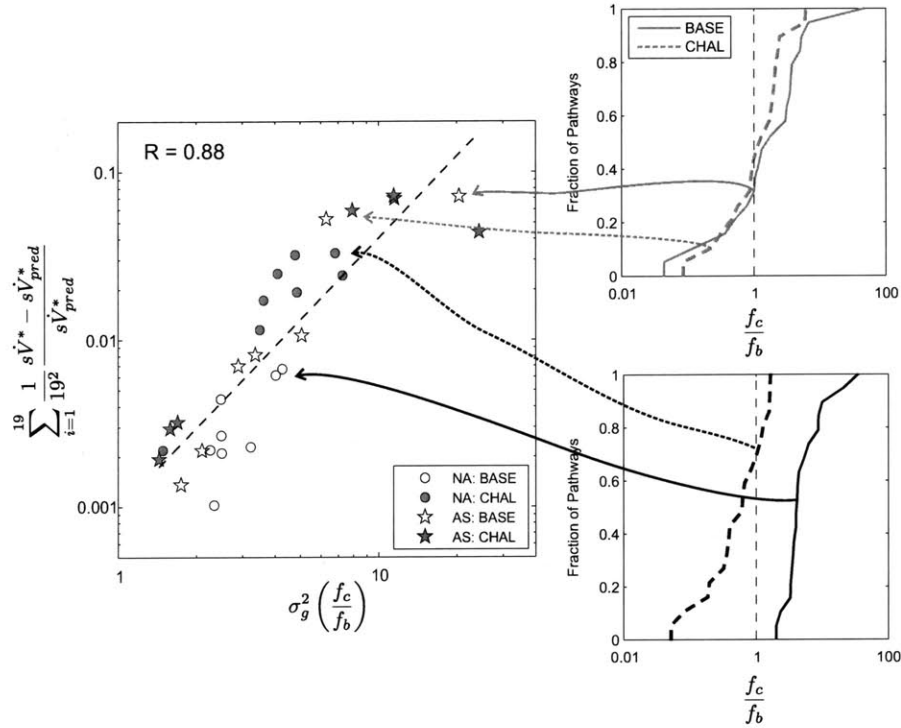


Figure 4-9: The sum of square (SS) of the relative difference between the mean normalized $s\dot{V}$ and $s\dot{V}_{pred}$ was plotted against the geometric variance of the normalized corner frequency (f_c/f_b). Each data point represents data from an individual subject at baseline (BASE-white) and after MCh challenge (CHAL-grey). Corresponding cumulative distributions from two representatives are plotted on the right with arrow indicating individual data points on the main plot. SS was highly correlated with geometric variance of f_c/f_b ($R=0.88$). Most geometric variance of f_c/f_b increased in NA subjects after the challenge, whereas the trend in the AS group is not clear.

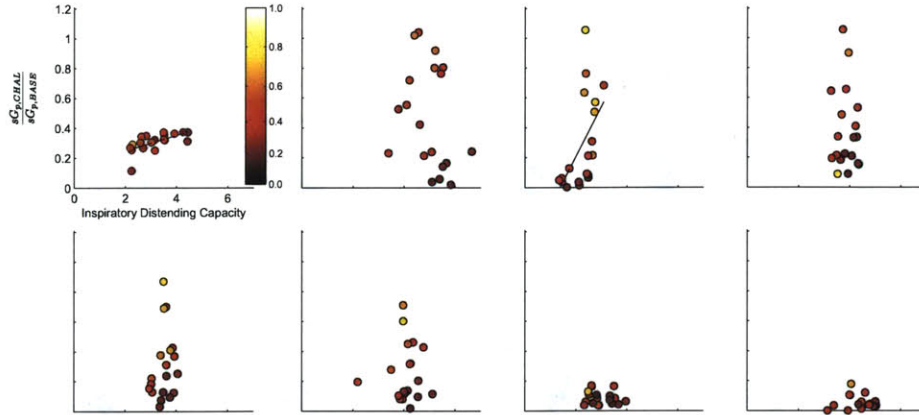


Figure 4-10: Parenchymal distending capacity δ_{IC} and peripheral airway response $\frac{R_{p,BASE}}{R_{p,CHAL}}$ in subjects without asthma (NA). We expected that regions of increased δ_{IC} should have an increased peripheral airway response (negative correlation). However, we found no significant negative correlation in any NA subjects.

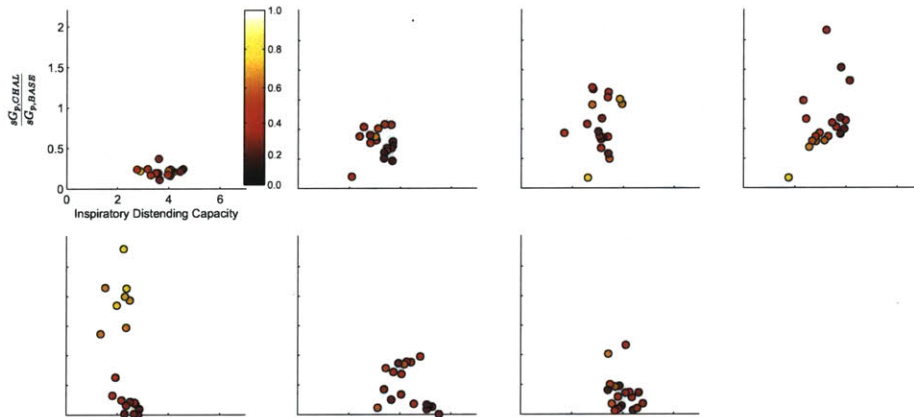


Figure 4-11: Parenchymal distending capacity δ_{IC} and peripheral airway response $\frac{R_{p,BASE}}{R_{p,CHAL}}$ in subjects without asthma. We expected that regions of increased δ_{IC} should have an increased peripheral airway response (negative correlation). However, we found no significant negative correlation in any AS subjects.

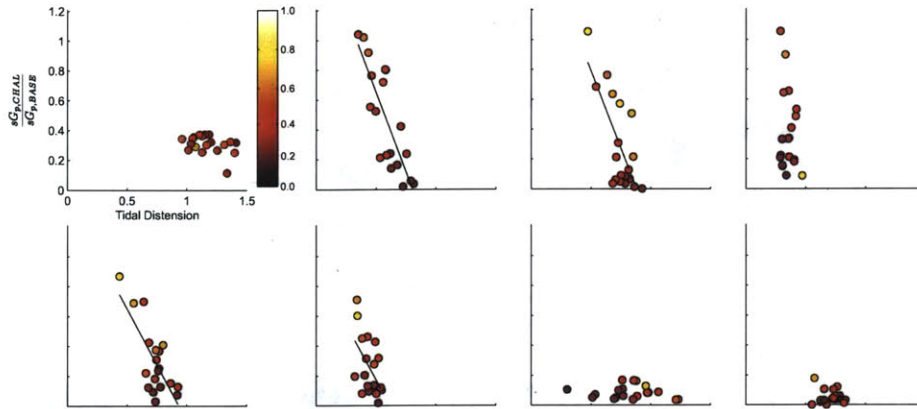


Figure 4-12: Tidal distension δ_T and peripheral airway response $\frac{R_{p,BASE}}{R_{p,CHAL}}$ in subjects without asthma. There was no positive correlation between tidal distension and peripheral airway response in any subject.

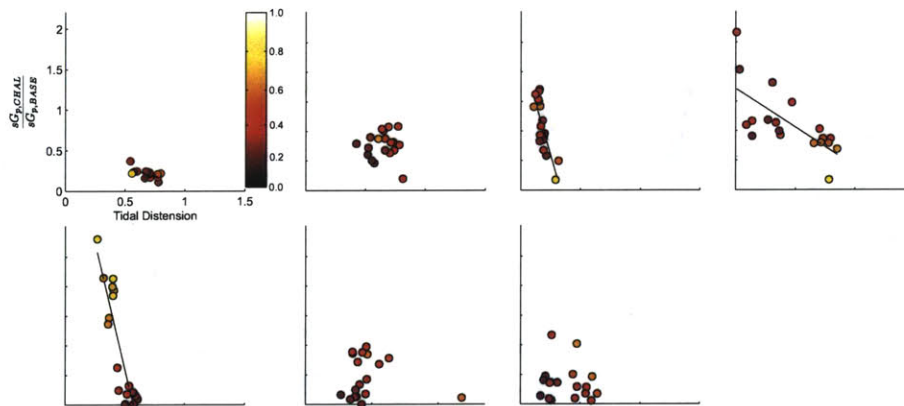


Figure 4-13: Tidal distension δ_T and peripheral airway response $\frac{R_{p,BASE}}{R_{p,CHAL}}$ in subjects with asthma. Similarly, there was no positive correlation between tidal distension and peripheral airway response in any subject.

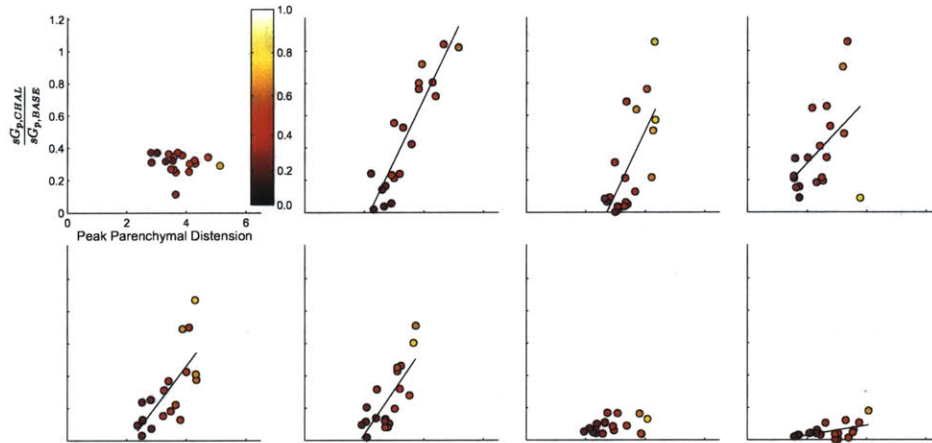


Figure 4-14: Peak parenchymal distension δ_P and peripheral airway response $\frac{R_{p,BASE}}{R_{p,CHAL}}$ in subjects without asthma. In 6 out of 8 NA subjects, there was a strong positive correlation suggesting that regions with high peak parenchymal distension had smaller response to MCh ($R = 0.68 \pm 0.07$ SEM).

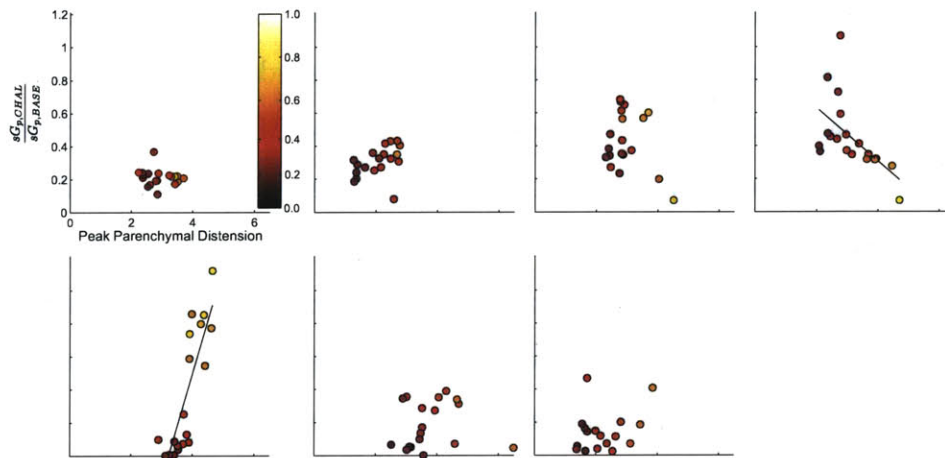


Figure 4-15: Peak parenchymal distension δ_P and peripheral airway response $\frac{R_{p,BASE}}{R_{p,CHAL}}$ in subjects with asthma. There was a significant positive correlation in two AS subjects with the least response to Mch challenge (highest PC20).

4.2.3 Discussion

Our study demonstrates that the effect of elastic and central airway viscous pressure drops on the distribution of airflow within the lung during an induced asthma attack is minimal compared to the effect of viscous pressure drops in peripheral airways. We estimated the peripheral airway resistance such that the predicted ventilation will match the observed ventilation derived from PET scans. Using this information, we investigated the correlation between different sources of heterogeneity that may give rise to the observed changes in peripheral airway resistance. We found that the source of heterogeneity associated with peripheral airway constriction in subjects without asthma was peak parenchymal distension, instead of tidal distension. Moreover, the amount of MCh dosing was also not associated with the degree of peripheral airway constriction. The distribution of ventilation in healthy lungs was dependent on tissue elastic pressure drops, which were linearly related to tissue compliance, and hence, the change in regional gas volume. This change in regional gas volume was postulated to be directly associated with tidal aeration and lung strain [6, 25].

It was taken that the distribution of inspired gas in the lung would describe regional distribution of ventilation in healthy lungs [64]. However, the contribution of central or peripheral airway resistance should also affect the regional distribution of ventilation particularly during a simulated asthma attack. Macklem and Mead concluded based on their measurements of resistance of peripheral airways that were at most 15% of the total lung resistance that central airway constriction would contribute greatly to a marked increase in pulmonary resistance [61]. However, we found the opposite to be true. The additional contribution of central airway viscous pressure drops on the distribution of ventilation was small and unable to explain the distribution during a simulated asthma attack. In fact, airway constriction occurs mostly in the periphery. The resistance of peripheral airways contributed to the majority of the total resistance at baseline and during bronchoconstriction in lungs of open-chest dogs [55] and rabbit [78], as well as in vivo human lung (journal in review). We postulated that this could be due to factors such as the increased secretion (inflammatory exudate or mucus) that might have replaced surfactant resulting in the instability of closure

in small airways during an induced bronchoconstriction [49]. Since small airways are less able to clear secretions due to a lack of cilia and a lack of high gas velocity generated during cough, it can exacerbate airway closure.

Our data suggests that pressure drops across peripheral airways are crucial in determining ventilation to sublobar regions. Additionally, we found that the extent to which peripheral resistance impacted regional ventilation was determined by the heterogeneity in the distribution of normalized corner frequency, that is the impact of peripheral resistance on ventilation was increased in patients with increased heterogeneity in the distribution of corner frequency. The effect of the three sources of heterogeneityairway dosing of Mch, tidal stretch on airway smooth muscle (ASM), and peak parenchymal forceson peripheral airway response during a simulated asthma attack was investigated.

First, using the inspiratory distending capacity (δ_{IC}) as a surrogate for Mch dosing, we found no significant correlation between δ_{IC} and peripheral airway response in any subject. This suggests that the distribution of Mch aerosols may not be the dominant source of the preferential clustering of airway constriction during bronchoconstriction in distal lungs. However, the lack of such correlation could be because the amount of Mch aerosols delivered in each sublobar region could be different from that deposited on airway walls, possibly due to aerosol agglomeration or other secondary phenomena.

Second, Fredberg et al. conducted a study on an isolated maximally contracted bovine tracheal smooth muscle subjected to tidal stretches and found that the steady state contractile ASM force reduced when the tidal stretch/strain increased [23]. Based on this experimental study, one can infer that airways inside a region with high tidal distension should have lower ASM force, and thus, less peripheral airway constriction compared to those in regions with low tidal distension. If this hypothesis holds in vivo, we should observe a preferential clustering of peripheral airway constriction in regions with low tidal distension (positive correlation). However, there was no significant positive correlation in any subject.

Two independent studies by Noble et al. [68] and Laprad et al. [51] conducted on intact airways could explain this finding. They demonstrated that the lack of tidal oscillations

in an intact airway did not result in an increase in airway response. It is possible that the hypothesis that oscillatory strains caused the breakage of actin-myosin cross bridges and reduction in ASM stiffness and contractile force was only applicable to the ASM strip, but not the intact airway. This could be because during activation in an intact airway, ASM shorted and thus moved away from the tensile strain required for yielding, making the argument of the breakage of actin-myosin crossbridges invalid in intact airways [50].

Additionally, opposite to what we expected from the hypothesis inferred from studies by Fredberg et al., we found that a region with high tidal distension had more peripheral airway constriction than that with low tidal distension in some subjects (4 asthmatic and 4 non-asthmatic subjects). This unexpected correlation could potentially be explained by a Chapman et al. study [16]. Their studies reported that in response to increased cyclic stretch, the production of reactive oxygen species (ROS) in lung epithelial cells increased. This increase in the production of ROS was hypothesized to induce inflammatory response [16] that could be related to increased airway responsiveness.

The third source of heterogeneity investigated was the regional peak parenchymal distension as a surrogate for peak parenchymal force. In a sublobar region with high peak parenchymal distension had reduced peripheral airway responses to Mch than in a region with low peak parenchymal distension in almost every non-asthmatic subject. Here we discussed two published studies that support our findings. The first is a study conducted on non-asthmatic subjects by Ding et al. investigating the impact of the increased lung volume (increased peak parenchymal distension) on changes in total lung resistance during a Mch-induced bronchoconstriction [20]. They found that, in healthy lungs, the increase in total lung resistance during bronchoconstriction was significantly higher at lower lung volume where the peak/average parenchymal distension was low. Given that most constriction in the lung occurs in the peripheral airways, their finding suggests that the heterogeneity in peak/average parenchymal distension was determined by the degree of peripheral airway constriction in healthy lungs. Worth noting was the fact that this observation was not true in almost all asthmatic subjects except one that turned out to be the least responsive to

Mch challenge (largest PC20).

In conclusion, this finding suggests that the ability for parenchymal distension to prevent airways from excessive narrowing during bronchoconstriction may be compromised in asthmatic lungs. Such reduced ability of the parenchyma could be due to the decreased interdependence between an airway and surrounding parenchyma. Several hypotheses that could cause reduced interdependence between airway and parenchyma include remodeling of peribronchial adventitia [73, 107, 59], a potential increase in parenchymal stiffness [88, 5, 10], or airway remodeling [19]. For example, in asthmatic airways where remodeling of the airway wall is prevalent, the transmission of stress from the expanding parenchyma to dilate airway lumen would be limited because of the thickened wall. Our work has the potential to help identify mechanisms responsible for excessive bronchoconstriction in asthma and offer suggestions for personalized treatment of asthma.

THIS PAGE INTENTIONALLY LEFT BLANK

Bibliography

- [1] T.A. Altes, P.L. Powers, J. Knight-Scott, G. Rakes, T.A.E. Platts-Mills, E.E. de Lange, B.A. Alford, J.P. Mugler III, and J.R. Brookeman. Hyperpolarized ^3He mr lung ventilation imaging in asthmatics: preliminary findings. Journal of Magnetic Resonance Imaging, 13(3):378–384, 2001.
- [2] S.D. Amin, A. Majumdar, U. Frey, and B. Suki. Modeling the dynamics of airway constriction: effects of agonist transport and binding. Journal of Applied Physiology, 109(2):553–563, 2010.
- [3] R.C. Anafi and T.A. Wilson. Airway stability and heterogeneity in the constricted lung. Journal of Applied Physiology, 91(3):1185–1192, 2001.
- [4] EM Baile, A. Sotres-Vega, and PD Pare. Airway blood flow and bronchovascular congestion in sheep. European Respiratory Journal, 7(7):1300–1307, 1994.
- [5] J.H.T. Bates and K.R. Lutchen. The interface between measurement and modeling of peripheral lung mechanics. Respiratory physiology & neurobiology, 148(1):153–164, 2005.
- [6] CL Bellardine Black, AM Hoffman, LW Tsai, EP Ingenito, B. Suki, DW Kaczka, BA Simon, and KR Lutchen. Impact of positive end-expiratory pressure during heterogeneous lung injury: insights from computed tomographic image functional modeling. Annals of biomedical engineering, 36(6):980–991, 2008.

- [7] W.A. Briscoe and A.B. Dubois. The relationship between airway resistance, airway conductance and lung volume in subjects of different age and body size. Journal of Clinical Investigation, 37(9):1279, 1958.
- [8] R.H. Brown, C.J. Herold, C.A. Hirshman, E.A. Zerhouni, and W. Mitzner. Individual airway constrictor response heterogeneity to histamine assessed by high-resolution computed tomography. Journal of Applied Physiology, 74(6):2615–2620, 1993.
- [9] R.H. Brown, D.W. Kaczka, K. Fallano, S. Chen, and W. Mitzner. Temporal variability in the responses of individual canine airways to methacholine. Journal of Applied Physiology, 104(5):1381–1386, 2008.
- [10] R.H. Brown, D.W. Kaczka, and W. Mitzner. Effect of parenchymal stiffness on canine airway size with lung inflation. PloS one, 5(4):e10332, 2010.
- [11] R.H. Brown and W. Mitzner. Airway response to deep inspiration: role of nitric oxide. European Respiratory Journal, 22(1):57–61, 2003.
- [12] R.H. Brown, D.B. Pearse, G. Pyrgos, M.C. Liu, A. Togias, and S. Permutt. The structural basis of airways hyperresponsiveness in asthma. Journal of Applied Physiology, 101(1):30–39, 2006.
- [13] R.H. Brown, E.A. Zerhouni, and W. Mitzner. Variability in the size of individual airways over the course of one year. American journal of respiratory and critical care medicine, 151(4):1159–1164, 1995.
- [14] V. Brusasco, E. Crimi, G. Barisione, A. Spanevello, J.R. Rodarte, and R. Pellegrino. Airway responsiveness to methacholine: effects of deep inhalations and airway inflammation. Journal of Applied Physiology, 87(2):567–573, 1999.
- [15] L. Campana, J. Kenyon, S. Zhalehdoust-Sani, Y.S. Tzeng, Y. Sun, M. Albert, and K.R. Lutchen. Probing airway conditions governing ventilation defects in asthma

- via hyperpolarized mri image functional modeling. Journal of Applied Physiology, 106(4):1293–1300, 2009.
- [16] K.E. Chapman, S.E. Sinclair, D. Zhuang, A. Hassid, L.P. Desai, and C.M. Waters. Cyclic mechanical strain increases reactive oxygen species production in pulmonary epithelial cells. American Journal of Physiology-Lung Cellular and Molecular Physiology, 289(5):L834–L841, 2005.
- [17] D.W. Cockcroft and B.E. Davis. Deep inhalation bronchoprotection in asthma: correlation with airway responsiveness. The Journal of allergy and clinical immunology, 117(4):951, 2006.
- [18] RO Crapo, R. Casaburi, AL Coates, PL Enright, JL Hankinson, CG Irvin, NR MacIntyre, RT McKay, JS Wanger, SD Anderson, et al. Guidelines for methacholine and exercise challenge testing-1999. this official statement of the american thoracic society was adopted by the ats board of directors, july 1999. American journal of respiratory and critical care medicine, 161(10):1023–1029, 2000.
- [19] D.E. Davies, J. Wicks, R.M. Powell, S.M. Puddicombe, and S.T. Holgate. Airway remodeling in asthma: new insights. Journal of allergy and clinical immunology, 111(2):215–225, 2003.
- [20] D.J. Ding, JG Martin, and PT Macklem. Effects of lung volume on maximal methacholine-induced bronchoconstriction in normal humans. Journal of Applied Physiology, 62(3):1324–1330, 1987.
- [21] S.B. Fain, G. Gonzalez-Fernandez, E.T. Peterson, M.D. Evans, R.L. Sorkness, N.N. Jarjour, W.W. Busse, and J.E. Kuhlman. Evaluation of structure-function relationships in asthma using multidetector ct and hyperpolarized he-3 mri. Academic radiology, 15(6):753–762, 2008.
- [22] KE Finucane and HJ Colebatch. Elastic behavior of the lung in patients with airway obstruction. Journal of applied physiology, 26(3):330–338, 1969.

- [23] J.J. Fredberg, D. Inouye, B. Miller, M. Nathan, S. Jafari, S.H. Raboudi, J.P. Butler, and S.A. Shore. Airway smooth muscle, tidal stretches, and dynamically determined contractile states. American journal of respiratory and critical care medicine, 156(6):1752–1759, 1997.
- [24] JJ Fredberg, KA Jones, M. Nathan, S. Raboudi, YS Prakash, SA Shore, JP Butler, and GC Sieck. Friction in airway smooth muscle: mechanism, latch, and implications in asthma. Journal of Applied Physiology, 81(6):2703–2703, 1996.
- [25] M.K. Fuld, R.B. Easley, O.I. Saba, D. Chon, J.M. Reinhardt, E.A. Hoffman, and B.A. Simon. Ct-measured regional specific volume change reflects regional ventilation in supine sheep. Journal of Applied Physiology, 104(4):1177–1184, 2008.
- [26] H.L. Gillis and K.R. Lutchen. Airway remodeling in asthma amplifies heterogeneities in smooth muscle shortening causing hyperresponsiveness. Journal of Applied Physiology, 86(6):2001–2012, 1999.
- [27] H.L. Gillis and K.R. Lutchen. How heterogeneous bronchoconstriction affects ventilation distribution in human lungs: a morphometric model. Annals of biomedical engineering, 27(1):14–22, 1999.
- [28] S.J. Gunst. Contractile force of canine airway smooth muscle during cyclical length changes. Journal of Applied Physiology, 55(3):759–769, 1983.
- [29] D. Halpern and JB Grotberg. Surfactant effects on fluid-elastic instabilities of liquid-lined flexible tubes: a model of airway closure. Journal of biomechanical engineering, 115:271, 1993.
- [30] Z. Hantos, B. Daroczy, B. Suki, S. Nagy, and JJ Fredberg. Input impedance and peripheral inhomogeneity of dog lungs. Journal of Applied Physiology, 72(1):168–178, 1992.

- [31] J.G. Hardman and A.R. Aitkenhead. Estimating alveolar dead space from the arterial to end-tidal co2 gradient: a modeling analysis. Anesthesia & Analgesia, 97(6):1846–1851, 2003.
- [32] R.S. Harris, T. Winkler, N. Tgavalekos, G. Musch, M.F.V. Melo, T. Schroeder, Y. Chang, and J.G. Venegas. Regional pulmonary perfusion, inflation, and ventilation defects in bronchoconstricted patients with asthma. American journal of respiratory and critical care medicine, 174(3):245–253, 2006.
- [33] E.A. Hoffman. Physiology and function from multidimensional images. Medical imaging, Bellingham, Wash, 1997.
- [34] J.H. Holmes, R.L. O’Halloran, E.K. Brodsky, T.A. Bley, C.J. Francois, J.V. Velikina, R.L. Sorkness, W.W. Busse, and S.B. Fain. Three-dimensional imaging of ventilation dynamics in asthmatics using multiecho projection acquisition with constrained reconstruction. Magnetic Resonance in Medicine, 62(6):1543–1556, 2009.
- [35] J.H. Holmes, R.L. O’Halloran, E.K. Brodsky, Y. Jung, W.F. Block, and S.B. Fain. 3d hyperpolarized he-3 mri of ventilation using a multi-echo projection acquisition. Magnetic Resonance in Medicine, 59(5):1062–1071, 2008.
- [36] K. Horsfield, G. Dart, D.E. Olson, G.F. Filley, and G. Cumming. Models of the human bronchial tree. Journal of Applied Physiology, 31(2):207–217, 1971.
- [37] JMB Hughes, JB Glazier, JE Maloney, and JB West. Effect of lung volume on the distribution of pulmonary blood flow in man. Respiration physiology, 4(1):58–72, 1968.
- [38] National Instruments. Extract single tone information.
- [39] A.L. James, J.C. Hogg, L.A. Dunn, and P.D. Paré. The use of the internal perimeter to compare airway size and to calculate smooth muscle shortening. American Journal of Respiratory and Critical Care Medicine, 138(1):136–139, 1988.

- [40] A.L. James, PD Pare, and J.C. Hogg. Effects of lung volume, bronchoconstriction, and cigarette smoke on morphometric airway dimensions. Journal of Applied Physiology, 64(3):913–919, 1988.
- [41] A.L. James, P.D. Paré, and J.C. Hogg. The mechanics of airway narrowing in asthma. American Journal of Respiratory and Critical Care Medicine, 139(1):242–246, 1989.
- [42] R.L. Jones and M.M.U. Nzekwu. The effects of body mass index on lung volumes*. Chest, 130(3):827–833, 2006.
- [43] D.W. Kaczka, R.H. Brown, and W. Mitzner. Assessment of heterogeneous airway constriction in dogs: a structure-function analysis. Journal of Applied Physiology, 106(2):520–530, 2009.
- [44] D.W. Kaczka, E.P. Ingenito, B. Suki, and K.R. Lutchen. Partitioning airway and lung tissue resistances in humans: effects of bronchoconstriction. Journal of Applied Physiology, 82(5):1531–1541, 1997.
- [45] I.M. Katz, A.R. Martin, P.A. Muller, K. Terzibachi, C.H. Feng, G. Caillibotte, J. Sandeau, et al. The ventilation distribution of helium-oxygen mixtures and the role of inertial losses in the presence of heterogeneous airway obstructions. Journal of Biomechanics, 44(6):1137–1143, 2011.
- [46] V.J. Kelly, N.J. Brown, G.G. King, and B.R. Thompson. A method to determine in vivo, specific airway compliance, in humans. Medical and Biological Engineering and Computing, 48(5):489–496, 2010.
- [47] Indu Khurana. Essentials of Medical Physiology. Elsevier, 2008.
- [48] GG King, JD Carroll, NL Müller, KP Whittall, M. Gao, Y. Nakano, and PD Pare. Heterogeneity of narrowing in normal and asthmatic airways measured by hrct. European Respiratory Journal, 24(2):211–218, 2004.

- [49] M. Kraft. The distal airways: are they important in asthma? European Respiratory Journal, 14(6):1403–1417, 1999.
- [50] A.S. LaPrad and K.R. Lutchen. The dissolution of intact airway responsiveness from breathing fluctuations: what went wrong? Journal of Applied Physiology, 110(6):1506–1507, 2011.
- [51] A.S. LaPrad, T.L. Szabo, B. Suki, and K.R. Lutchen. Tidal stretches do not modulate responsiveness of intact airways in vitro. Journal of applied physiology, 109(2):295–304, 2010.
- [52] A.M. Lauzon, G. Dechman, and JHT Bates. On the use of the alveolar capsule technique to study bronchoconstriction. Respiration physiology, 99(1):139–146, 1995.
- [53] K. Li, X. Wu, D.Z. Chen, and M. Sonka. Optimal surface segmentation in volumetric images—a graph-theoretic approach. Pattern Analysis and Machine Intelligence, IEEE Transactions on, 28(1):119–134, 2006.
- [54] Bustinza A de Lucas N Carrillo A. Lopez-Herce J, Gari M. On pressure-controlled ventilation in severe asthma. Pediatric Pulmonology, 21(6):401–403, 1996.
- [55] M.S. Ludwig, P.V. Romero, and JH Bates. A comparison of the dose-response behavior of canine airways and parenchyma. Journal of Applied Physiology, 67(3):1220–1225, 1989.
- [56] K.R. Lutchen and H. Gillis. Relationship between heterogeneous changes in airway morphometry and lung resistance and elastance. Journal of Applied Physiology, 83(4):1192–1201, 1997.
- [57] K.R. Lutchen, A. Jensen, H. Atilah, D.W. Kaczka, E. Israel, B. Suki, and E.P. Ingenito. Airway constriction pattern is a central component of asthma severity. American journal of respiratory and critical care medicine, 164(2):207–215, 2001.

- [58] P.T. Macklem. Bronchial hyporesponsiveness*. Chest, 91(6 Supplement):189S–191S, 1987.
- [59] P.T. Macklem. A theoretical analysis of the effect of airway smooth muscle load on airway narrowing. American journal of respiratory and critical care medicine, 153(1):83–89, 1996.
- [60] P.T. Macklem. The physiology of small airways. American journal of respiratory and critical care medicine, 157(5):S181–S183, 1998.
- [61] P.T. Macklem and J. Mead. Resistance of central and peripheral airways measured by a retrograde catheter. Journal of applied physiology, 22(3):395–401, 1967.
- [62] A.T. Mariassy, H. Gazeroglu, and A. Wanner. Morphometry of the subepithelial circulation in sheep airways: effect of vascular congestion. American Journal of Respiratory and Critical Care Medicine, 143(1):162–166, 1991.
- [63] DS McCarthy and M. Sigurdson. Lung elastic recoil and reduced airflow in clinically stable asthma. Thorax, 35(4):298–302, 1980.
- [64] J. Milic-Emili, JAM Henderson, MB Dolovich, D. Trop, K. Kaneko, et al. Regional distribution of inspired gas in the lung. J Appl Physiol, 21(3):749–759, 1966.
- [65] RH Moreno, JC Hogg, PD Pare, et al. Mechanics of airway narrowing. The American review of respiratory disease, 133(6):1171, 1986.
- [66] K. Murata, H. Itoh, G. Todo, T. Itoh, M. Kanaoka, M. Furuta, K. Torizuka, et al. Bronchial venous plexus and its communication with pulmonary circulation. Investigative radiology, 21(1):24, 1986.
- [67] G. Musch, J.D.H. Layfield, R.S. Harris, M.F.V. Melo, T. Winkler, R.J. Callahan, A.J. Fischman, and J.G. Venegas. Topographical distribution of pulmonary perfusion and ventilation, assessed by pet in supine and prone humans. Journal of Applied Physiology, 93(5):1841–1851, 2002.

- [68] P.B. Noble, R.L. Jones, E.T. Needi, A. Cairncross, H.W. Mitchell, A.L. James, and P.K. McFawn. Responsiveness of the human airway in vitro during deep inspiration and tidal oscillation. Journal of Applied Physiology, 110(6):1510–1518, 2011.
- [69] PB Noble, DJ Turner, and HW Mitchell. Relationship of airway narrowing, compliance, and cartilage in isolated bronchial segments. Journal of Applied Physiology, 92(3):1119–1124, 2002.
- [70] G. Nucci, B. Suki, and K. Lutchen. Modeling airflow-related shear stress during heterogeneous constriction and mechanical ventilation. Journal of Applied Physiology, 95(1):348–356, 2003.
- [71] M. Okazawa, N. Müller, A.E. McNamara, S. Child, L. Verburgt, and P.D. Pare. Human airway narrowing measured using high resolution computed tomography. American journal of respiratory and critical care medicine, 154(5):1557–1562, 1996.
- [72] Hogg JC Okazawa M, Paré PD and Lambert RK. Mechanical consequences of remodeling of the airway wall. London: Academic, 1994.
- [73] PD Pare, BR Wiggs, A. James, JC Hogg, and C. Bosken. The comparative mechanics and morphology of airways in asthma and in chronic obstructive pulmonary disease. American Journal of Respiratory and Critical Care Medicine, 143(5 Pt 1):1189–1193, 1991.
- [74] TJ Pedley, RC Schroter, and MF Sudlow. The prediction of pressure drop and variation of resistance within the human bronchial airways. Respiration physiology, 9(3):387–405, 1970.
- [75] Fredburg J. Peslin R. Oscillation mechanics of the respiratory system, volume 3 of Handbook of Physiology. The Respiratory System. Mechanics of Breathing. Am. Physiol. Soc, 1986.
- [76] J.M. Reinhardt, N. D’Souza, and E.A. Hoffman. Accurate measurement of intrathoracic airways. Medical Imaging, IEEE Transactions on, 16(6):820–827, 1997.

- [77] M. Rietkerk, S.C. Dekker, P.C. De Ruiter, and J. Van De Koppel. Self-organized patchiness and catastrophic shifts in ecosystems. Science, 305(5692):1926–1929, 2004.
- [78] PV Romero and MS Ludwig. Maximal methacholine-induced constriction in rabbit lung: interactions between airways and tissue? Journal of Applied Physiology, 70(3):1044–1050, 1991.
- [79] A.P. Sarnaik, K.M. Daphtary, K.L. Meert, M.W. Lieh-Lai, and S.M. Heidemann. Pressure-controlled ventilation in children with severe status asthmaticus*. Pediatric Critical Care Medicine, 5(2):133, 2004.
- [80] F. Sasaki, Y. Saitoh, L. Verburgt, and M. Okazawa. Airway wall dimensions during carbachol-induced bronchoconstriction in rabbits. Journal of Applied Physiology, 81(4):1578–1583, 1996.
- [81] C.F. Schiller-Scotland, R. Hlawa, and J. Gebhart. Experimental data for total deposition in the respiratory tract of children. Toxicology letters, 72(1):137–144, 1994.
- [82] N. Scichilone, T. Kapsali, S. Permutt, and A. Togias. Deep inspiration-induced bronchoprotection is stronger than bronchodilation. American journal of respiratory and critical care medicine, 162(3):910–916, 2000.
- [83] N. Scichilone, R. Marchese, F. Catalano, A. Togias, A.M. Vignola, and V. Bellia. The bronchodilatory effect of deep inspiration diminishes with aging. Respiratory medicine, 98(9):838–843, 2004.
- [84] N. Scichilone, S. Permutt, and A. Togias. The lack of the bronchoprotective and not the bronchodilatory ability of deep inspiration is associated with airway hyperresponsiveness. American journal of respiratory and critical care medicine, 163(2):413–419, 2001.
- [85] N. Scichilone and A. Togias. The role of lung inflation in airway hyperresponsiveness and in asthma. Current allergy and asthma reports, 4(2):166–174, 2004.

- [86] S. Sell and E.E. Max. Immunology, immunopathology, and immunity. Amer Society for Microbiology, 2001.
- [87] X. Shen, MF Wu, RS Tepper, and SJ Gunst. Mechanisms for the mechanical response of airway smooth muscle to length oscillation. Journal of Applied Physiology, 83(3):731–738, 1997.
- [88] P.L. Silva, C.P. Passaro, V.R. Cagido, M. Bozza, M. Dolhnikoff, E.M. Negri, M. Morales, V.L. Capelozzi, W.A. Zin, and P.R.M. Rocco. Impact of lung remodelling on respiratory mechanics in a model of severe allergic inflammation. Respiratory physiology & neurobiology, 160(3):239–248, 2008.
- [89] B.A. Simon. Regional ventilation and lung mechanics using x-ray ct. Academic radiology, 12(11):1414–1422, 2005.
- [90] S. Sircar. Principles of medical physiology. Thieme Medical Pub, 2007.
- [91] G. Skloot and A. Togias. Bronchodilation and bronchoprotection by deep inspiration and their relationship to bronchial hyperresponsiveness. Clinical reviews in allergy and immunology, 24(1):55–71, 2003.
- [92] M.H. Tawhai, P. Hunter, J. Tschirren, J. Reinhardt, G. McLennan, and E.A. Hoffman. Ct-based geometry analysis and finite element models of the human and ovine bronchial tree. Journal of applied physiology, 97(6):2310–2321, 2004.
- [93] N.T. Tgavalekos, G. Musch, RS Harris, M.F.V. Melo, T. Winkler, T. Schroeder, R. Callahan, KR Lutchen, and JG Venegas. Relationship between airway narrowing, patchy ventilation and lung mechanics in asthmatics. European Respiratory Journal, 29(6):1174–1181, 2007.
- [94] N.T. Tgavalekos, M. Tawhai, R.S. Harris, G. Mush, M. Vidal-Melo, J.G. Venegas, and K.R. Lutchen. Identifying airways responsible for heterogeneous ventilation and

- mechanical dysfunction in asthma: an image functional modeling approach. Journal of Applied Physiology, 99(6):2388–2397, 2005.
- [95] M.J. Tobin. Principles and practice of mechanical ventilation. Shock, 26(4):426, 2006.
- [96] J. Tschirren, E.A. Hoffman, G. McLennan, and M. Sonka. Intrathoracic airway trees: segmentation and airway morphology analysis from low-dose ct scans. Medical Imaging, IEEE Transactions on, 24(12):1529–1539, 2005.
- [97] H. Van Brabandt, M. Cauberghe, E. Verbeken, P. Moerman, JM Lauweryns, and KP Van de Woestijne. Partitioning of pulmonary impedance in excised human and canine lungs. Journal of Applied Physiology, 55(6):1733–1742, 1983.
- [98] J. Venegas. Linking ventilation heterogeneity and airway hyperresponsiveness in asthma. Thorax, 62(8):653–654, 2007.
- [99] J.G. Venegas. Viscoelastic properties of the contracting detrusor. i. theoretical basis. American Journal of Physiology-Cell Physiology, 261(2):C355–C363, 1991.
- [100] J.G. Venegas, T. Schroeder, S. Harris, R.T. Winkler, and M.F.V. Melo. The distribution of ventilation during bronchoconstriction is patchy and bimodal: a pet imaging study. Respiratory physiology & neurobiology, 148(1):57–64, 2005.
- [101] J.G. Venegas, T. Winkler, G. Musch, M.F.V. Melo, D. Layfield, N. Tgavalekos, A.J. Fischman, R.J. Callahan, G. Bellani, and R.S. Harris. Self-organized patchiness in asthma as a prelude to catastrophic shifts. Nature, 434(7034):777–782, 2005.
- [102] J.G. Venegas, J.P. Woll, S.B. Woolfson, E.G. Cravalho, N. Resnick, and S.V. Yalla. Viscoelastic properties of the contracting detrusor. ii. experimental approach. American Journal of Physiology-Cell Physiology, 261(2):C364–C375, 1991.
- [103] M.F. Vidal-Melo, D. Layfield, R.S. Harris, K. O’Neill, G. Musch, T. Richter, T. Winkler, A.J. Fischman, and J.G. Venegas. Quantification of regional ventilation-perfusion ratios with pet. Journal of Nuclear Medicine, 44(12):1982–1991, 2003.

- [104] E.M. Wagner, E.R. Bleeker, S. Permutt, and M.C. Liu. Direct assessment of small airways reactivity in human subjects. American journal of respiratory and critical care medicine, 157(2):447–452, 1998.
- [105] ER Weibel et al. Morphometry of the human lung: the state of the art after two decades. Bulletin europeen de physiopathologie respiratoire, 15(5):999, 1979.
- [106] T.J. Wellman, T. Winkler, E.L.V. Costa, G. Musch, R.S. Harris, J.G. Venegas, and M.F.V. Melo. Measurement of regional specific lung volume change using respiratory-gated pet of inhaled ^{13}N -nitrogen. Journal of Nuclear Medicine, 51(4):646–653, 2010.
- [107] BR Wiggs, C. Bosken, PD Pare, A. James, and JC Hogg. A model of airway narrowing in asthma and in chronic obstructive pulmonary disease. American Journal of Respiratory and Critical Care Medicine, 145(6):1251–1258, 1992.
- [108] BR Wiggs, R. Moreno, JC Hogg, C. Hilliam, and PD Pare. A model of the mechanics of airway narrowing. Journal of Applied Physiology, 69(3):849–860, 1990.
- [109] T. Winkler and J.G. Venegas. Complex airway behavior and paradoxical responses to bronchoprovocation. Journal of Applied Physiology, 103(2):655–663, 2007.
- [110] C. Wongviriyawong, R.S. Harris, H. Zheng, M. Kone, T. Winkler, and J.G. Venegas. Functional effect of longitudinal heterogeneity in constricted airways before and after lung expansion. Journal of Applied Physiology, 112(1):237–245, 2012.
- [111] AJ Woolcock and J. Read. The static elastic properties of the lungs in asthma. The American review of respiratory disease, 98(5):788, 1968.
- [112] D.A. Yablonskiy, A.L. Sukstanskii, J.C. Woods, D.S. Gierada, J.D. Quirk, J.C. Hogg, J.D. Cooper, and M.S. Conradi. Quantification of lung microstructure with hyperpolarized ^3He diffusion mri. Journal of Applied Physiology, 107(4):1258–1265, 2009.
- [113] H. Yuan, B. Suki, and K.R. Lutchen. Sensitivity analysis for evaluating nonlinear models of lung mechanics. Annals of biomedical engineering, 26(2):230–241, 1998.

THIS PAGE INTENTIONALLY LEFT BLANK

Appendix A

Derivations of Specific Pathway Admittance

A.1 Model 1

Each pathway in Model 1 consisted of elastic elements with different apparent compliance of each sublobar regions ($C_{a,i}$) (all resistive elements were assumed to be zero). Airflow through each pathway (i) was assumed to be sinusoidal with maximum flow rate ($\dot{V}_{max,i}$), average flow rate (\bar{V}_i), and constant breathing frequency (f).

$$\dot{V}_i = \dot{V}_{max,i} \cos(2\pi f \cdot t) = \frac{\pi}{2} \bar{V}_i \cos(2\pi f \cdot t) \quad (\text{A.1})$$

The average pressure drop across $C_{a,i}$ in each pathway ($i = 1, \dots, 19$) during inspiration ($P_{pw,i}$) to the flow rate through each pathway (\dot{V}_i).

$$P_{pw,i} = \int_0^{T/2} \frac{\dot{V}_i(t)}{C_{a,i}} dt \quad (\text{A.2})$$

In the Laplace domain,

$$P_{pw,i}(s) = \frac{1}{C_{a,i}} \frac{\dot{V}_i(s)}{s} \quad (\text{A.3})$$

where $s = j(2\pi f)$ and $j = \sqrt{-1}$

Therefore, the pathway admittance ($Y_{pw,i}$) of Model 1 is,

$$Y_{pw,i} = \left| \frac{\dot{V}_i}{P_{pw,i}} \right| = 2\pi f C_{a,i} \quad (\text{A.4})$$

A.2 Model 2

The network in Model 2 consisted of conductance of central airways ($G_{c,k}$) and C_a (i.e. peripheral resistance ($R_{p,i}$) was neglected). The total pressure drop, therefore, $P_{pw,i}$ was the sum of the resistive pressure drop and the pressure drop across the apparent compliance.

In the Laplace domain,

$$P_{pw,i}(s) = \frac{1}{C_{a,i}} \frac{\dot{V}_i(s)}{s} + \sum_{k \in pw_i} \frac{\dot{V}_k(s)}{G_{c,k}} \quad (\text{A.5})$$

where k is the index of an airway leading to the sublobar region i , and is the flow through the airway k . Hence,

$$P_{pw,i} = \left(\sum_{k \in pw_i} \frac{\dot{V}_k}{G_{c,k}} \right) - j \left(\frac{1}{C_{a,i}} \frac{\dot{V}_i}{2\pi f} \right) \quad (\text{A.6})$$

And,

$$Y_{pw,i} = \left| \frac{\dot{V}_i}{\left(\sum_{k \in pw_i} \frac{\dot{V}_k}{G_{c,k}} \right) - j \left(\frac{1}{C_{a,i}} \frac{\dot{V}_i}{2\pi f} \right)} \right| \quad (\text{A.7})$$

A.3 Model 3

The network in Model 3 consisted of $G_{c,i}$, peripheral resistance ($R_{p,i}$), and $C_{a,i}$ connected in the order listed. A unique set of $R_{p,i}$ was determined to satisfy the pressure drop boundary condition both in magnitude and phase.

Similar to the analysis above,

$$P_{pw,i} = \left(\sum_{k \in pw_i} \frac{1}{G_{c,k}} \dot{V}_k + R_{p,i} \dot{V}_i \right) - j \left(\frac{1}{C_{a,i}} \frac{\dot{V}_i}{2\pi f} \right) \quad (\text{A.8})$$

Solve for $R_{p,i}$ such that $P_{pw,i} = -P_{pl}$

$$-P_{pl} = \left(\sum_{k \in pw_i} \frac{1}{G_{c,k}} \dot{V}_k + R_{p,i} \dot{V}_i \right) - j \left(\frac{1}{C_{a,i}} \frac{\dot{V}_i}{2\pi f} \right) \quad (\text{A.9})$$

THIS PAGE INTENTIONALLY LEFT BLANK

Appendix B

Estimating Apparent Compliance

Regional Apparent Compliance ($C_{a,i}$) for each sublobar region (index $i = 1, 2, \dots, 19$) was computed as,

$$C_{a,i} \equiv \frac{\Delta V_i}{\Delta P_{tp}} \quad (\text{B.1})$$

where

$$\Delta V_i = Vgas_{i,TLC} - Vgas_{i,MLV} \quad (\text{B.2})$$

and ΔP_{tp} was found from the relationship below,

$$sC \equiv \frac{\Delta V_L / FRC}{\Delta P_{tp}} = \frac{(Vgas_{L,TLC} - Vgas_{L,MLV})}{\Delta P_{tp}} \quad (\text{B.3})$$

Hence,

$$C_{a,i} = \frac{Vgas_{i,TLC} - Vgas_{i,MLV}}{\frac{Vgas_{L,TLC} - Vgas_{L,MLV}}{sC \cdot FRC}} \quad (\text{B.4})$$

where $Vgas_i$ and $Vgas_L$ were the gas volume in the segmental region and whole lung, respectively; the subscript MLV and TLC denoted the lung volume during HRCT imaging from which $Vgas$ was calculated; sC was the specific compliance and assumed to be 0.1

L/cmH₂O per 1L of Functional Residual Capacity (FRC). This method was equivalent to those described in the literature by Fuld et al. [25].